CONTROL OF DISTRIBUTED GENERATION FOR GRID-CONNECTED AND INTENTIONAL ISLANDING OPERATIONS

By

Irvin Joel Balaguer Álvarez

A DISSERTATION

Submitted to
Michigan State University
in partial fulfillment of the requirements
for the degree of

DOCTOR OF PHILOSOPHY

Electrical Engineering

2011

ABSTRACT

CONTROL OF DISTRIBUTED GENERATION FOR GRID-CONNECTED AND INTENTIONAL ISLANDING OPERATIONS

By

Irvin Joel Balaguer Álvarez

The current model for electricity generation and distribution in the United States is dominated by centralized power plants. The power at these plants is typically combustion (coal, oil, and natural) or nuclear generated. Centralized power models, like this, require distribution from the center to outlying consumers. This system of centralized power plants has many disadvantages. Electric utilities are becoming more and more stressed since existing transmission and distribution systems are facing their operating constraints with growing load. Greenhouse gas emissions have resulted in a call for cleaner renewable power sources. Under such circumstances, distributed generation (DG) with alternative sources; such as fuel-cell, wind-turbine, bio-mass, micro-turbine and solar-cell systems; has been considered as a promising solution to the above problems.

DG is defined as small, modular electricity generators located close to the end customer's load connection point. DGs can enable utilities to decrease investment costs in transmission and distribution system upgrades while still meeting increasing power demands. Also, DGs provide customers with improved quality and reliability of energy supplies without imposing undesirable effects on environment. In general, DG can be intended as small sized power plants that are designed to be installed and operated within a local load center.

This research presents the development and test of a control strategy for DG capable of working in both intentional islanding (stand-alone) and grid-connected modes. In the grid-connected mode of operation, the DG is connected to the utility. The utility, which is assumed to be stiff, sets the voltage at the terminal of the DG inverter. The inverter controls the power being injected into the grid by controlling the injected current. Thus, in this mode, the inverter operates in the current control mode. In the stand-alone mode, the inverter supplies power to the load. It has to maintain the voltage at the terminals of the load, irrespective of any changes in the load. Thus, in this mode, the inverter operates in the voltage controlled mode.

The stand-alone control features an output voltage controller capable of handling deficit of generated power (load shedding) and synchronization for grid reconnection with a seamless transition from stand-alone to grid-connected operation modes. The grid-connected mode with current control is also enabled for the case of power grid connection. This grid-connected control features an output current controller capable of loss of main detection, synchronization with the grid, and seamless transition from grid-connected to stand-alone operation modes with minimum interruption to the load.

The operational principle and control method of the proposed system are explained in detail. A 10kW DG inverter has been designed, built and set up for testing. Simulation and experimental results are provided in order to verify the validity of the developed DG system.

To the only wise God our Savior, be glory and majesty, dominion and power, both now and ever. Amen. (Jude 1:25 King James Version)

To my wife Raquel, my son Kevin, and my daughters Kelly and Kiara, for their patience, unconditional love, and support.

ACKNOWLEDGMENTS

First and foremost I would like to thank *God* for giving me the drive, ability and patience to strive for the completion of this dissertation.

I am forever grateful to Dr. Fang Z. Peng for providing me the opportunity to work with him and for his kind words of advice, guidance and encouragement throughout my stay at Michigan State University.

I would also like to thank Dr. Robert Schlueter, Dr. Elias Strangas, and Dr. Robert Ofoli for agreeing to be members of my doctoral guidance committee, for their invaluable comments and time.

I extend a special thank you to Dr. Percy Pierre and Dr. Barbara O'Kelly of the Sloan Engineering Program in MSU's College of Engineering and to Professor Aníbal Romney, Chairperson of the Department of Electronics Engineering Technology of the University of Puerto Rico-Aguadilla Campus, for the generous financial support without which this work would not have been possible.

I deeply appreciate the continued support, cooperation, and valuable discussions that I engaged in with the Power Electronics and Motor Drives Laboratory colleagues who I was involved with: Dr. Eduardo Ortiz, Dr. Lihua Chen, Dr. Miaosen Shen, Dr. Haiping Xu, Dr. Heung-Geun Kim, Dr. Nam-Sup Choi, Dr. Yuan Li, Dr. Honnyong Cha, Dr. Yi Huang, Miss Qin Lei, Mr. Uthane Supatti, Mr. Shuitao Yang, Mr. Craig Rogers, Mr. Matthew Gebben, Mr. Jorge Cintrón, Mr. Dong Cao, Miss Xi Lu, Miss Wei Qian, Mr. Varun Chengalvala, Mr. Richard Badin, Mr. Alan Joseph, Mr. Joel Anderson, and Mr. Carlos Niño. This long list is still not complete and I apologize to those not listed as you all contributed to my experience in the lab.

A special thanks to Miss Qin Lei, Mr. Shuitao Yang, Mr. Jorge Cintrón, and Mr. Uthane Supatti for all their help with the hardware and experimental setups. To my proofreaders Mr. Craig Rogers, Mr. Matthew Gebben, Mrs. Deana Hutchins, Mr. Erick Rivas, Mrs. Aurelia Rivas, Mr. Jason Lounds, Mr. Alex Fitzpatrick, and Mrs. Deb Fitzpatrick, thanks all you very much.

I would also like to express my gratitude to Mrs. Sheryl Hulet, former graduate secretary and Mrs. Meagan Kroll, the current graduate secretary at the Department of Electrical and Computer Engineering at Michigan State University for their tremendous help with all the procedural paper work throughout my time in the Ph.D. program.

From the bottom of my heart, I'm most grateful to my parents, Mr. Ramón Balaguer and Mrs. Carmen Rita Álvarez, and my brothers, Victor and José, for their unwavering support, constant encouragement, and extraordinary understanding throughout my graduate studies. I'm equally grateful to my parents-in-law, Mr. Adalberto Lebrón, Mrs. Esther Salas, and my brothers-in-law, Adalberto Jr. and Marcos, for their good wishes, and specifically, for their faith in my abilities. I truly believe that this work could only have been brought to completion via the blessings and good wishes from all of them.

A special thank you goes out to all of our extended family from the Lansing Seventh-day Adventist Church, Greater Lansing Adventist School, Lansing Spanish Seventh-day Adventist Church, and the University Seventh-day Adventist Church in East Lansing.

Finally, words cannot articulate the companionship and support provided to me by my lovely wife, Raquel, my son Kevin and my two daughters, Kelly and Kiara. I would have left this work long ago without their presence in my life. Obtaining a Ph.D. is a complex undertaking. At times it is uncomfortable and challenging, and at others utterly rewarding. There have been many peaks and troughs along the way. Raquel has been my pillar through them all. She has always

been willing to make sacrifices in her life to accommodate my work schedule. I could not have asked for more, and I genuinely thank her for the role she has played in making this endeavor a success.

TABLE OF CONTENTS

LIST OF FIGURES

CHAPTER 1. INTRODUCTION

The current model for electricity generation and distribution in the United States is dominated by centralized power plants. The power at these plants is typically combustion (coal, oil, and natural) or nuclear generated. Centralized power models like this require distribution from the center to outlying consumers.

This system of centralized power plants has many disadvantages. Electric utilities are becoming more and more stressed since existing transmission and distribution systems are facing their operating constraints with growing load. Greenhouse gas emissions have resulted in a call for cleaner renewable power sources. Under such circumstances, distributed generation (DG) with alternative sources such as fuel-cell, wind-turbine, bio-mass, micro-turbine and solar-cell systems, has been considered as a promising solution to the above problems.

1.1. The Distributed Generation Concept

DG is defined as small, modular electricity generators located close to the end customer's load connection point. They can enable utilities to decrease investment costs in transmission and distribution system upgrades while still meeting increasing power demands and provide customers with improved quality and reliability of energy supplies without imposing undesirable effects on environment [1-2]. In general, DG can be intended as small sized power plants that are designed to be installed and operated within a local load center.

To effectively and efficiently connect any of the DG sources to the existing power systems power electronics-based conversion systems need to be developed for the proper control and conditioning of the energy to be delivered [3]. Specifically, with most of the DG sources such as

variable frequency AC microturbines, DC fuel cells, DC photovoltaic cells and low power variable frequency AC wind turbines, electrical power is generated as DC voltage or converted to DC voltage, then converted to AC using a voltage sourced inverter. This voltage sourced inverter performs the interface function between the DC bus and the AC world. Through the proper control and conditioning of the DG, benefits such as voltage support and improved power quality, diversification of power sources, reduction in transmission and distribution losses, transmission and distribution capacity release and improved reliability, among others, can enhance the utility grid without having to add or replace the existing transmission/distribution system.

Some issues and concerns must be addressed when dealing with DG systems. Particularly, attention must be taken into account when a design is being done for the support of power delivery to the utility and when incorporating the concepts of both grid-connected and stand-alone. During the grid-connected operation, each DG system is usually operated to provide or inject pre-set power to the grid, which is the current control mode in stiff synchronization with the grid [4-6]. When the main grid is cut off from the DG system, stand-alone operation or intentional islanding, the DG system has to detect this islanding situation and must be switched to a voltage control mode to provide constant voltage to the local sensitive loads [7-9]. The trend is that they should be able to work in stand-alone mode but also connected to the power grid (grid-connected) [10]. Thus some new challenges on the control side of the DG occurred. Among these challenges are: reasonable voltage regulation in stand-alone mode, grid-connection mode enabled, and automatic detection of grid disconnection. Also grid disconnection detection and an automatic mode switching are required. In order to manage these challenges, relative complex control strategies need to be developed.

1.2. Benefits associated with DG

In distribution systems, DG can provide benefits for the consumers as well as for the utilities, especially in sites where there are deficiencies in the transmission system. Some of the expected benefits of DG are [11-19]:

- Green house emissions reductions: By the increase of the use of renewable energy units, as well as high efficiency generation units, operated in an optimum manner, the green house emissions will be decreased with respect to the conventional generation.
- Energy efficiency: By an adequate planning and operation of the generation and storage units of the DG, the electric and heat generation or combined heat and power (CHP) can be mixed, increasing the energy efficiency of the installation. It can also be made in a profitable way.
- Reduced transmission and distribution investments: DG helps bypass ‘‘congestion’’ in existing transmission grids. DG could serve as a substitute for investments in transmission and distribution capacity. DG can postpone the need for new infrastructure. Because of opportunities for integration in buildings, DG development often occurs in the same location as demand. In such cases, if production output is concurrent with demand – such as demand for air-conditioning in hot regions – network reinforcement may be unnecessary while generation remains in the same order of magnitude as demand. Moreover, normal development of the grid in response to growing demand may also be postponed or even avoided as DG has the net effect of decreasing demand in that area.
- Minimization of the electric losses: On-site production reduces the amount of power that must be transmitted from a centralized plant, and avoids resulting transmission losses and

distribution losses, as well as the transmission and distribution costs, a significant part of the total electricity cost, due to the fact that generation buses and consumption are closer.

- Network (voltage) support: The connection of distributed generators to networks generally leads to a rise in voltage in the network.
- Quality of supply improvement: In areas where voltage support is difficult, installation of a distributed generator may improve quality of supply. As the demand for more and better quality electric power increases, DG can provide alternatives for reliable, cost-effective, premium power for homes and businesses.
- New market opportunities and enhanced industrial competitiveness: DG can also stimulate competition in supply; adjusting price via market forces. In a free market environment, DG operator can buy or sell power to the electricity grid, exporting only at peak demand and purchasing power at off-peak prices.
- Reduction of the energy costs: Thanks to the intelligence and control capabilities of the DG, its operator will schedule the operation of its generation and storage sources, depending on the electricity and gas actual prices, climatic conditions and their forecast.
- Locality, i.e. improved utilization of local resources: Distributed energy generation may also promote local business opportunities, and develop products and services based on local raw materials and labor. Local employment can be improved by creating new jobs related to distributed energy generation. This, in turn, causes a need for high-quality education. Locality also means the absence of transmission lines, large power plants, and fuel storage, which spoil the landscape. The environmental load is also reduced due to the avoidance of additional energy required to compensate transmission losses.

1.3. Issues associated with DG

Despite the above mentioned benefits provided by DG, there are technical limits regarding the degree to which DG can be connected. Indiscriminate application of individual DG systems can cause as many problems as it may solve [11]. This is because the distribution system was intended to cope with the conventional load supply by central generation, where power flows radially from the transmission network. Changing the power flow causes problems since DG does not behave the same way as conventional load. The issues associated with DG can be summarized as [14, 17, 19-27]:

- Interface with AC System: The main DG requirement for interfacing with the utility system is that it must not compromise the stability and reliability of the grid. The interface must also guarantee compliance with already existing protection schemes.
- Protection: DG needs to be retrofitted in its protection algorithms to include the contributions of micro-sources. DG can impact a variety of levels of short-circuit current. The DG systems have to provide enough fault current to operate the protective devices, including circuit breakers, fuses, and fault-protection relays. The addition of DG on a circuit may need to be studied to establish whether changes are needed for coordination or protection equipment. Different hardware setups may be required: the rating of the breakers responsible to implement protection may need to be revisited, and surely they will have to be controlled with a different algorithm.
- Power quality: DG can negatively affect power quality. Power quality refers to the degree to which power characteristics align with the ideal sinusoidal voltage and current waveform, with current and voltage in balance.
    - Voltage Regulation: The primary objective of voltage regulation is to provide each customer connected to the utility with voltage that conforms to limits voltage

range for normal operation. The operating window for DG systems is 106-132 V_{rms} on a 120 V_{rms} base, that is, 88 - 110% of nominal voltage [28].

- Harmonics: Due to the power electronics and digital methods used to form the AC waveform from DC, inverter-based DG technologies produce various harmonics of the power system frequency. Standards states that the total harmonic distortion (THD) must not exceed 5% of the fundamental 60 Hz frequency, nor 3% of the fundamental for any individual harmonic [28].
- Power Factor: Power factor measures the apparent power that is generated when the voltage and current waveforms are out of synchronism. Power factor is the ratio of true electric power (watts), to the apparent power (kVA). Although not strictly the case, power factor problems can be thought of as contributing to utility system inefficiencies [29]. The DG inverter should operate at a power factor > 0.85 (lagging or leading) [28]. Most DG inverters designed for utility-interconnected service operate close to unity power factor. Specially designed systems that provide reactive power compensation may operate outside of this limit with utility approval.
- Frequency: DG systems have to operate in synchronism with the utility. DG systems installed in North America should have a fixed operating frequency range of 59.3 - 60.5 Hz [28]. Systems installed in another country should follow the frequency operating window standards of that country.
- DC injection: DC injection occurs when an inverter passes unwanted DC current into the AC or output side of the inverter. The DG inverter should not inject dc current > 0.5% of rated inverter output current into the ac interface under either normal or abnormal operating conditions [28]. Inverter manufacturers generally use one of two methods to prevent the injection of dc current into the utility interface. One method is to incorporate an ac output isolation transformer in the inverter. The other method, which uses a shunt or dc-current sensor, initiates

inverter shutdown when the dc component of the current exceeds the specified threshold.

- Instantaneous power tracking: The requested power from the load coming on-line is a step function, while the prime mover in the micro-source always takes a finite amount of time to ramp up to the newly requested value. Micro-sources have a slow response to changes in commands and the inverter interface by itself does not provide any kind of internal form of energy storage. This inertia-less system is not well suited to handle step changes in the requested output power. If the connection to the grid is missing due to a temporary malfunction then the need for some sort of storage is manifest. Storage is required to satisfy the instantaneous power balance as a new load comes on-line without penalizing the quality of other network quantities, such as bus voltage magnitude. Load changes resulting in fast transients that exceed the ramping capability of generation require storage availability from which to draw the required transient energy.
- Unidirectional Area Electric Power System (EPS) Relaying: Due to the traditional radial nature of distribution systems, most protective devices on the EPS are unidirectional in nature and respond to a given value of current without regard to the direction of flow of that current. Because DG produces fault current of various magnitudes for faults on the EPS, the traditional radial nature of the distribution system is disrupted and unidirectional relays could operate improperly.
- Paralleling DG: One of the selling points for DG is that the local generation follows a scalable system model, where due to the typical small size of the units, one can install as many units as needed to satisfy the requests of the loads, without having too much of extra capacity sitting idle. But this concept requires that the micro-sources can be installed in parallel without any restrictions.

- Plug and Play Configuration: When looking into the future and envisioning micro-sources being installed by the thousands, the need for plug and play configuration becomes manifest. The plug and play mode of operation implies simplicity of installation and therefore speeds up the process of diffusion of the DG in the system. The ideal case would be purchasing a unit and plugging it in a three-phase socket, having power injected immediately (after synchronization).
- Synchronization with the Grid: One of the most important issues of a DG system connected to the utility network is the synchronization with the grid voltage vector. The synchronization algorithm mainly outputs the phase of the grid voltage vector. The phase angle of the utility voltage is a critical piece of information for grid connected systems. This information can be used to synchronize the turning on/off of the power devices, calculate and control the flow of active/reactive power or transform the feedback variables to a reference frame suitable for control purposes. Because of these, the accurate and fast detection of this phase angle is essential to assure the correct generation of the reference signals.
- Loss of Main Detection (Grid condition detection) or Islanding Detection: One of the major concerns in operating DG systems connected to the grid is the possibility of islanding due to grid disturbances, intentional disconnect for servicing, accidental opening, intentional disconnect from the utility, and an act of nature, among others. Islanding is the condition in which a portion of the utility system, which contains both load and DG, is isolated from the remainder of the utility system and continues to operate. Islanding is either due to preplanned (intentional) events or due to non-planned or accidental (un-intentional) events [10]. Some distinctions of islanding are:

- *non-intentional* islanding occurs if it is not possible to disconnect the DG after the fault, non-intentional islands must then be detected and eliminated as fast as possible;
- *intentional* islanding refers to the formation of islands of predetermined or variable extension; these islands have to be supplied from suitable sources able to guarantee acceptable voltage support and frequency, controllability and quality of the supply, and may play a significant role in assisting the service restoration process;
- *microgrids* are seen as particular types of intentional islands basically operated in autonomous mode, not connected to the supply system; the whole microgrid can be seen from the distribution system as a single load and has to be designed to satisfy the local reliability requirements, in addition to other technical characteristics concerning frequency, voltage control and quality of supply.

In a deregulated market environment, current practices of disconnecting the DG following a disturbance will no longer be a practical or reliable solution. As a result, the IEEE Std. 1547-2003 states as one of its tasks for future consideration of the implementation of stand-alone operation of DG (IEEE P1547.4: Guide for Design, Operation, and Integration of Distributed Resource Island Systems with Electric Power Systems) [28].

- Transitions from grid-connected to stand-alone: One of the problems to face during the transfer to stand-alone is to ensure minimal to none transients at all the load bus. The DG inverter should operate in grid-connected and stand-alone modes in order to provide power to the emergency load during system outages. However, grid current controller

(for grid-connected) and output voltage controller (for stand-alone) are switched between the two modes, so the outputs of both controllers may not be equal during the transfer instant, which will cause the current or voltage spikes during the switch process.

- Load shedding: Another problem to face during the transfer to stand-alone is to automatically readjust the power output of the units to compensate for the missing quota of injected power from the utility system. This issue brings a challenge because of the assumption that there is no previous knowledge of the loading levels as the system transfer to island and also because of the assumption that no communication may exist between the micro-sources to enforce a coordinated behavior during and after the transfer to island.
- Reclosing: Automatic circuit reclosers may also be deployed in the feeder circuit to automatically clear faults and quickly restore service on the feeder. Reclosers reenergize the circuit automatically at a predetermined time after a trip resulting from a feeder fault. The response of the DG unit needs to be coordinated with the reclosing strategy and the settings of the recloser isolation operations. Coordination and synchronization are required to prevent possible damage to the equipment connected to the DG.
- Transitions from stand-alone to grid-connected: When the grid-disconnection cause disappears, the transition from stand-alone mode to grid-connected mode can be started. The voltage amplitude and phase of the DG have to be synchronized with the grid to avoid hard transients in the reconnection. Once the synchronization process is completed, the DG can be reconnected to the grid.

1.4. Scope of the Dissertation

This research presents the development and test of a control strategy for DG capable of working in both stand-alone and grid-connected modes. The stand-alone control features an output voltage controller capable of handling excess or deficit of generated power and synchronization for grid reconnection with a seamless transition from stand-alone to grid-connected operation modes. The grid-connected mode with current control is also enabled for the case of power grid connection. This grid-connected control features an output current controller capable of loss of main detection, synchronization with the grid, and seamless transition from grid-connected to stand-alone operation modes with minimum interruption to the load.

A method to automatically switch between both modes of operation is described. This method, based on a phase-locked loop (PLL), detects the power grid disconnection or recovery, and switches the operation mode accordingly.

The proposed control strategy will have the following characteristics:

1. Interface with AC System
2. Power quality
    a. Voltage Regulation
    b. Harmonics
3. Synchronization with the Grid
4. Loss of Main Detection or Islanding
5. Transitions from grid-connected to stand-alone
6. Load shedding
7. Reclosing
8. Transitions from stand-alone to grid-connected

Operation modes as well as the involved voltage and current controllers will be described in detail. The design of an LCL filter to achieve attenuation of the switching frequency ripple in the output voltage will be also described. A PLL for grid synchronization and loss of main detection will be presented. Also, a re-connection algorithm and automatic mode switching will be delineated**.**

1.5. Outline of the Dissertation

A brief description of the Distributed Generation Concept is presented in this chapter. Chapter 2 presents a literature review of the techniques used for the control of an inverter unit in grid-connected and stand-alone modes. The system description including circuit topology, voltage source inverter, LCL filter, simulation set-up, and experimental set-up are given in Chapter 3. Chapter 4 discusses the proposed control for grid-connected operation of DG. The proposed control for intentional islanding operation is presented in Chapter 5. Conclusions and the scope for future work are presented in Chapter 6.

CHAPTER 2. LITERATURE REVIEW

This section summarizes the techniques used for the control of an inverter unit in grid-connected and stand-alone modes.

R. Tirumala, *et al.* [30] presented an algorithm for a utility interactive DG system with a seamless transition between grid-tied (current controller) and off-grid (voltage controller) modes of operation. A static transfer switch (STS) was used to disconnect and reconnect the load bus to the grid. The control ensured a smooth voltage profile across the load when the grid was disconnected or reconnected. The control algorithm ensured that the static transfer switch was turned off before the inverter was shifted to the voltage-controlled mode. Also, the algorithm ensured that the voltage applied across the load matched the load voltage just before disconnection. The steps to perform this algorithm can be summarized as follows:

1. Detect a fault on the grid and give a turn off signal to the STS.
2. Monitor the magnitude and phase of the load voltage.
3. When the STS current goes to zero, switch the inverter to a voltage-controlled mode, with the voltage reference being derived from the load voltage.
4. Ramp up the magnitude of the load voltage from its initial value to the rated value.

For the transfer between the voltage-controlled mode and the current controlled mode, the inverter voltage matched the grid voltage both in magnitude and phase before the static transfer switch was turned on. The STS would be turned on when there is essentially zero voltage across it. Once the STS was turned on, the grid current would be slowly ramped up to prevent any voltage spikes caused by the grid inductance. The steps to perform this algorithm can be summarized as follows:

1. Detect that the grid is within nominal operating parameters.

2. Adjust the load voltage to match the magnitude and phase of the grid voltage.

3. Once the load voltage is equal to the grid voltage, turn on the STS and switch from voltage-controlled mode to current-controlled mode, with the reference current being equal to the load current.

4. Change the reference current slowly to the desired current (both magnitude and phase).

L. Yunwei, *et al.* [31] proposed a unified controller for use with DG system. By regulating the output voltage, the proposed controller controlled power flow in the grid-connected mode of operation, enabling the operation of DG when the system islands, and resynchronized the DG with the utility before reconnecting them. The presented controller responded fast, allowing the controlled DG to transit smoothly between the grid-connected and islanding modes without disrupting critical loads connected to it. The resynchronization process when the utility grid returned back to normal operating conditions form was achieved by aligning the voltage at the DG and utility ends of a STS separation device. This process was implemented by adding two synchronization compensators to the real and reactive power control loop, as shown in the dashed frames of Fig. 2.1 and Fig. 2.2. To summarize, the final block diagram representation of their proposed unified controller is shown in Fig. 2.3.

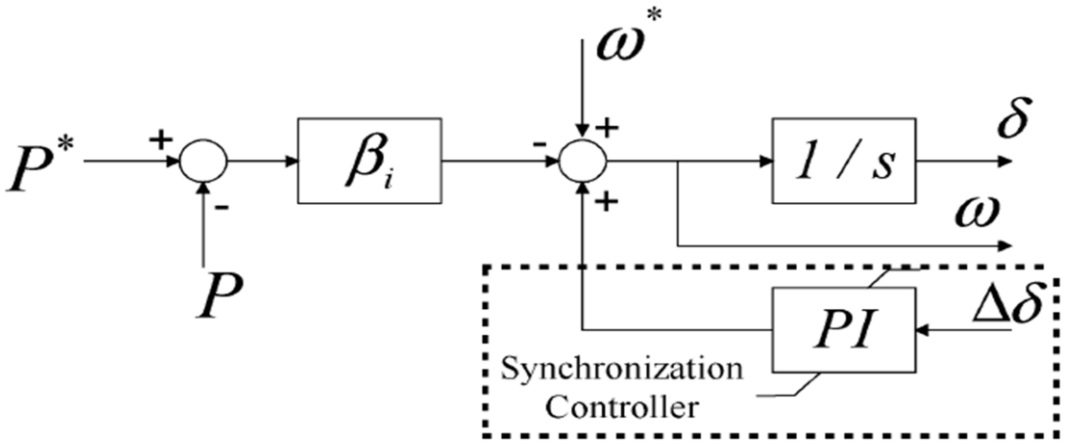

Fig. 2. 1 Real power compensator with synchronization function [31]

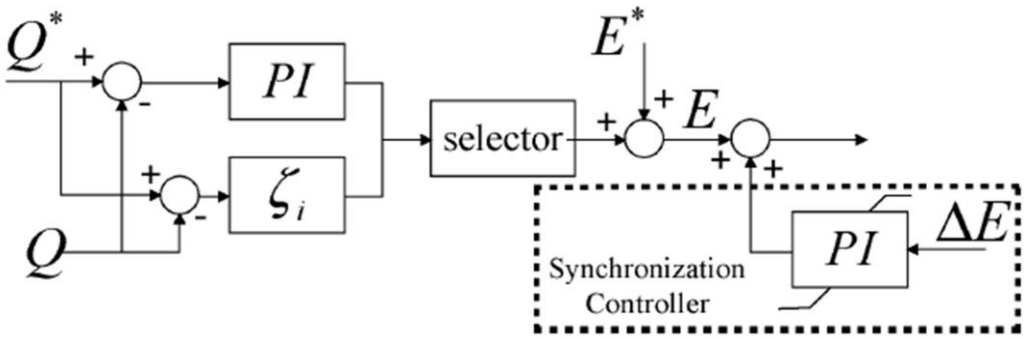

Fig. 2. 2 Reactive power compensator with synchronization function [31]

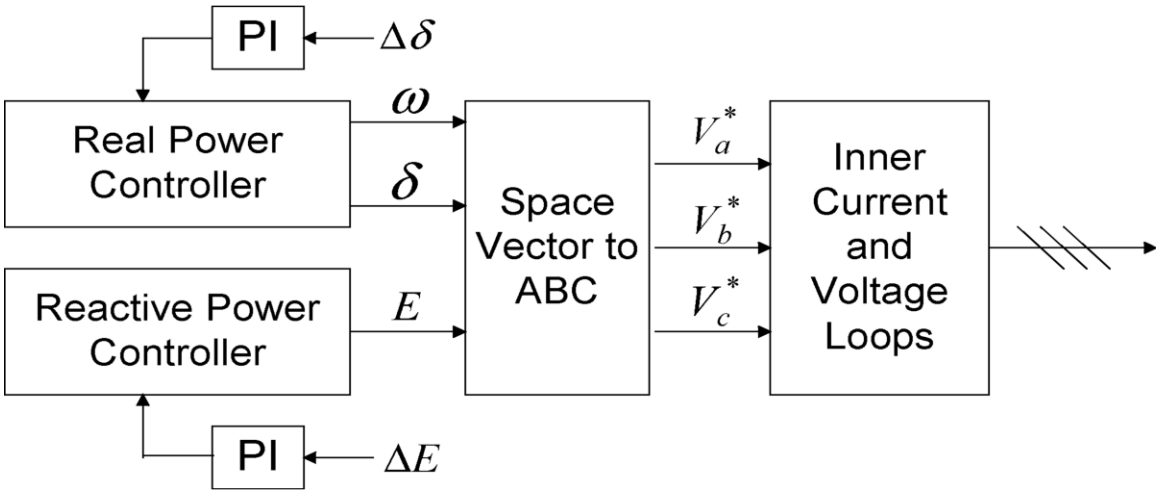

Fig. 2. 3 Overview of proposed unified controller [31]

T. Thacker, *et al.* [32-33] proposed a switched-mode control with detection and re-closure algorithms scheme to regulate between the grid-connected and stand-alone modes of operation. Their proposed system configuration can be seen in Fig. 2.4.

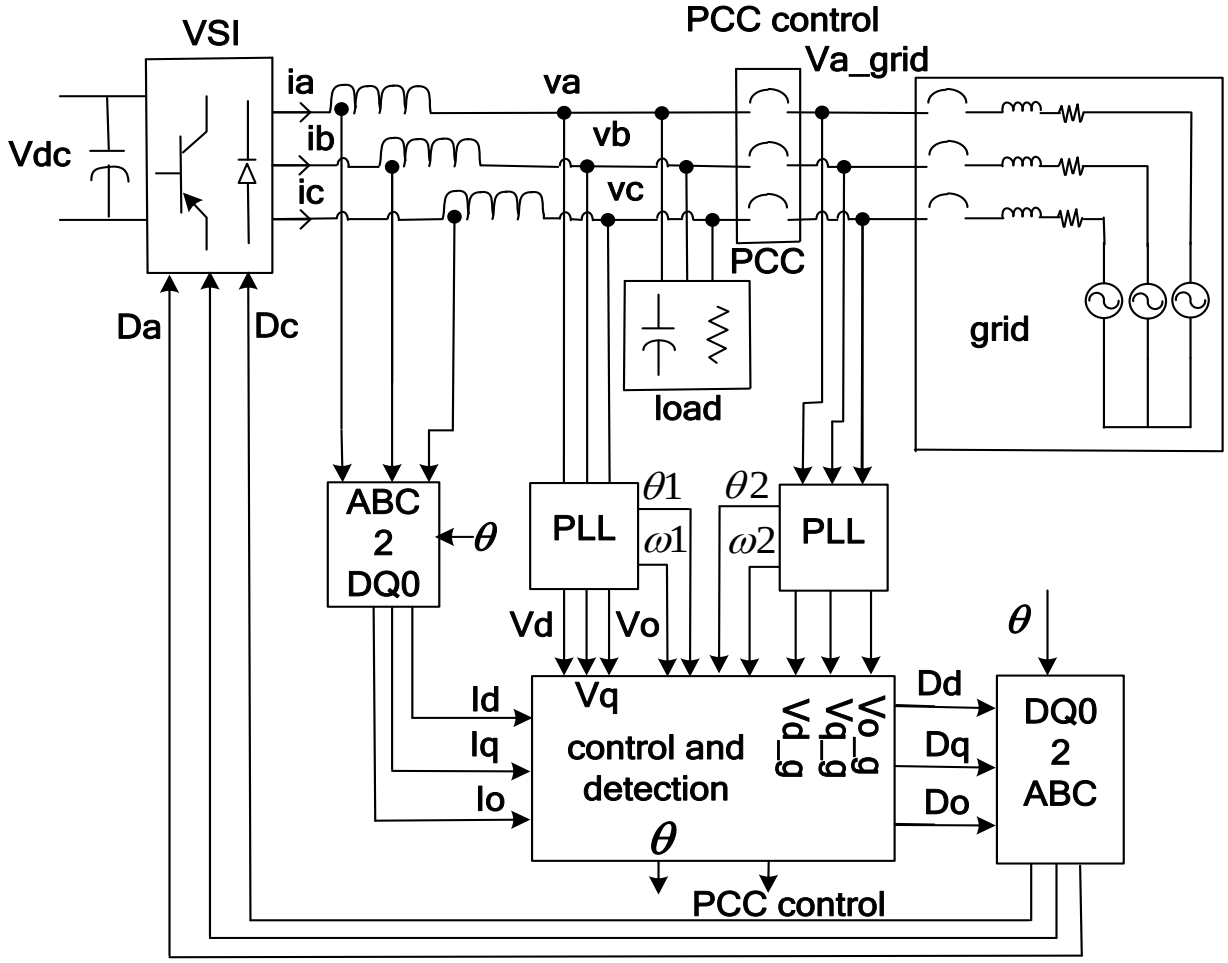

Fig. 2. 4 System configuration for simulated and experimental results [32-33]

Their proposed detection scheme, Fig. 2.5, used passive sensing parameters (over/under voltage & frequency, real/reactive power deviation) with a BPF loop being fed directly to the duty cycles instead of being fed to the current references. The advantage of BPF going directly to the duty-cycles is that the current limiters can still be implemented without special considerations. When an islanding event was detected, the system was automatically disconnected from the grid and switched to voltage mode control.

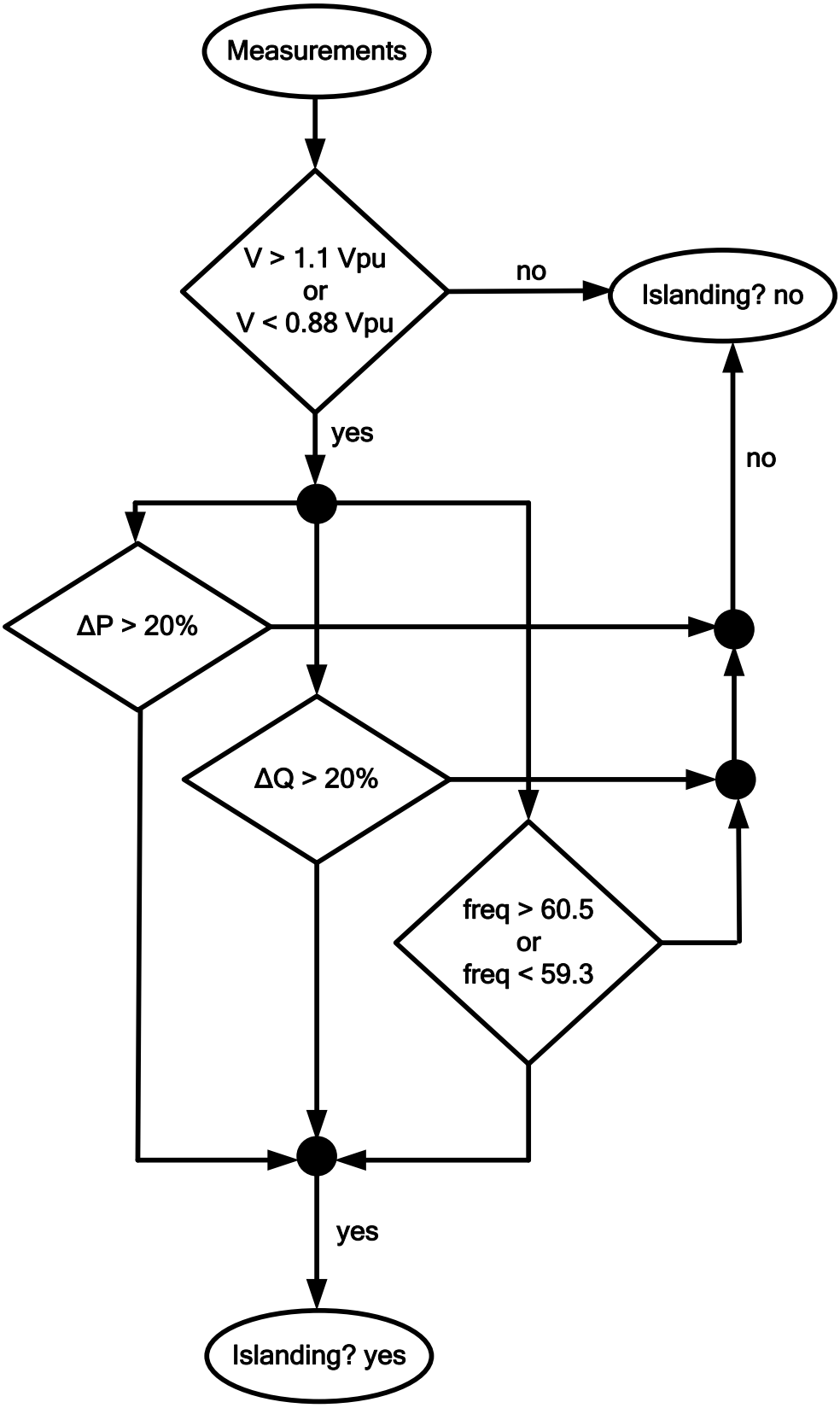

Fig. 2. 5 Islanding Detection Flowchart [32-33]

Their proposed re-closing scheme is seen in Fig. 2.6. Like the detection algorithm, this algorithm was autonomous and incorporated into the control of the DG. The idea was that by measuring four key parameters: the grid voltage, VSI voltage, VSI frequency, and the line angle difference between the grid and VSI, the system could safely reclose to the utility without having to de-energize the DG. The scheme first measured and detected if the grid voltage had been recovered from its fault and was back in nominal operating conditions. With the grid back to nominal conditions, the signal coordinate transforms and detection started to use the grid's line angle as a reference. This caused the VSI's PLL to start tracking the grid. Next, the magnitudes of the VSI voltage and grid voltage were compared to ensure that they were on the same order of magnitude before re-closing. The VSI frequency was then checked to make sure that the VSI had not left the nominal frequency range. Finally, the system checked to see that the phase angle difference between the VSI and grid were near zero. Once all of these conditions were satisfied, concurrently, the DG would re-close with the grid.

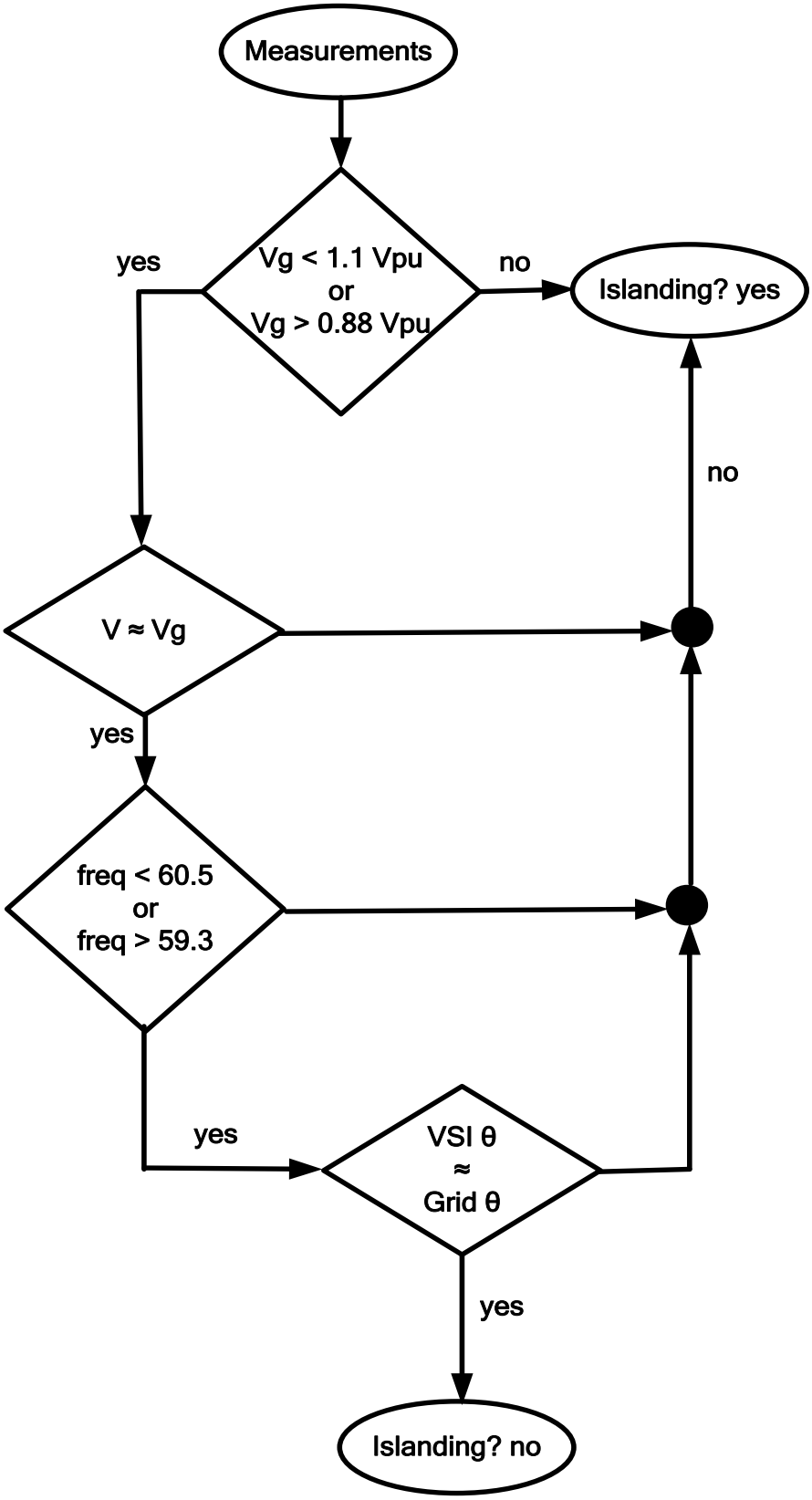

Fig. 2. 6 Re-closure Flowchart [32-33]

The work presented in [34] by H. Zeineldin, *et al.*, proposed a control strategy to implement intentional islanding of inverter based DG. The proposed method was based on designing two control algorithms, one for normal operation and the other for islanded operation. The DG provided constant power and constant voltage during normal operation. A hybrid passive islanding detection method was implemented to detect DG islanding. The detection algorithm sent a signal to declare an islanded operation and the DG switched to the voltage control mode. To overcome a large delay in detecting islanding for matching load condition cases, the Rate of Change of Frequency (ROCOF) was used, in parallel with the OFP/UFP, as another measure to detect islanding. The algorithm stated by monitoring both the frequency and voltage at the PCC and calculating the ROCOF. The time at which the frequency exceeded its thresholds and the time when ROCOF exceeded its threshold were denoted by T1 and T2 respectively and were stored. The difference between the actual time T and T1 and T2 respectively were calculated. If the difference exceeded a certain predetermined delay time, islanding was declared and the DG was operated in the islanded mode. The islanding detection algorithm was responsible for sending a signal that switched the inverter to the suitable interface control. Once islanding was detected, the DG switched to the voltage control interface. To assure safe islanded operation of the DG, the output active power of the DG was monitored to assure that it was less than the DG capacity. If the load on the island was greater than the DG capacity, the DG would become overloaded and a signal was sent to disconnect it. Fig. 2.7 and Fig. 2.8 show the flowcharts of their designed control strategy.

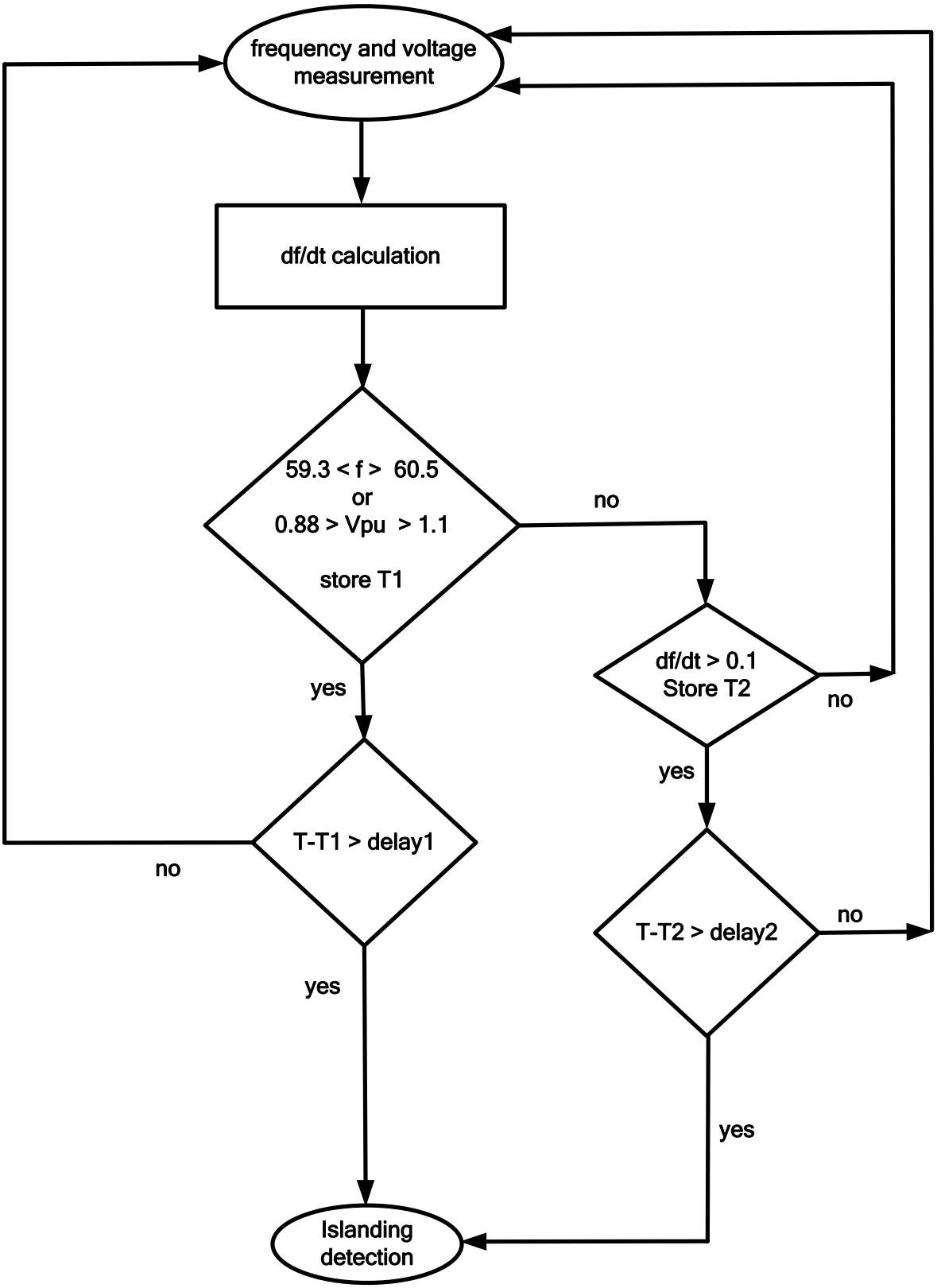

Fig. 2. 7 Proposed islanding detection algorithm [34]

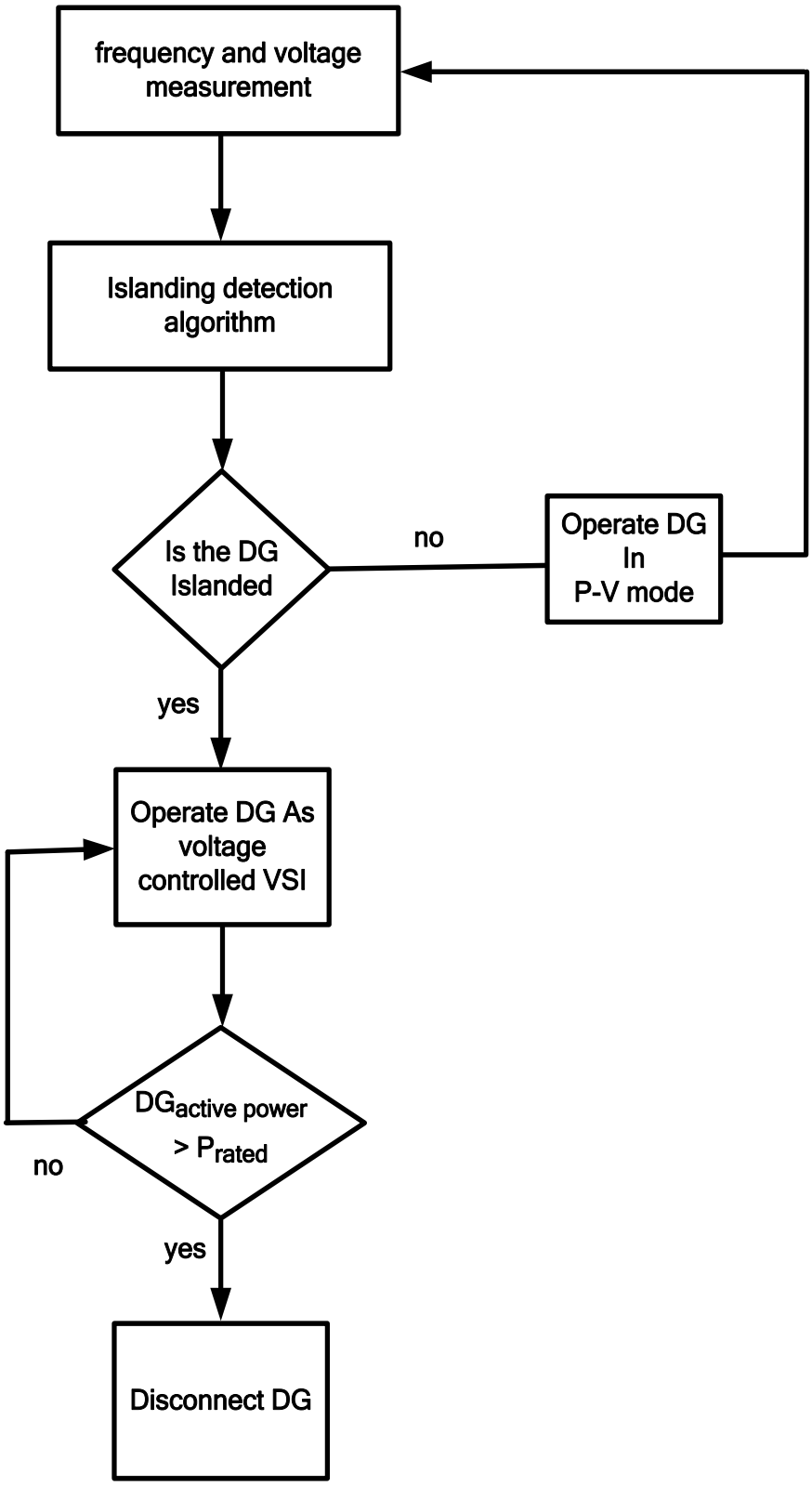

Fig. 2. 8 Flowchart of the control strategy implemented to produce intentional islanding [34]

In [14], a control strategy for grid-connected and islanded operation was designed and implemented by Y. Zhou, *et al.* Their proposed controller solved the following issues: how to detect system separation fast and accurately, how to control DG in an islanded power system to stabilize frequency and voltage, and how the controller of the DG can be transferred through grid connected operation to islanding operation and vice versa seamlessly in order to protect the critical load. Voltage angle difference between the local power system and the main power grid was measured. If the angle difference was increased to an abnormal value, which cannot happen under grid connected operation, then it was determined that the local power system was disconnected from the main power grid. Before synchronization, voltage magnitudes and phase angles of the islanded system at the point of common coupling (PCC) and grid were measured. When the magnitude and angle differences between the islanded system and the main grid approached zero the synchronization began and the hybrid power system was connected with the power grid again.

G. Fang and M. R. Iravani [35] reported a control strategy that provided control over frequency and voltage permitting the operation of the DG unit in both grid-connected and autonomous modes. The features of the control strategy presented were: it provided smooth transition capability from grid-connected mode to autonomous (islanded) mode, and it included an islanding detection capability. Reactive power control (upper path of Fig. 2.9), which drove the system to an unstable condition during an autonomous mode of operation, was exploited for islanding detection. To decrease the detection time, positive feedback based on the instantaneous PCC voltage, was added to the controller as shown in Fig. 2.10. This positive feedback ensured that the feedback process was only effective during transients, did not impact the dc steady state error signal, and provided attenuations for high-frequency noise.

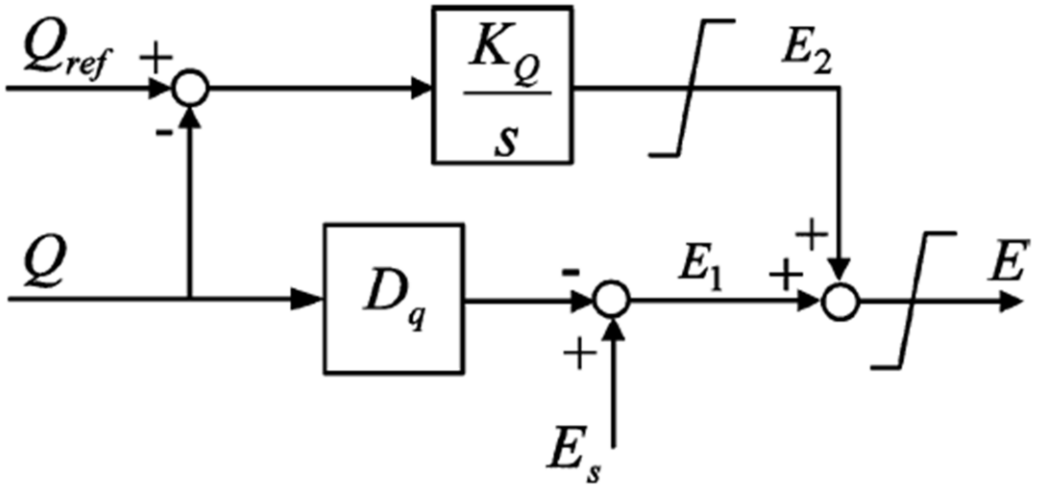

Fig. 2. 9 Block diagram of voltage control [35]

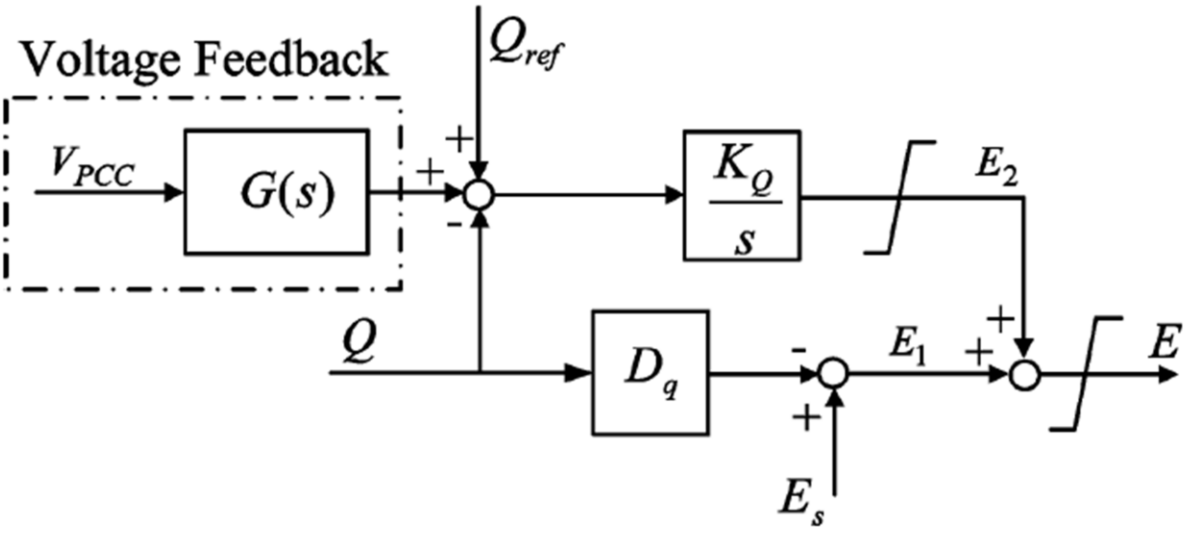

Fig. 2. 10 Block diagram of voltage control with positive feedback [35]

In [36], presented by G. Iwanski and W. Koczara, the loss of mains was detected using two methods. The first method was based on the voltage amplitude calculation and the second method, used for detection of grid voltage failures, was based on the monitoring of the frequency of the stator voltage provided by the grid. The mains outage detection implicated soft disconnection of the generator from grid by STS opening, and transition to standalone operation.

This way the selected load was supplied uninterruptedly. On the other hand, recovery of the grid voltage caused that the stator voltage was synchronized with the grid and the generator was softly connected to the grid by closing the STS. Their strategy for synchronization of the stator and grid voltages was:

1. The angle between the stator voltage vector and the grid voltage vector was calculated.
2. This angle was reduced by iterative turning of the synchronously rotating frame in the direction of the grid voltage vector.
3. The original transformation angle, calculated by integration of reference angular speed, was decreased iteratively in every computation cycle and in each cycle a new angle was determined.
4. When the stator voltage was synchronized with the power grid, two PLL structures were operated simultaneously. During synchronization, the reference *dq* frame connected with the stator voltage rotates with an angular speed Ω while the grid voltage vector rotates synchronously with the reference synchronous speed of the *dq* frame (Ω_S^*).
5. The relative speed and position of the grid voltage vector and the synchronously rotating frame were decreased to zero.
6. Thus, the synchronously rotating frame was synchronized with the grid voltage, whereas the stator voltage was synchronized with the rotating frame controller and consequently provided stator voltage and grid voltage synchronization.
7. If the angle was close to zero, the STS was closed and the generator was connected to the grid.

They proposed two methods for the main outage detection and soft disconnection. The first method was based on the voltage amplitude calculation. If the power of load connected between

the stator and breaking point was much higher or much lower than the power delivered to the grid, the amplitude was increased or decreased rapidly after line breaking. This way the loss of main was quickly detected. The second method used for detection of grid voltage failures was based on the monitoring of the frequency of the stator voltage provided by the grid. The output frequency could not be controlled using a power control method which was applied during the grid connection operation. The frequency was continuously increased or decreased in case of the main outage.

The aim of the research presented by R. Majumder, et al. [22, 37] was to set up a power electronics interfaced DG system. A seamless transfer between islanded and grid connected mode was proposed that uses an online load flow study. During resynchronization, the reference voltage of the DG was changed to achieve the same voltage magnitude and angle at PCC as the grid voltage while simultaneously supplying the total power demand of the DG in desired ratio. Once the breaker was closed, the DG started to supply its rated power and the rest of the power requirement was supplied by the grid. Their proposed sequence of control from a grid connected operation to islanded mode and then again back to grid connected can be summarize as:

1. Detect the islanding by zero current in the breaker connecting the grid with the DG.
2. If islanded, switch to voltage control mode.
3. Calculate the reference voltage required for the DG to maintain the load power requirement.
4. Check for the clearing of the fault.
5. If resynchronization is desired, detect the grid voltage and frequency.
6. Calculate the reference voltages for the DG to make the PCC voltage the same as the grid voltage while continuing to supply the load requirement.

7. Calculate the change in angle required to match the phase for proper synchronization.

8. Change the voltage reference to the new calculated value.

9. Connect the breaker.

10. Switch to the state feedback control mode.

Aiming to solve the transition problem from grid-tied mode to off-grid mode, H. Shengli, *et al.* [38] presented a control strategy based on a controlled voltage method whether connected to the grid or stand-alone. In grid-tied mode, the inverter worked as a controlled voltage source by controlling the phase and magnitude of the filter capacitor voltage, the injection current to the grid was regulated indirectly, so the output active and reactive powers were also successfully controlled. Once the grid failed, the inverter regulated its output voltage amplitude quickly, while the voltage fluctuated within permissible levels during this period, the grid currents forced through the STS decreased to zero at a highly accelerated rate. The controller cancelled all the gate drive pulses of the STS and reduced the inverter output voltage lower than the grid voltage simultaneously, which introduced a reverse voltage across the coupling inductor and forced the grid current to decrease to zero quickly. As soon as the grid current reached zero, the STS was turned off and the controller promptly regulated the inverter output voltage to its rated value. After disconnection from the grid, the inverter recovered its voltage amplitude to a rated level. Based on the SST forced turn-off strategy, the inverter operated as a controlled voltage source whether grid-tied or not. By controlling the phase and magnitude of the filter capacitor voltage, the grid current was regulated indirectly; accordingly the output active and reactive powers were also successfully controlled.

C.-S. Wu, *et al.* [4] introduced a power supply system designed with grid-connected operation and autonomous operation modes. Through a novel anti-island (AI) detection method,

the current status of the electricity network was detected quickly and the operation mode of the inverter was ascertained. Based on analysis of transition between grid-connected operation and autonomous operation modes, the output conditions of the inverter were adjusted optimally and a seamless transition process was acquired. All transitions were conducted in zero-crossing in order to reduce the voltage ripple of the sensitive load. Their seamless transition from autonomous operation mode to grid-connected operation mode in detail is as follows:

1) Detects the voltage, frequency of the electricity network and judges the operation status of the grid;

2) Adjusts the output voltage of the inverter, and makes it equal to those of the electricity networks;

3) After adjusting, translates the operation mode of inverter (from voltage source to current source) and closes the switch. In order to reduce the voltage ripple on the sensitive load, the initial current is given as the current of the load;

4) Increases the output current step by step up to maximization.

Similar to the transition process described above, the seamless transition from grid-connected operation mode to autonomous operation mode in detail is as followings:

1) Detect a fault in the electricity networks (by means of AI method introduced in next chapter);

2) Set the output current to that of load in order to reduce the voltage ripple impact;

3) Open the switch and change the operation mode of inverter.

For the AI detection two positive feedback mechanisms were established. One was magnitude of voltage feedback (Fig. 2.11); the other was frequency of voltage feedback (Fig. 2.12).

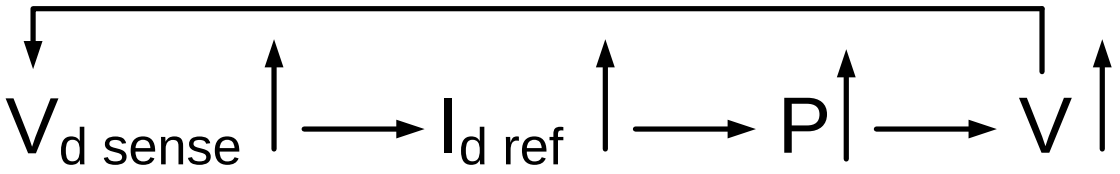

Fig. 2. 11 Diagram of magnitude of voltage feedback in dq frame

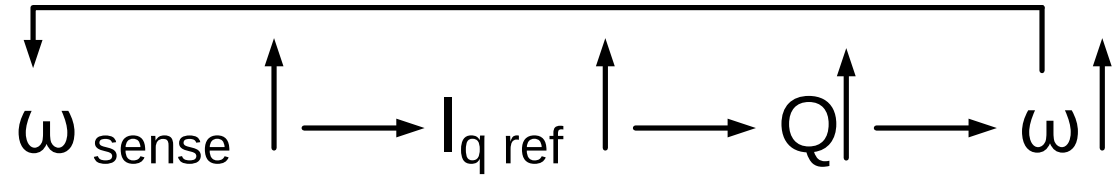

Fig. 2. 12 Diagram of frequency feedback in dq frame

A novel scheme for seamless transfer of MTG (Microturbine Generation) system operation between grid-connected and islanding modes and vice versa was proposed by D. N. Gaonkar, *et al.,* [39]. The presented scheme used the estimated phase angle error obtained by the PLL for islanding detection and re-synchronizing DG to grid. A converter control strategy for both grid-connected and islanding modes was presented. The proposed seamless transfer scheme consisted of a passive islanding detection and re-closure method. The presented islanding detection method used the phase angle estimated by the PLL to detect the islanding condition. Their algorithm devised for the detection scheme is shown in Fig. 2.13. Their re-closure scheme continuously monitored the phase angle and terminal voltage magnitude to determine whether or not the disturbance in the grid was over. This was necessary in order to synchronize the MTG system and to connect back to the grid without any down-time. The re-closure algorithm continuously monitored the terminal voltage of the grid and MTG system. Both voltage magnitudes were compared. Both voltages had to be approximately equal to avoid large transients during re-connection to grid. Once the voltages were approximately equal, the algorithm compared the $\Delta\theta$

value obtained from the PLL with the set threshold limit. As long as these minimum requirements were met (voltage and phase angle), there were no major issues in reconnection of islanded systems to the utility. The re-closure algorithm for connecting the MTG system to the grid, when the utility recovers from the disturbance, is shown in Fig. 2.14.

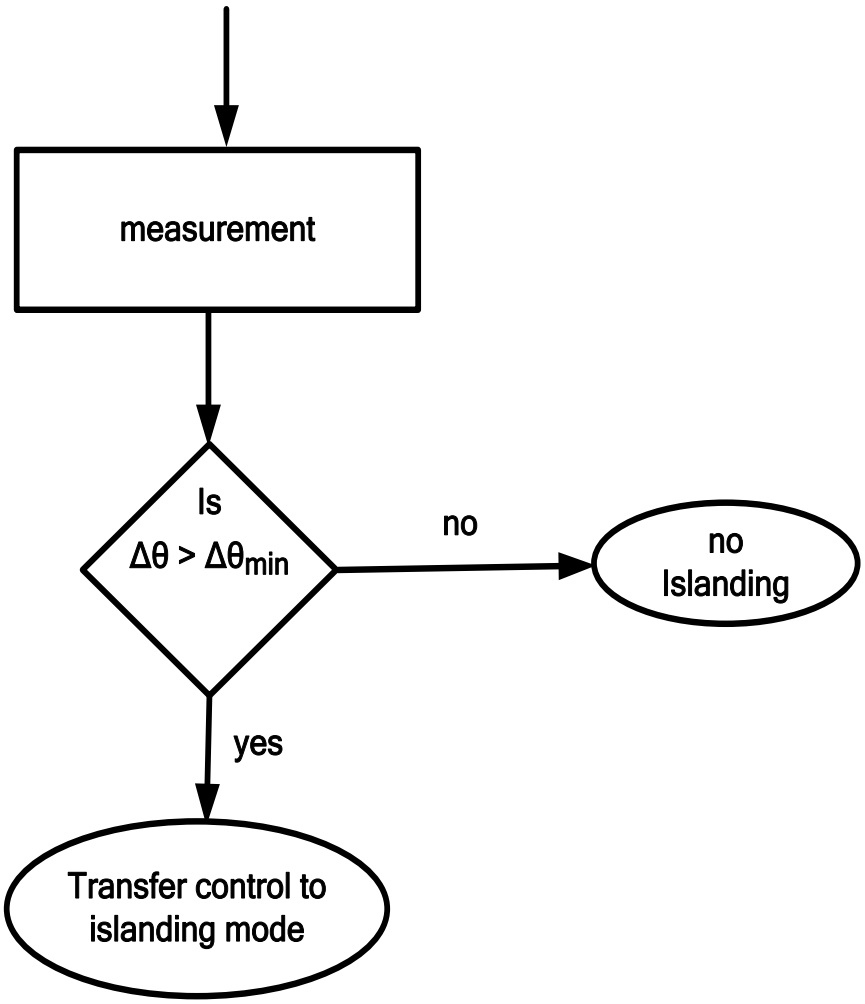

Fig. 2. 13 Islanding-detection scheme [39]

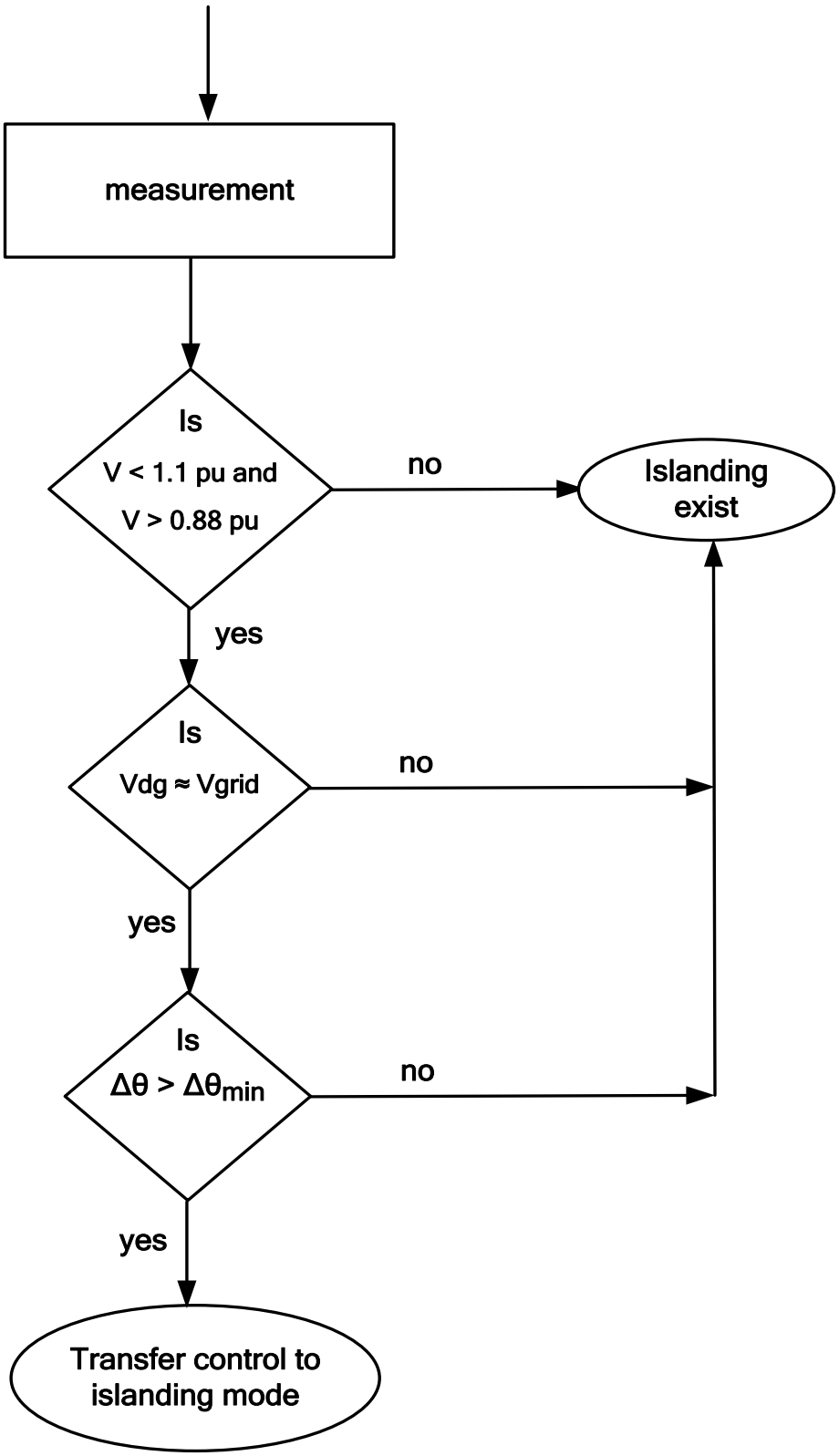

Fig. 2. 14 Re-closure scheme [39]

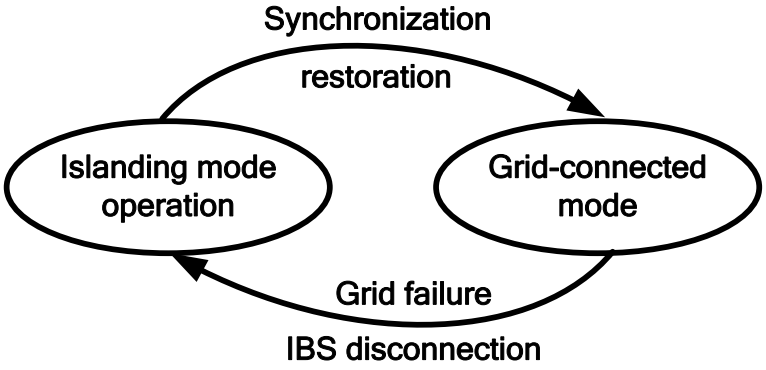

Fig. 2. 15 Flowchart diagram of the modes of the VSI [3]

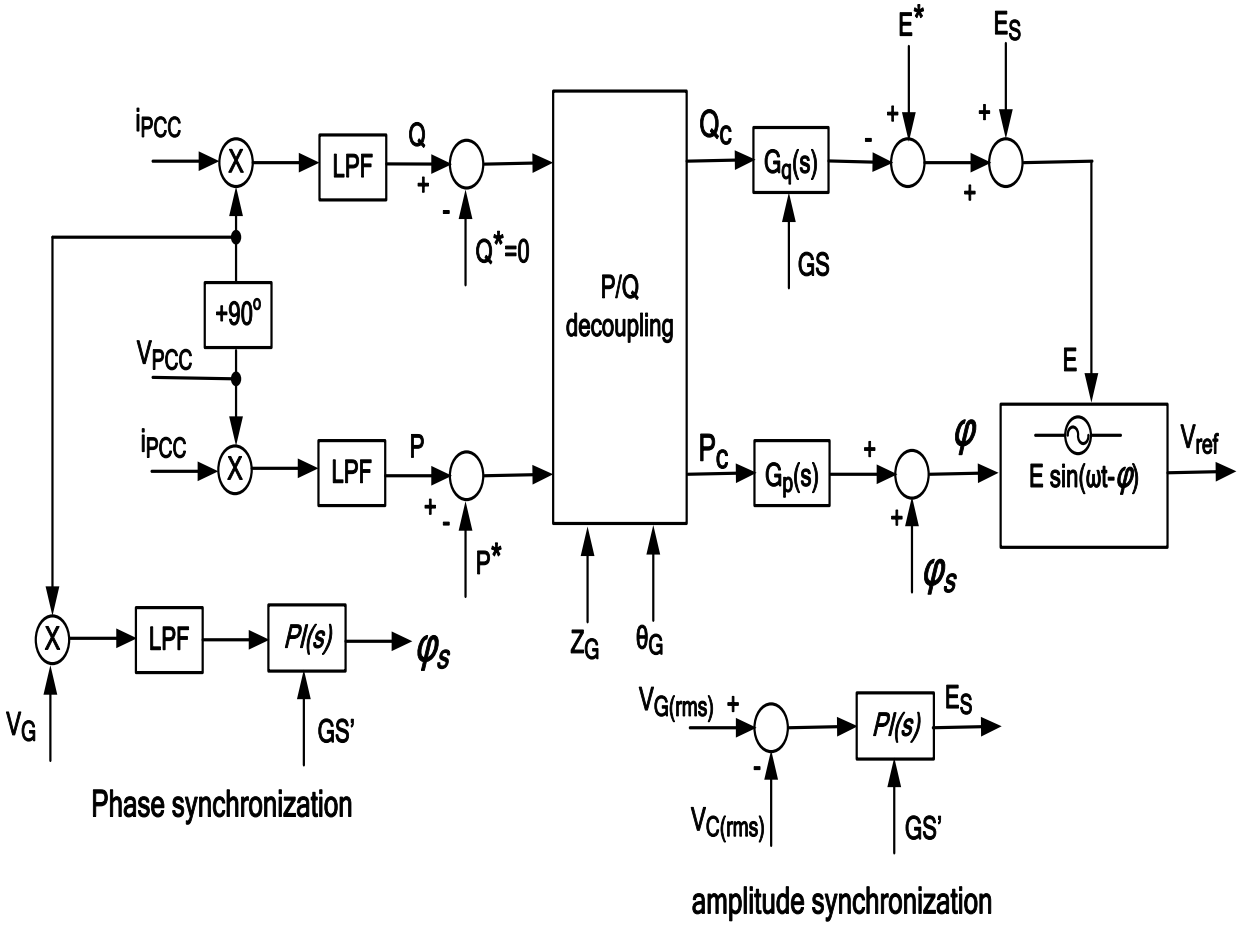

Fig. 2. 16 Block diagram of the whole proposed controller using the synchronization control loops [3]

The intent of the research that has been presented in [40] by C. Chien-Liang, *et al.*, was to introduce a practical inverter based DG system that ensured smooth mode transfer between islanding and grid-tie modes while maintained accurate current sharing and high quality output waveforms. The key features of the proposed DG system include: a single current loop controller designed for a grid-tie operation to reduce the steady-state error while maintaining system stability; for islanding operation, a dual-loop control system for outer voltage loop and a controller for inner current loop control is proposed to limit peak current magnitude under transient, enhance voltage loop stability, and reduce the voltage steady-state error; a phase synchronization is implemented with PLL and an automatic phase adjustment to synchronize the output currents among the inverters; and, a proper mode transfer procedure with smooth current transition are suggested to minimize the excessive electrical stresses. Their proposed procedure to change from grid-tie to islanding mode is summarized as follows.

1) The upper level controller detects the fault on the voltage grid and extracts the current information.

2) Through a CAN bus, the upper level controller provides the current information and commands the current-controlled inverters to change their outputs so that the current on the STS can be minimized to avoid mode transfer transient.

3) The upper level controller provides the turn OFF signal for the STS after a certain waiting time.

4) Through the CAN bus, the upper level controller commands a selected inverter to change from current-controlled mode to voltage-controlled mode at the next zero crossing.

5) That inverter regulates the bus voltage to a desired level and provides the output current information.

Their procedure to change from islanding to grid-tie mode is summarized as follows.

1) The upper level controller detects if the grid voltage recovers, and keeps detecting the grid voltage magnitude and phase information.

2) Through the CAN bus, the upper level controller provides the grid voltage information and commands the inverter to adjust its voltage to track the grid voltage in both magnitude and phase.

3) The upper level controller keeps monitoring both voltages. It turns on the STS once the two voltages are synchronized in phase and magnitude.

4) Through the CAN bus, the upper level controller commands the inverter to change its controller from voltage controlled mode to current-controlled mode at the next zero crossing. It assigns the current references so that zero current goes through the STS during transfer transient.

5) The current controlled inverters change the current reference to a desired level.

In [41], presented by L. Qin, *et al.,* the transition from grid-connected to standalone operation using a Solid State Relay (SSR) was discussed. A feed-forward that could boost the dynamic response and benefited the transition from grid-connected to stand-alone was added to the controller. They proposed to force the grid current to be zero by using a voltage amplitude regulation method. Then, the SSR was turned off and the reference output voltage was recovered to the rated value. The principle of zero current regulation was to retain the current control mode in transition but change the current reference to zero. After the current dropped to zero, the SSR was turned off and the system was switched to voltage control.

A seamless transfer of grid-interactive inverters between grid-connected and stand-alone modes was proposed by Y. Zhilei, *et al.* [42]. In grid-tied mode, an output voltage controller was used for compensating the filter capacitor current, and a grid current controller was used to control the grid current. In stand-alone mode, the output voltage controller was used to regulate the output voltage and to set the output of the grid current controller to zero. Therefore, the transfer between the two controllers did not exist with their proposed method. In order to realize a seamless transfer between grid-tied and off-grid modes, they proposed a controller that matched the magnitude, frequency, and phase of the grid voltage before connecting to the utility. The detailed process of their seamless transfer between the two modes is as follows:

1) *Off-grid mode to grid-tied mode:*

a) Detect that the grid is operating in nominal condition.

b) Adjust the reference voltage to match the frequency and phase of the grid voltage.

c) Change the voltage reference to the grid voltage at the positive zero-crossing of the output voltage, which makes the output voltage equal to the grid voltage, even in polluted grid voltage.

d) Once the load voltage is equal to the grid voltage, the STS is turned on.

e) Increase the reference grid current slowly from zero to the desired value (both magnitude and phase).

2) *Grid-tied mode to off-grid mode:*

a) Detect a fault on the utility.

b) Decrease the reference current to zero at zero crossing of the grid current.

c) Change the STS voltage from high level to low level at zero crossing of the grid voltage. This will turned off the STS.

d) Synchronize the reference voltage with the grid voltage.

e) Change the reference voltage at zero-crossing of the grid voltage.

From this algorithm, the transfer between both modes was only the change of the reference voltage between the two modes. The transfer between the output voltage controller and the grid current controller did not exist in their proposed method.

CHAPTER 3. SYSTEM DESCRIPTION

3.1. Circuit Topology

Fig. 3.1 shows the proposed main circuit topology for grid-connected and stand-alone operations voltage source inverter. The system consists of a DG unit that is modeled by a DC source, a sinusoidal pulse-width-modulated (SPWM) voltage source inverter, an LCL filter to achieve attenuation of the switching frequency ripple in the output voltage, a load, and the controller needed to implement grid connected and stand-alone operations.

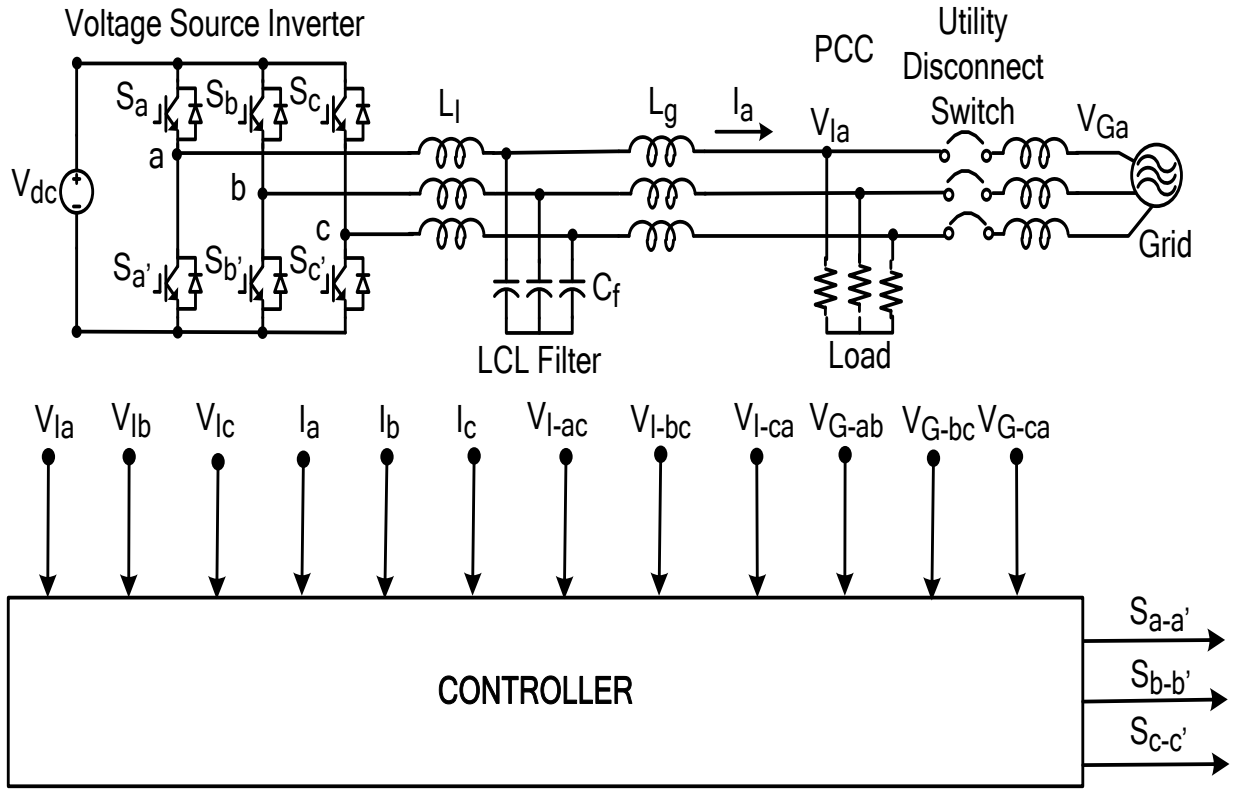

Fig. 3. 1 Schematic diagram of the grid-connected inverter system

The voltage source inverter performs the interface function between the DC bus and the three phase AC world. The inverter consists of power electronics devices actuated by gate pulses:

these devices are high frequency static switches that periodically apply repetitive pulses with different widths and polarities at the AC terminals, with the goal to create an AC waveform of desired magnitude and phase.

The controller includes control for grid-connected and stand-alone operations, PLL, coordinate transforms, parallel interconnection to the grid (represented by ideal, sinusoidal voltage sources behind line impedances) through the Point of Common Coupling (PCC) breakers. The loss of main detection, load shedding algorithm, and re-connection to the grid are also included.

3.2. Voltage Source Inverter

A typical DG system based on micro-source is depicted in Fig. 3.2. There are two basic elements: the part where the electricity is generated (micro-source) and the part that performs the interface with the rest of the system (voltage source inverter).

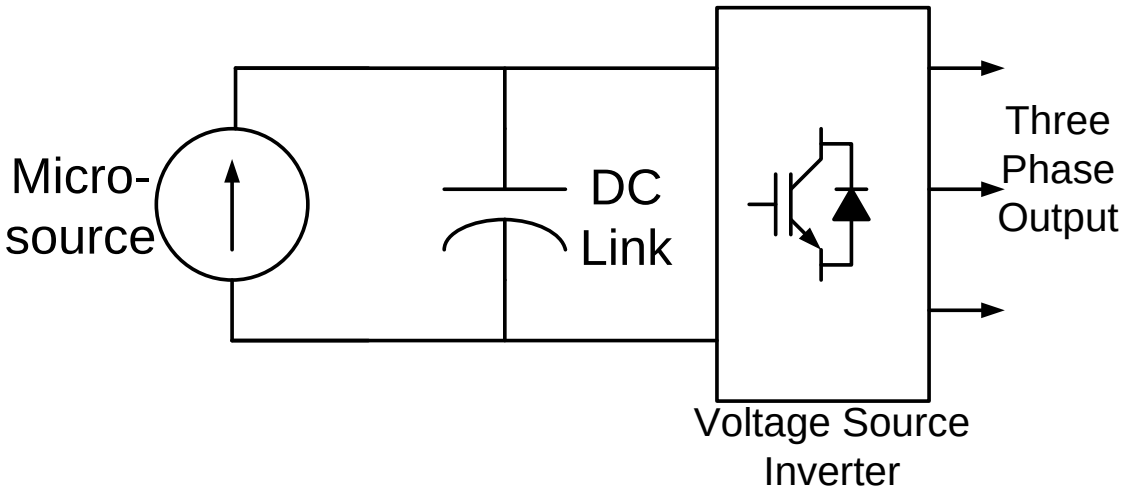

Fig. 3. 2 Typical diagram of micro-source generation system

All the power, DC or non-power frequency AC, generated by each DG must use an electronic inverter (to convert DC voltage to a three-phase AC voltage with desired magnitude and phase) to interface with the electrical power system. This power electronic interface provides significant flexibility and permits the DG to function as a semi-autonomous power system [31].

There are two main requirements to convert DC voltage to a three-phase AC voltage: a matrix of switches and a switching sequence. Fig. 3.3 shows the circuit that allows synthesizing the AC voltage at the three-phase terminals starting from a DC voltage. From left to right, there is the DC bus and then the matrix of six power electronics devices. Each device has bi-directional current flow capability. The flow of current out of the DC bus is regulated by signals sent to the gates to each of the devices present in the inverter.

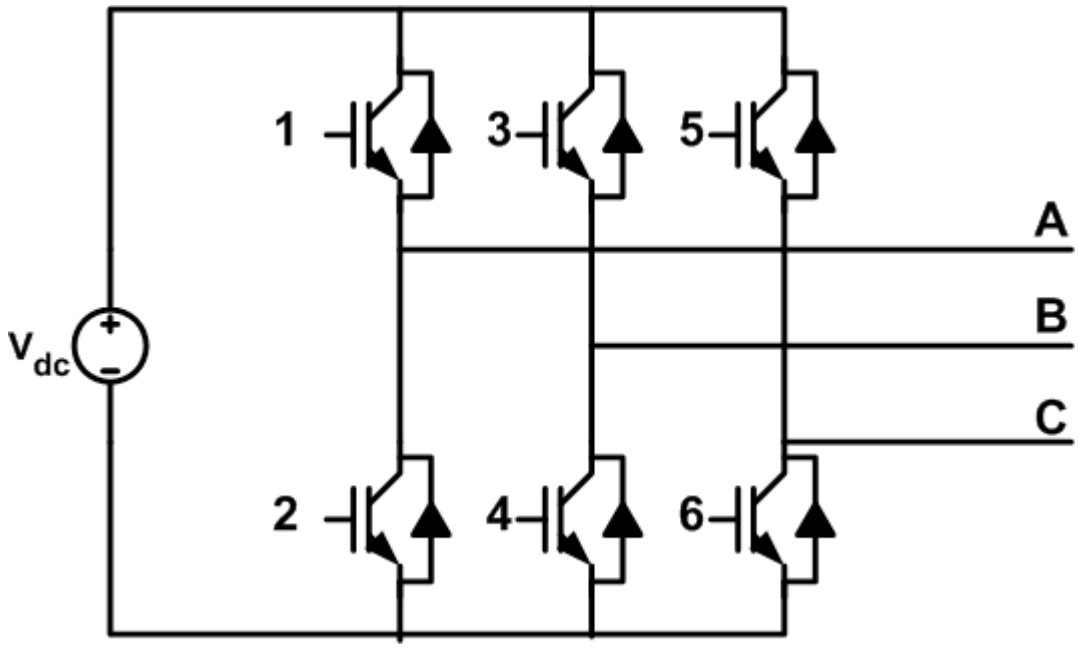

Fig. 3. 3 DC to Three-Phase AC Inverter Diagram

The operation of this bridge requires two restrictions. First, two devices on the same leg may never be conducting. Second, at least one device per leg must be conducting. The first constraint

comes from the fact that if for example, devices numbered 1 and 2 are conducting at the same time then the DC source is shorted, resulting in very high currents that will destroy both devices. The second constraint stems from the fact that the current flowing in each of the phases on the AC side must have a path where to flow: if for instance neither device numbered 1 and 2 is closed, then the current flowing on the AC side in the 'a' phase would have no path where to flow.

Consider the switching sequence shown in Fig. 3.4, where devices 1, 4, and 5 are closed: this configuration satisfies both the above constraints. The voltages at the AC terminals are:

$$V_{ab} = +V_{dc} \tag{3.1}$$

$$V_{bc} = -V_{dc} \tag{3.2}$$

$$V_{ca} = 0 \tag{3.3}$$

From Eq. 3.1 to Eq. 3.3 it can be noticed that the output voltages can be either $+V_{dc}$, $-V_{dc}$ or zero. By carefully selecting a switching sequence it is possible to make those three levels of voltage appear in one particular phase. Furthermore, it is possible to create a three phase system of sinusoidal voltages with desired amplitude and phase. This is called a six pulse operation of the bridge. In reality the output waveform of the AC voltage is a squared wave with a particular amplitude and phase at the fundamental frequency. In order to solve this problem, more complex switching sequences with higher switching frequencies are needed.

One of these complex switching sequences is the pulse width modulation (PWM) technique. This PWM technique works on an averaging effect using the switching frequency as a base period where the averaging occurs. Fig. 3.4 shows how the basic principle of the PWM technique works: it allows the instantaneous average output to be held closer to the desired fundamental

output. The voltage waveform is made of pulses of different widths: hence the name pulse width modulation. The sinusoidal signal is compared with a sawtooth waveform (carrier). When the carrier is less than the sinusoidal signal, the PWM signal will be in high state (1). Otherwise it will be in the low state (0).

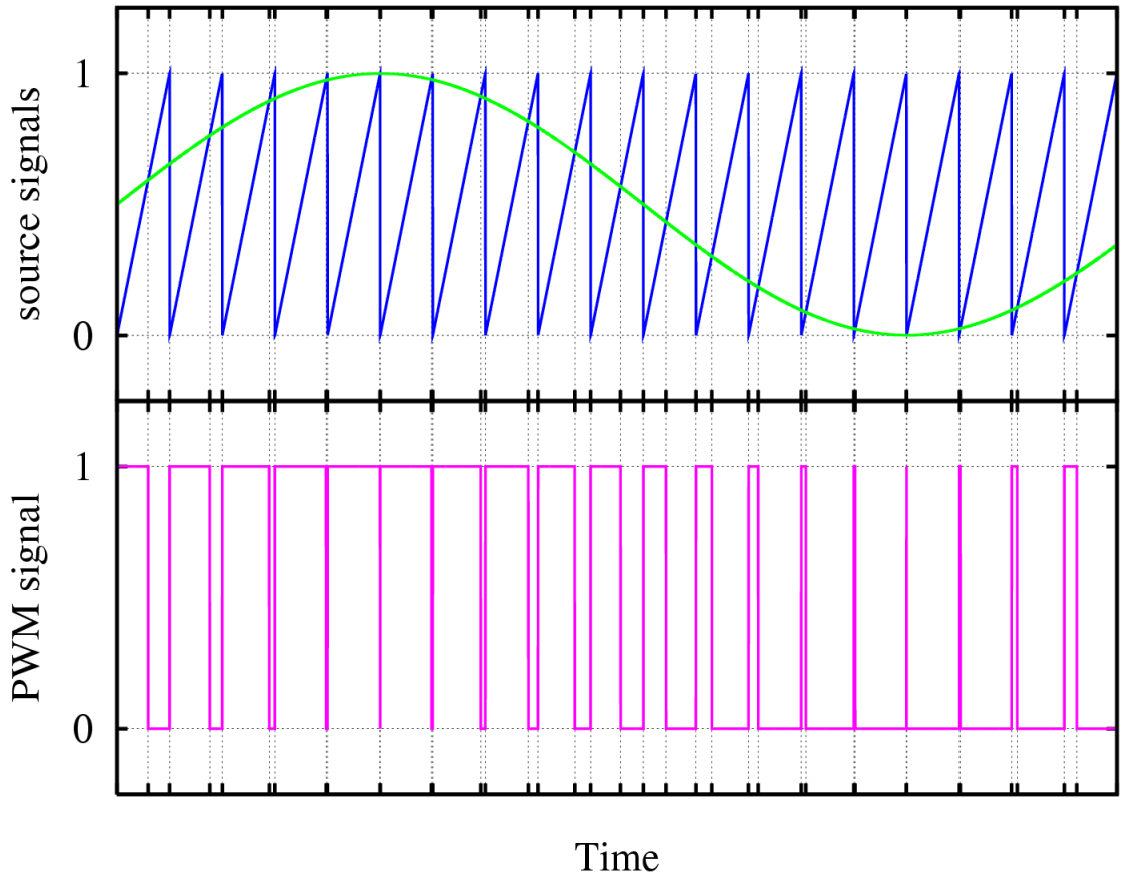

Fig. 3. 4 PWM Operation of the Bridge
(For interpretation of the references to color in this and all other figures, the reader is referred to the electronic version of this dissertation)

3.3. LCL filter

For attenuating the current ripple produced at the output of the inverter, an LCL filter is placed in between inverter and grid. An LCL filter can achieve reduced levels of harmonic

distortion with lower switching frequencies and with less overall stored energy [43]. Fig. 3.5 shows the LCL filter where L_i and L_g are inductors on inverter side and grid side respectively.

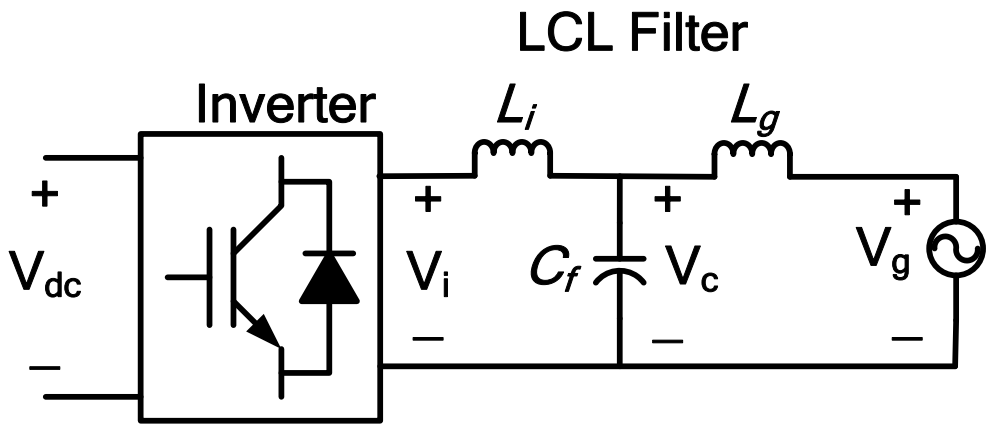

Fig. 3. 5 LCL Filter configuration circuit

$$Z_i = L_i s \tag{3.4}$$

$$Z_g = L_g s \tag{3.5}$$

$$Z_c = \frac{1}{sC_f} \tag{3.6}$$

From the economical point of view, the design of the LCL filter is made in such a way that the magnitude of the inductor should be minimum and the magnitude of the capacitor should be maximum. By selecting large capacitor the filter volume is reduced [44-45].

3.3.1. Specifications for the design of LCL filter

The following are the parameters for the design of the LCL filter:

Output Power of inverter: $P_{i-3\phi} = 10\ kW$

Apparent Power of inverter: $S_i = 10\ kVA$

Output Voltage of Inverter: $V_i = 208\ V_{ll}$

Switching frequency: $f_s = 10\ kHz$

Input DC voltage: $V_{dc} = 400\ V$
$(V_{dc} = V_{ll-rms} / 0.612 = 208 / 0.612 = 339.869\ V)$

Grid Voltage: $V_g = 208\ V_{ll}$

Inverter current: $\hat{I}_L = \frac{P_{load-1\phi}}{V_{load-1\phi}} = \frac{3.33kW}{120V} = 27.5A \approx 28A$

Inverter ripple current: $\Delta\hat{I}_L = 10\% = (0.10)\left(\hat{I}_L\right) \approx (0.10)(28) \approx 2.8A$

Reactive Power storage at C_f : $\Delta Q = 5\%$

3.3.2. Design of L_I

The ripple current depends on the DC link voltage, inductance, and the switching frequency. The DC link voltage and switching frequency are constant, thus the inductance can be calculated using the following procedure:

$$V_L = L\frac{\Delta\hat{I}_L}{\hat{\delta}T_s} \tag{3.7}$$

where $\hat{\delta}$ is the phase voltage duty cycle at maximum output and is given by:

$$\hat{\delta} = \frac{2V_{g-pk-1\phi}}{V_{dc}} = \frac{2\left(208\sqrt{2}\right)}{\sqrt{3}(400)} = 0.85 \tag{3.8}$$

$$\Delta\hat{I}_L = \hat{\delta}\frac{V_L}{Lf_s} = \frac{1}{6}\frac{\hat{\delta}V_{dc}}{Lf_s} \tag{3.9}$$

$$L = (0.1416)\left(\frac{V_{dc}}{\Delta\hat{I}_L f_s}\right) \tag{3.10}$$

$$L = (0.1416)\left(\frac{200}{(2.8)(10x10^3)}\right) = 1mH \tag{3.11}$$

3.3.3. Design of C_f

Considering the capacitor stores 5% of the system power as reactive power, maximum capacitance is:

$$Q = 5\%S \tag{3. 12}$$

$$Q = 5\%S_{3-\phi} = (0.05)(10kVA) = 500VA \tag{3.13}$$

$$C_f = \frac{Q}{3\cdot V_i^2\cdot\omega} \tag{3.14}$$

$$C_f = \frac{Q}{3\cdot V_i^2\cdot\omega} = \frac{500}{(3)(120^2)(2\pi 60)} = 31\mu F \tag{3.15}$$

3.3.4. Design of L_g

As most of the ripple is filtered by L_I & C_f, grid side inductor value is taken as half the value of L_I.

$$L_g = 0.5L_I = L_g = 0.5(1mH) = 0.5mH \tag{3.16}$$

3.4. Simulation and Experimental Set-ups

3.4.1. Simulation Set-up

The performance of the proposed control strategies will be evaluated by computer simulation using SABER. Fig. 3.6 shows the simulated system. This system will be tested under the following conditions:

- Switching frequency, f_s, 10 kHz
- Filter inductor, L_I, 1 mH
- Filter inductor, L_g, 0.5 mH
- Filter capacitor, C_f, 31 μF
- Output voltage 208 V_{rms-ll}, 3Φ @ 60 Hz grid connection, with V_{dc} = 400 V
- Output capacity 10 kW from DG
- Total load 10 kW

The load will be adjusted to consume 10 kW. The DG system will be simulated to supply 10 kW and zero reactive power. The system will be operated initially in grid-connected operation.

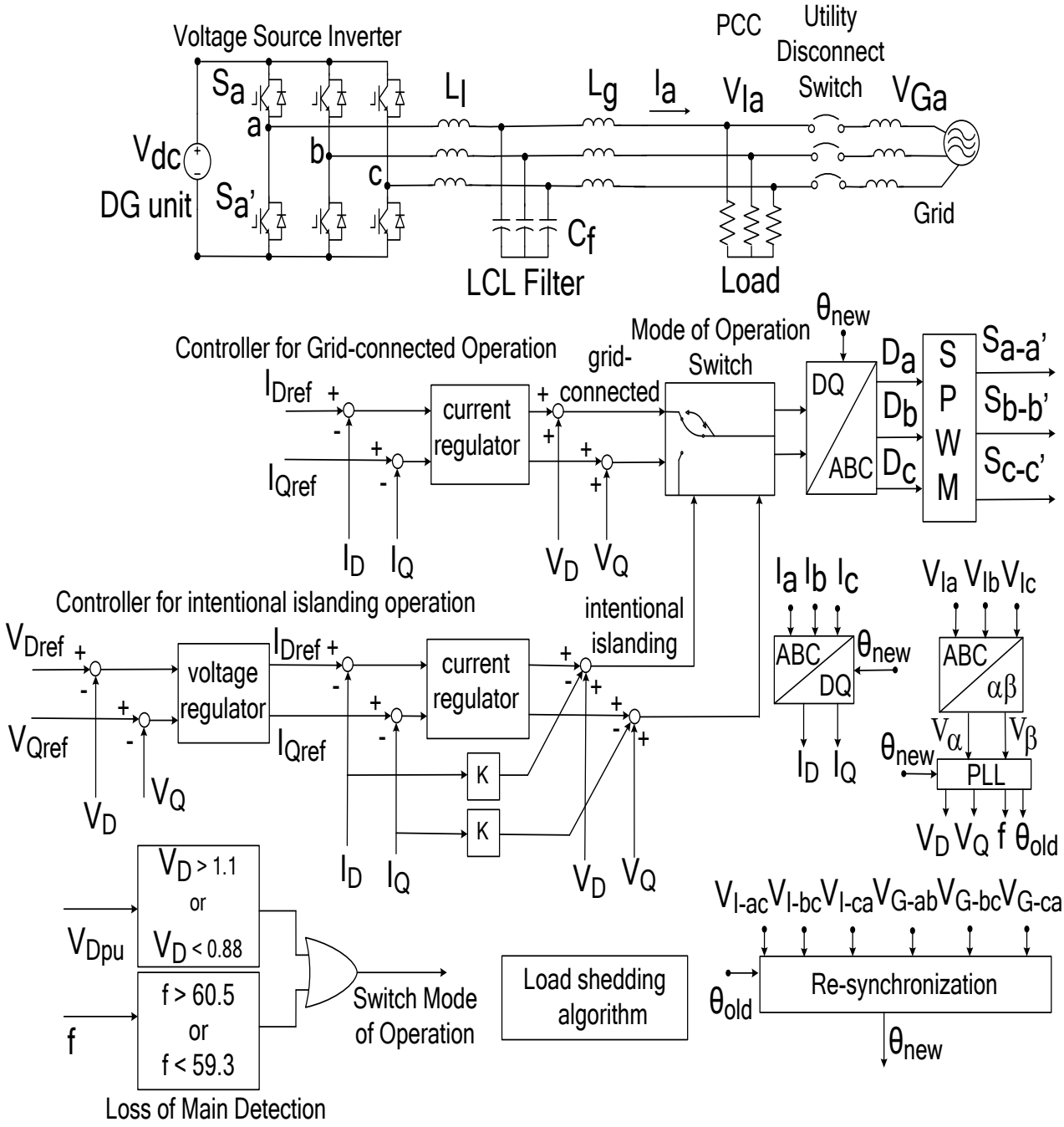

Fig. 3. 6 Simulated system

3.4.2. Experimental Set-up

The hardware prototype of Fig. 3.6 will be implemented for experimental verification. The control, PLL, grid condition detection, and re-closure algorithms will be programmed using a

universal DSP control board developed at the Power Electronics and Motor Drives Laboratory at Michigan State University. The system will be tested under the following conditions to experimentally verify the simulation results:

- Switching frequency, f_s, 10 *kHz*
- Dead time 3μs
- Filter inductor, L_I, 1 *mH*
- Filter inductor, L_g, 0.5 *mH*
- Filter capacitor, C_f, 50 μF
- Simulated Output voltage 104 V_{rms-ll}, 3Φ @ 60 *Hz* grid connection, with $V_{dc} = 200\ V$
- Output capacity 2.5 kW from DG
- Total load 2.5 kW

The reason for simulating the output voltage is to ensure the algorithms and controllers are functioning properly under low-power tests; such that there is a reduced risk of operator and equipment damage if the system fails.

Shown in Fig. 3.7 are the inverter, the DSP board, the filter, and the rectifier.

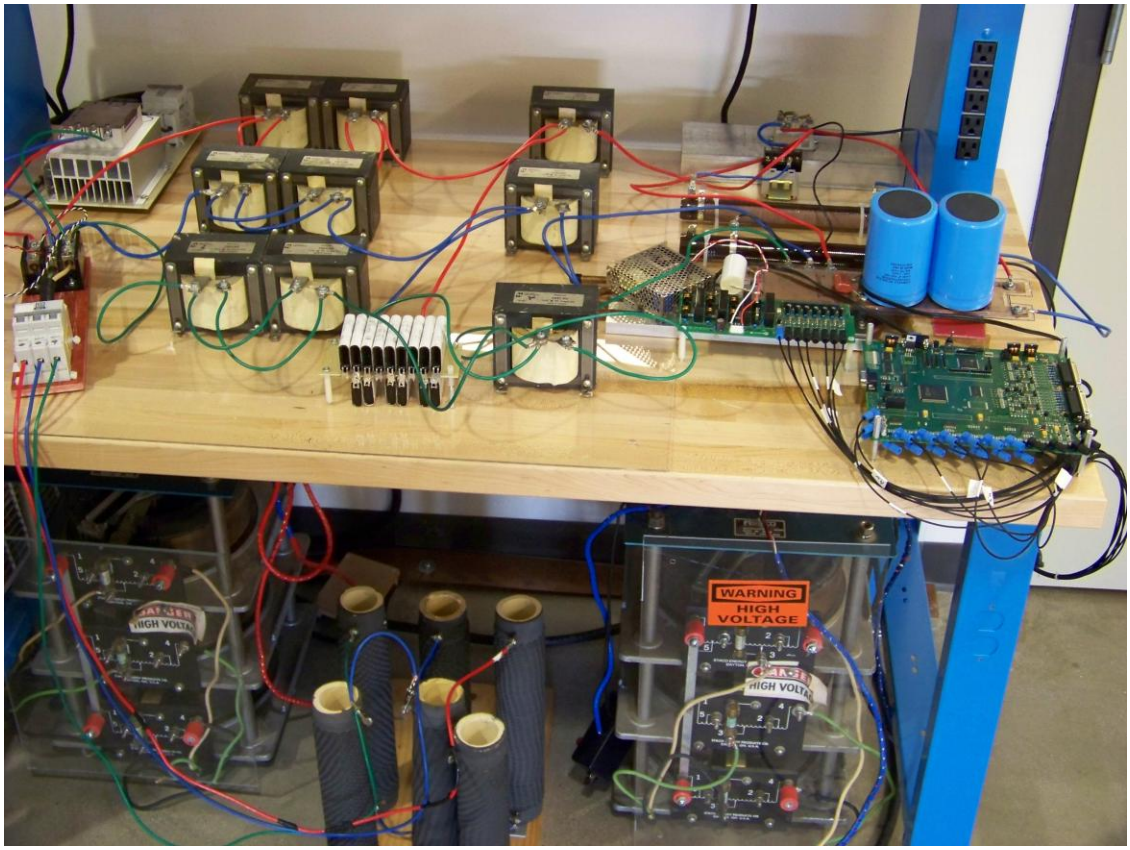

Fig. 3. 7 Experimental set-up

The DG will be started up in grid-connected operation mode, and then the separation device will be opened. When the DG is disconnected from the grid it operates in stand-alone mode.

CHAPTER 4. PROPOSED CONTROL FOR GRID-CONNECTED OPERATION OF DG

4.1. Introduction

There are two modes of operation for the DG inverter – the grid-connected mode and the stand-alone mode. Each mode has its own control requirements and control structure. In the grid-connected mode of operation, the DG is connected to the utility. The utility, which is assumed to be stiff, sets the voltage at the terminal of the DG inverter [10]. The inverter controls the power being injected into the grid by controlling the injected current. Thus, in this mode, the inverter operates in the current control mode.

In the stand-alone mode, the inverter supplies power to the load. It has to maintain the voltage at the terminals of the load, irrespective of any changes in the load. Thus, in this mode, the inverter operates in the voltage controlled mode.

This chapter discusses the grid-connected mode of operation and its controller design, while the stand-alone mode will be discuss in the next chapter.

4.2. Circuit Topology

Fig. 4.1 shows the main circuit topology. This system consists of the micro-source represented by the DC source, the conversion unit which performs the interface function between the DC bus and the three phase AC world, and the LCL filter that attenuates the current ripple produced at the output of the inverter. The controller presented provides constant DG output and maintains the voltage at the PCC before and after the grid is disconnected.

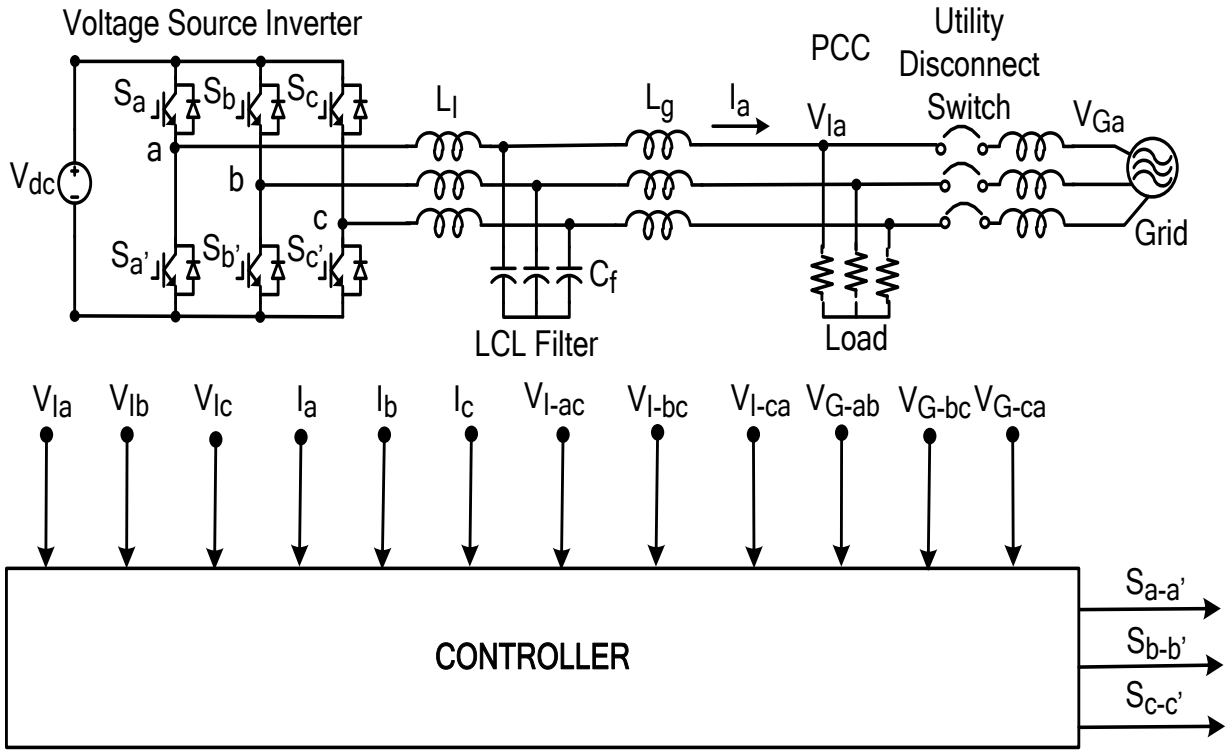

Fig. 4. 1 Schematic diagram of the grid-connected inverter system

4.3. Controller

For grid-connected operation, the controller shown in Fig. 4.1 is designed to supply constant current output in order to provide a pre-set power to the main grid [46]. An important aspect to consider in grid-connected operation is the synchronization with the grid voltage [47]. For unity power factor operation, it is essential that the grid current reference signal be in phase with the grid voltage. This grid synchronization can be carried out by using a PLL [48-49]. Also, the PLL is used to determine the frequency and angle reference of the PCC [3]. Fig. 4.2 shows the control topology used.

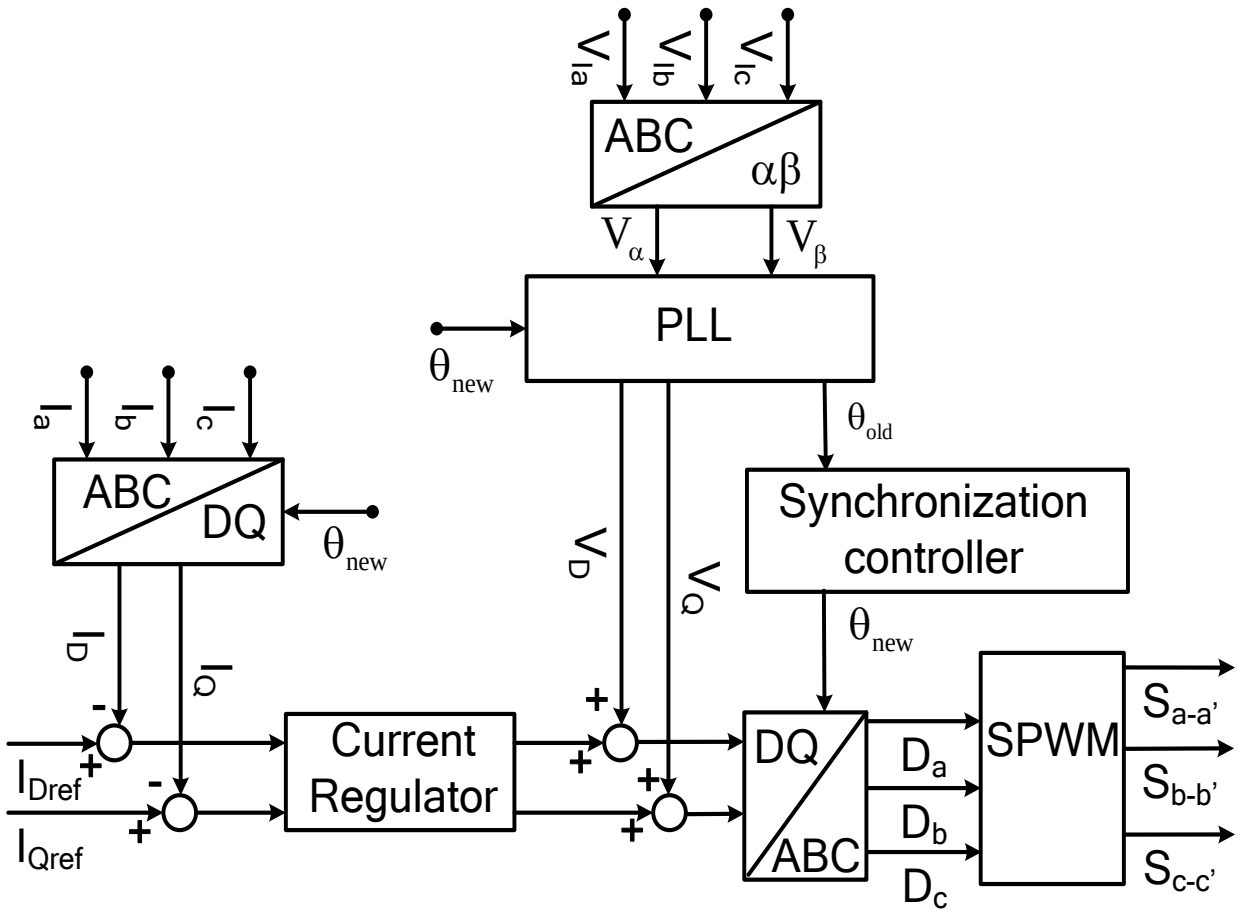

Fig. 4. 2 Block diagram of the current controller for grid-connected

When using the current control, the output current from the filter, which has been transformed into a synchronous frame by Park's transformation (Eq. 4.1) and regulated in DC-quantity, is fed back and compared with reference currents I_{DQref}. This generates a current error that is passed to the current regulator (PI controller) to generate voltage references for the inverter. In order to get a good dynamic response V_{DQ} is fed forward. This is done because the terminal voltage of the inverter is treated as a disturbance and the feed-forward is used to compensate for it. The voltage references in DC-quantities, V_{DQref}, are transformed into a

stationary frame by the inverse of Park's transformation (Eq. 4.2) and utilized as command voltages for generating high frequency pulse width modulated (PWM) voltages.

$$\begin{bmatrix} X_D \\ X_Q \\ X_0 \end{bmatrix} = \frac{2}{3}\begin{bmatrix} -\cos\theta & -\cos(\theta+2\pi/3) & -\cos(\theta-2\pi/3) \\ \sin\theta & \sin(\theta+2\pi/3) & \sin(\theta-2\pi/3) \\ 1/2 & 1/2 & 1/2 \end{bmatrix}\begin{bmatrix} X_a \\ X_b \\ X_c \end{bmatrix} \tag{4.1}$$

where $\theta = \omega t$ and ω is the frequency of the electric system.

$$\begin{bmatrix} X_a \\ X_b \\ X_b \end{bmatrix} = \begin{bmatrix} -\cos\theta & \sin\theta & 1/2 \\ -\cos(\theta-2\pi/3) & \sin(\theta-2\pi/3) & 1/2 \\ -\cos(\theta+2\pi/3) & \sin(\theta+2\pi/3) & 1/2 \end{bmatrix}\begin{bmatrix} X_D \\ X_Q \\ X_0 \end{bmatrix} \tag{4.2}$$

4.3.1. Synchronization Controller for Grid Reconnection: Proposed Algorithm

When the DG is in islanded mode operation and the grid-disconnection cause disappears, the transition from stand-alone to grid-connected mode can be started [42]. To avoid hard transients in the reconnection, the DG has to be synchronized with the grid voltage [50-52]. The DG is operated in synchronous island mode until both systems are synchronized. Once the voltage in the DG is synchronized with the utility voltage, the DG is reconnected to the grid and the controller will pass from voltage control mode to current control mode. This synchronization is achieved by implementing the following algorithm:

- Assume that the phase difference between grid voltage and inverter voltage is given by:

$$\phi = \angle V_G - \angle V_I \tag{4.3}$$

- In order to obtain information of ϕ, two sets of voltage values are used:

$$k = V_{Ia}V_{Ga} + V_{Ib}V_{Gb} + V_{Ic}V_{Gc} = \frac{3}{2}[\cos(\phi)] \tag{4.4}$$

$$g = V_{Ia}V_{Gb} + V_{Ib}V_{Gc} + V_{Ic}V_{Ga} = \frac{3}{4}\left[-\cos(\theta) + \sqrt{3}\sin(\phi)\right] \tag{4.5}$$

where,

$$V_{Ga} = V_{Gm}\sin(\omega t)$$

$$V_{Gb} = V_{Gm}\sin(\omega t + 120^{o})$$

$$V_{Gc} = V_{Gm}\sin(\omega t - 120^{o})$$

$$V_{Ia} = V_{Im}\sin(\omega t + \theta)$$

$$V_{Ib} = V_{Im}\sin(\omega t + 120^{o} + \theta)$$

$$V_{Ic} = V_{Im}\sin(\omega t - 120^{o} + \theta)$$

Using the variables *k* and *g*, $\sin(\phi)$ can be found as:

$$\sin(\phi) = \frac{\frac{4}{3}g + \frac{2}{3}k}{\sqrt{3}} \tag{4.6}$$

Fig. 4.3 shows how $\sin(\phi)$ is used to obtain the compensated phase angle for which the grid voltage and the DG voltage are synchronized. When the grid is recovered, a PLL observer, whose output will generate the grid frequency and phase, processes the grid phase voltages. If the amplitude and frequency of the voltages are within the limits defined by standards, a synchronizing signal will be generated. When the sine of the phase error is between -0.04 and 0.04 radians, the voltages are considered to be synchronized and the control of the supply-side inverter will be switched from stand-alone to grid-connected control mode.

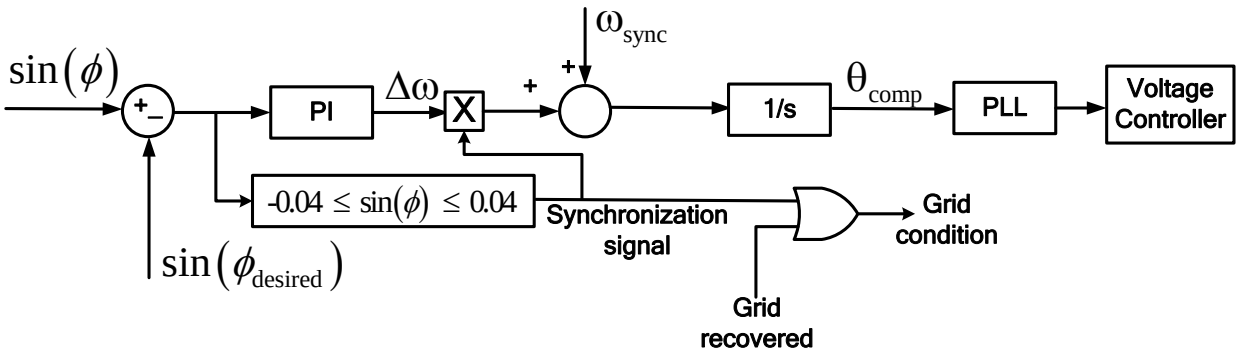

Fig. 4. 3 Synchronization controller

4.4. Transfer Functions

Fig. 4.4 shows the block diagram of the DG interface control for grid-connected operation.

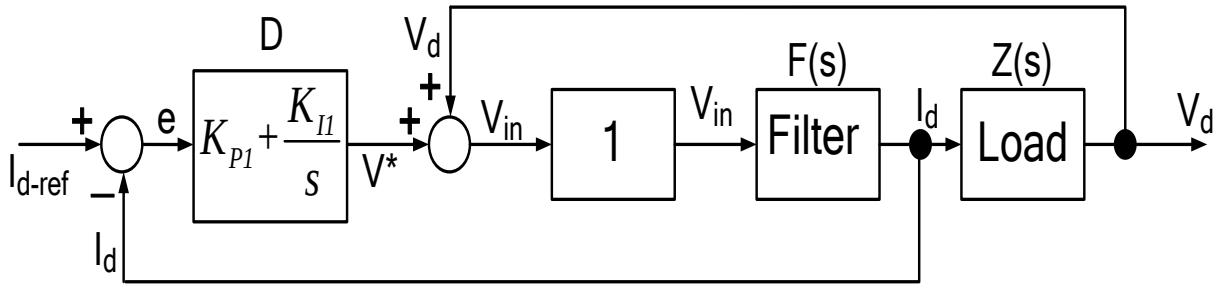

Fig. 4. 4 Block diagram of the current controlled inverter

The PI controller produces a signal that is proportional to the time integral of the controller. The transfer function of the PI controller is given by:

$$D = K_{P1} + \frac{K_{I1}}{s} \tag{4.7}$$

where K_P is the proportional gain and K_I the integral gain.

The inverter stage does not have any significant transient time associated with it and hence it is modeled as an ideal gain. This ideal gain can be given by $G_I(s) = 1$.

The schematic circuit of the filter stage is shown in Fig. 4.5. It consists of an LCL filter and a parallel RLC load.

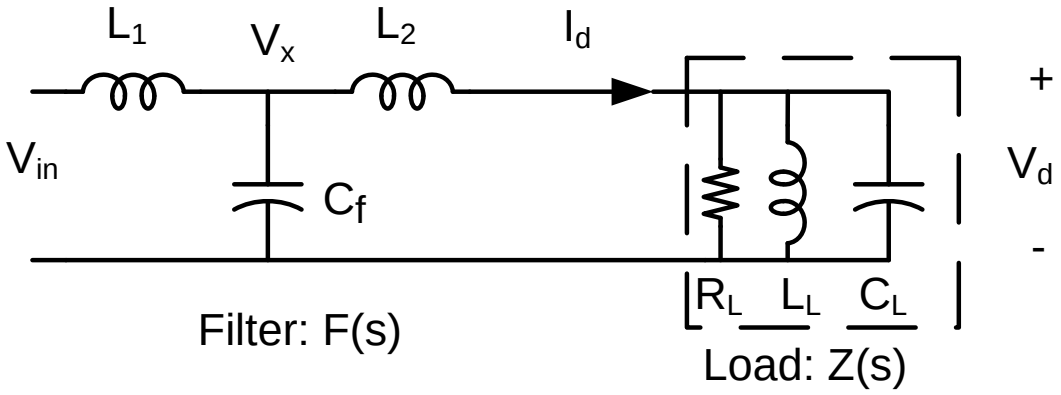

Fig. 4. 5 LCL Filter and parallel RLC load

The transfer function of the filter is given by:

$$F(s)=\frac{I_d(s)}{V_{in}(s)}=\frac{1}{s^3C_fL_1L_2+s^2C_fL_1Z+s\left(L_1+L_2\right)+Z} \tag{4.8}$$

The transfer function of the load, Z(s), is given by:

$$Z(s)=\frac{V_d(s)}{I_d(s)}=\frac{1}{\frac{1}{R_L}+\frac{1}{sL_L}+sC_L} \tag{4.9}$$

This can be re-expressed as:

$$Z(s)=\frac{sL_LR_L}{s^2R_LC_LL_L+sL_L+R_L} \tag{4.10}$$

Using Fig. 4.4 and equations (4.7), (4.8) and (4.10), the transfer function of the current controlled system is derived as:

$$H(s)=\frac{V_d(s)}{I_{d\text{-}ref}(s)}=\frac{FZD}{(1-FZ+FD)} \tag{4.11}$$

$$Z(s)=\frac{651.466s}{s^2+150.454s+142117} \tag{4.12}$$

$$F(s)=\frac{6.4516x10^{10}\left(s^2+150.454s+142117\right)}{s^5+150.454s^4+9.8219x10^7 s^3+1.456x10^{10}s^2+5.5783x10^{13}s+0.4187} \tag{4.13}$$

$$D=0.8+\frac{25}{s} \tag{4.14}$$

$$H(s)=\frac{3.365x10^{13}s^2+1.051s}{s^6+150.108s^5+9.83x10^7 s^4+6.62x10^{10}s^3+2.31x10^{13}s^2+7.58x10^{15}s+2.28x10^{17}} \tag{4.15}$$

where $R_L=4.33\Omega$, $L_L=4.584mH$, $C_L=1.535mF$, $L_1=1mH$, $L_2=0.5mH$, $C_f=31\mu F$, $K_{P1}=0.8$, $K_{I1}=25$

4.5. Simulation Results

The performance of the proposed control strategies was evaluated by computer simulation using SABER. Fig. 4.6 shows the simulated system.

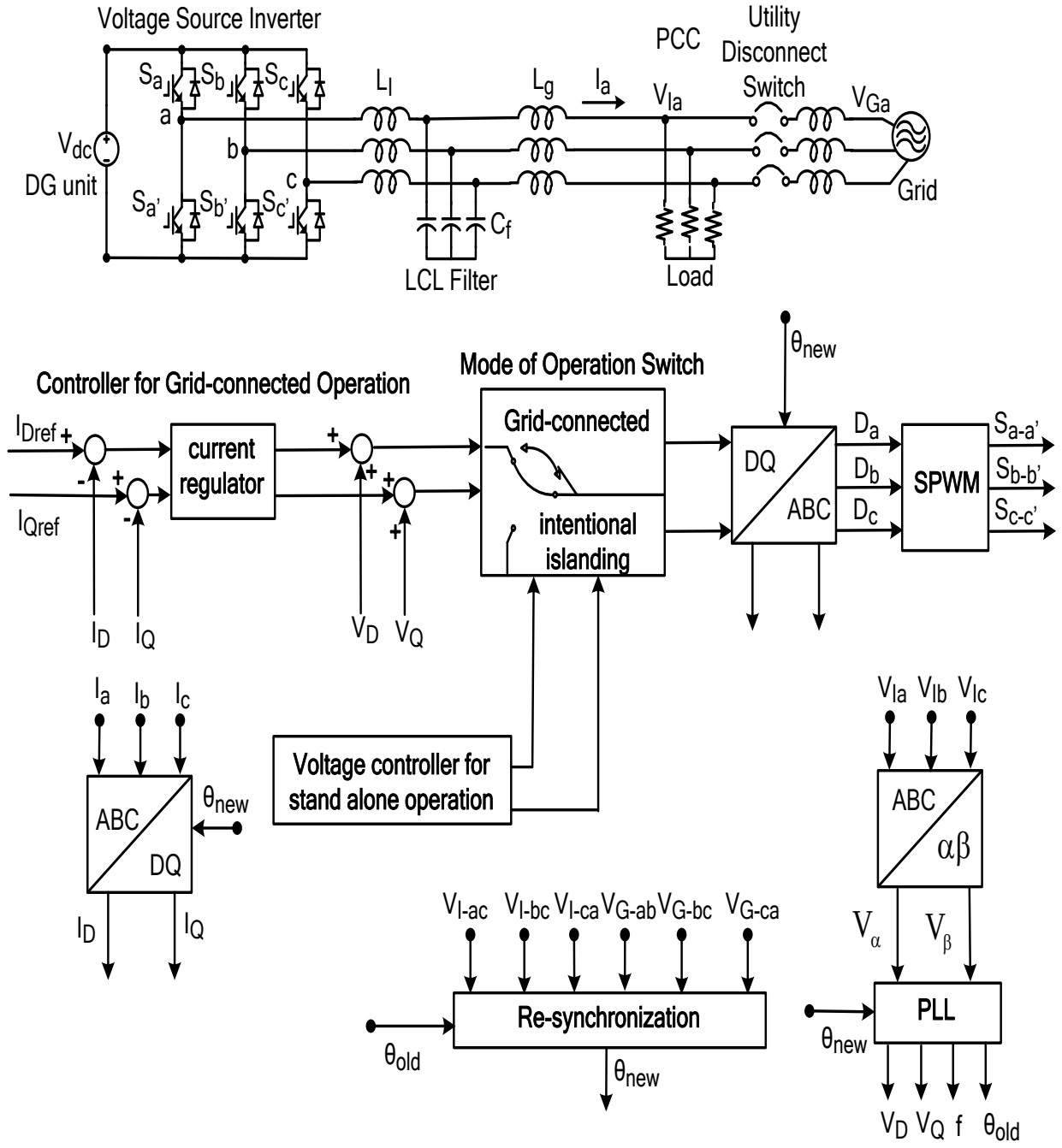

Fig. 4. 6 Current controller for grid-connected operation

The R load was adjusted to consume 10 kW. The DG system was designed to supply 10 kW and zero reactive power. The system was operated initially in grid-connected operation. Fig. 4.7 shows the voltages and currents at the PCC during grid-connected operation.

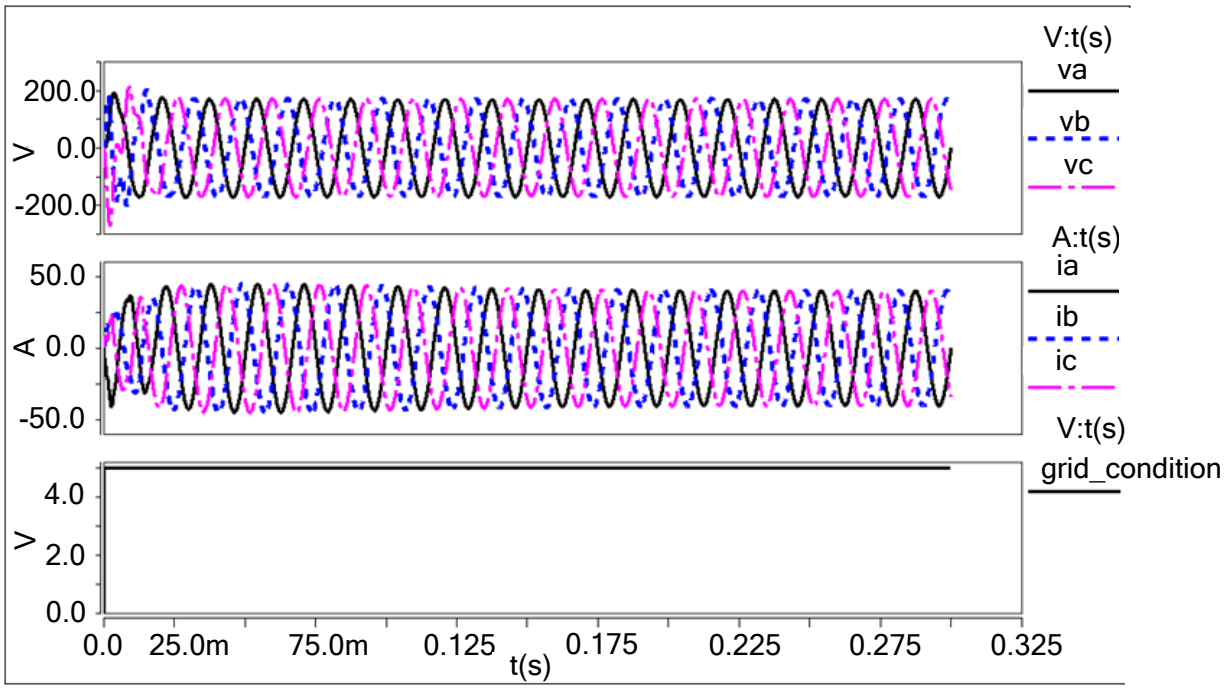

Fig. 4. 7 Phase voltages and currents during grid-connected operation

When the grid-disconnection cause disappears, the transition from stand-alone mode to grid-connected mode can be started. The DG was operated in synchronous island mode until both systems were re-synchronized. While in synchronous island mode, the synchronization controller decreases or decreases the frequency to a limited value, as seen in Fig. 4.8. Also seen in that figure are the voltages of the DG and grid; here the DG voltage can be seen to synchronize with the grid and when the phase angle between the two voltages are approximately equal, the algorithm reconnects the system to the utility and switches the mode of control from voltage control to current control. As can be seen, the proposed algorithm successfully forces the voltage at the DG to track the voltage at the grid.

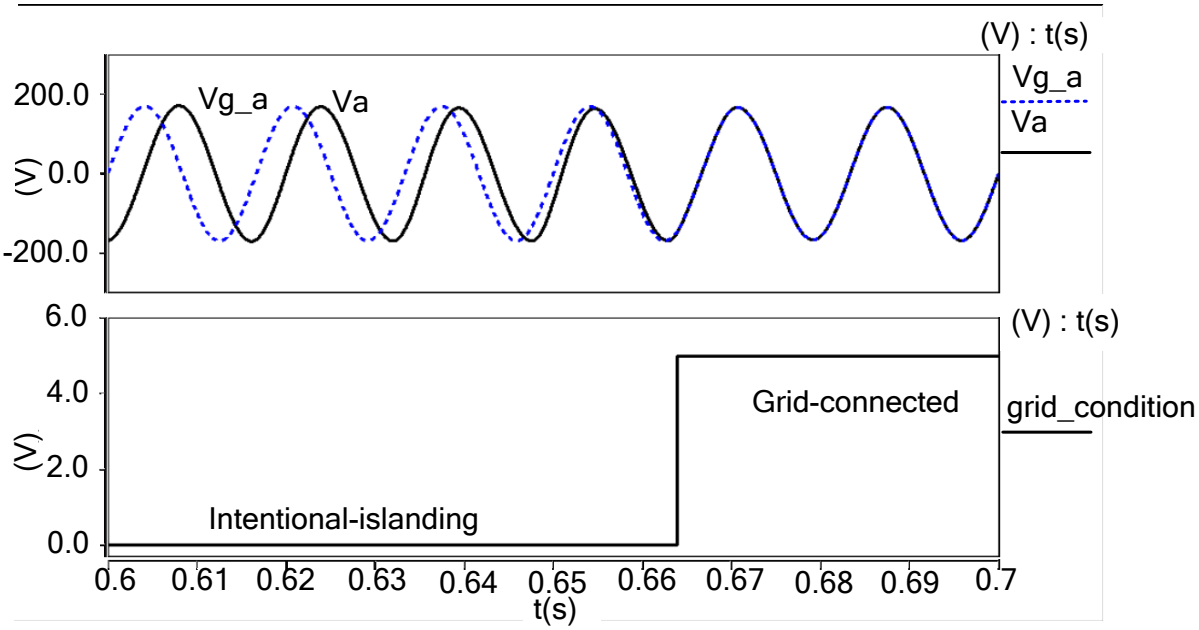

Fig. 4. 8 Synchronization for grid re-connection

Once the synchronization was completed, the DG was reconnected to the grid and the controller was switched from voltage control mode to current control mode. Fig. 4.9 shows the phase voltage V_a without and with the synchronization algorithm implemented. As can be noticed, the transients are minimal and virtually negligible indicating that the algorithm avoids a hard transient in the reconnection from stand-alone operation to grid-connected operation.

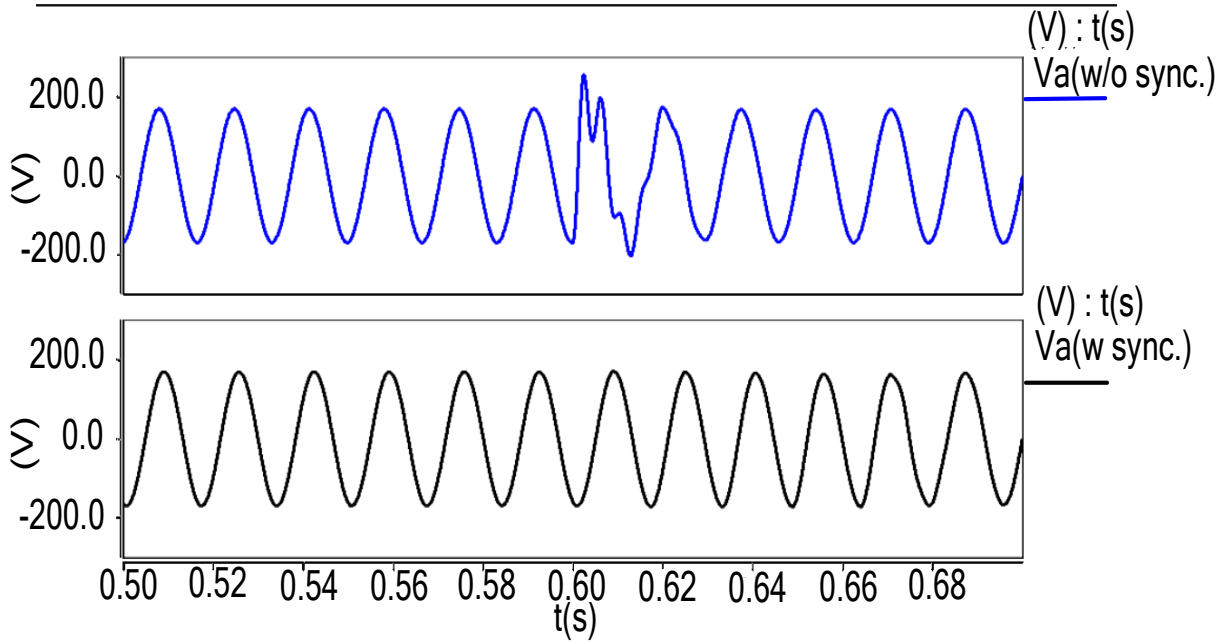

Fig. 4. 9 Phase voltage without (top) and with (bottom) synchronization

4.6. Experimental Results

A hardware prototype has been implemented for experimental verification. The control, PLL, grid condition detection, and re-closure algorithms have been programmed using a universal DSP control board developed at the Power Electronics and Motor Drives Laboratory at Michigan State University. The DG is started up in grid-connected operation mode. Fig. 4.10 demonstrates how the system line to line voltage and phase current behaves during grid-connected mode.

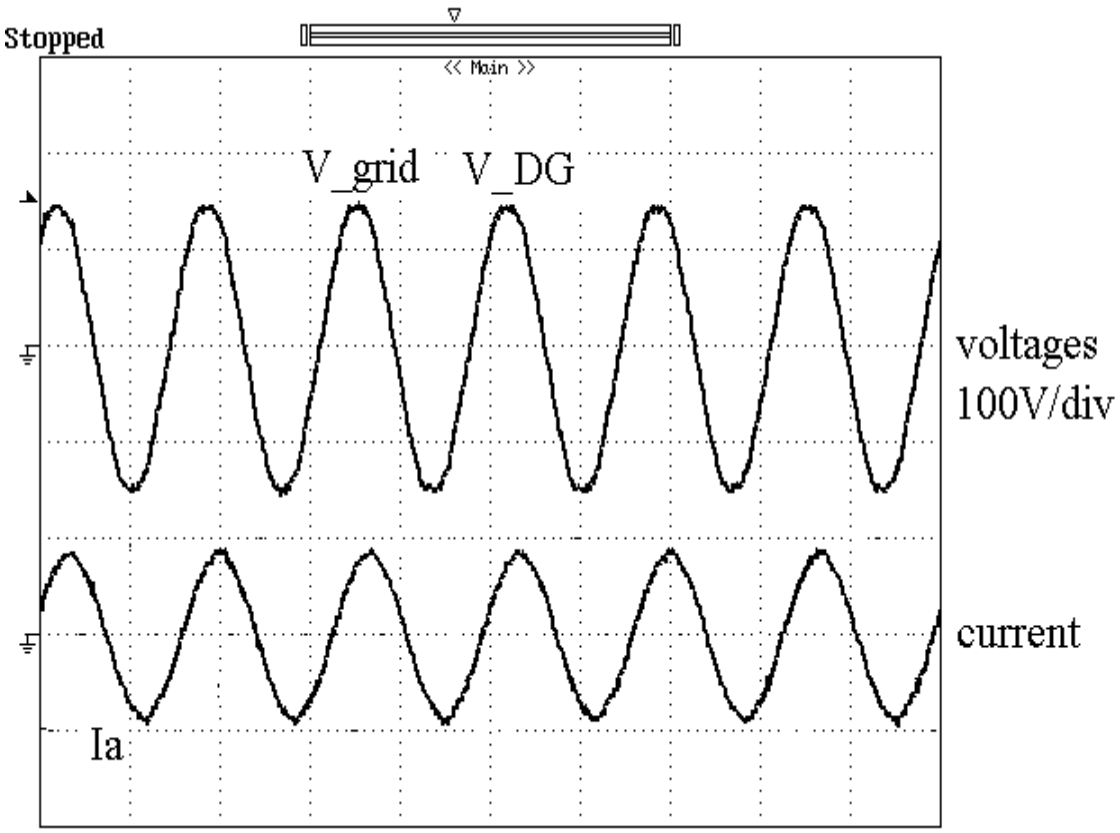

Fig. 4. 10 Line to line voltages and phase current during grid-connected operation

Fig. 4.11 shows the process of synchronization where the line to line voltage at both ends of the separation device is illustrated. At the beginning of the synchronization, both voltages are out of phase. As can be seen, the proposed algorithm successfully forces the voltage at the DG to track the voltage at the grid until the synchronization process is completed. Also shown is the smooth transition of the currents.

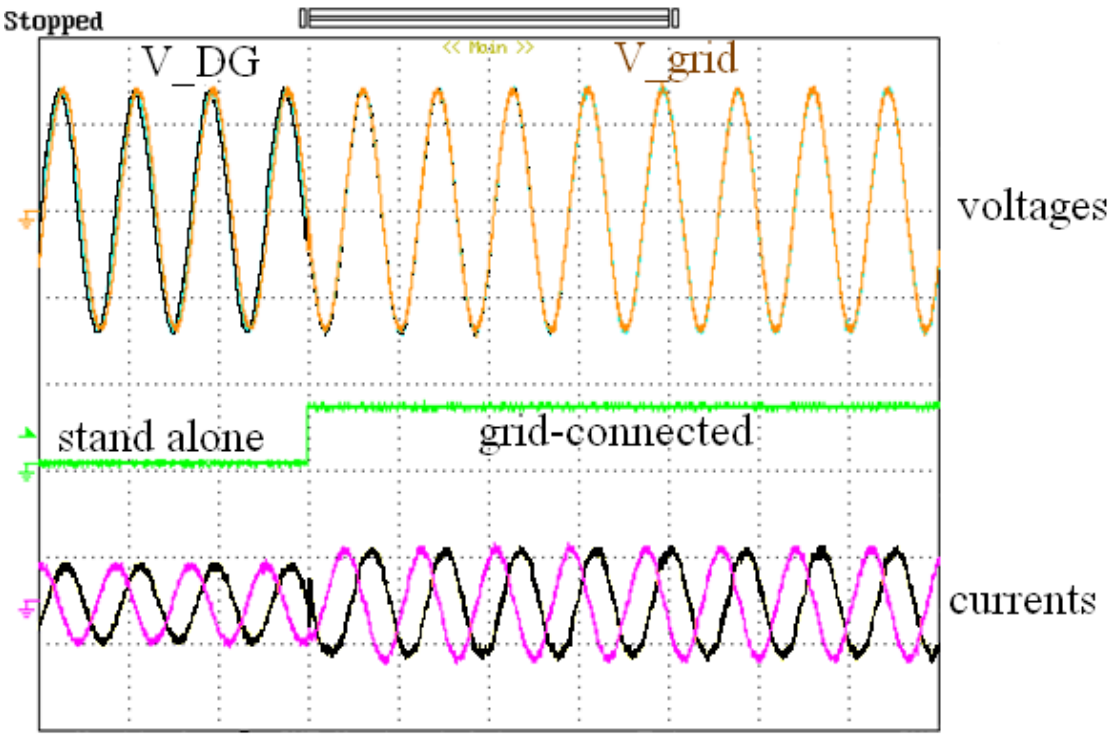

Fig. 4. 11 Transition from stand-alone to grid connected operation

CHAPTER 5. PROPOSED CONTROL FOR INTENTIONAL ISLANDING OPERATION OF DG WITH SEAMLESS TRANSITION FROM GRID CONNECTED OPERATION

5.1. Introduction

The control of the DG system is important in both grid-connected and stand-alone modes and the system stability becomes very crucial during the transfer between these two modes. If the system does not have a proper transfer procedure, severe transient voltages or currents will occur, which may damage the entire system [40]. Fig. 5.1 shows a waveform showing this situation after grid disconnection at time t_1. A seamless transfer can ensure smooth operation and quick attainment of steady state.

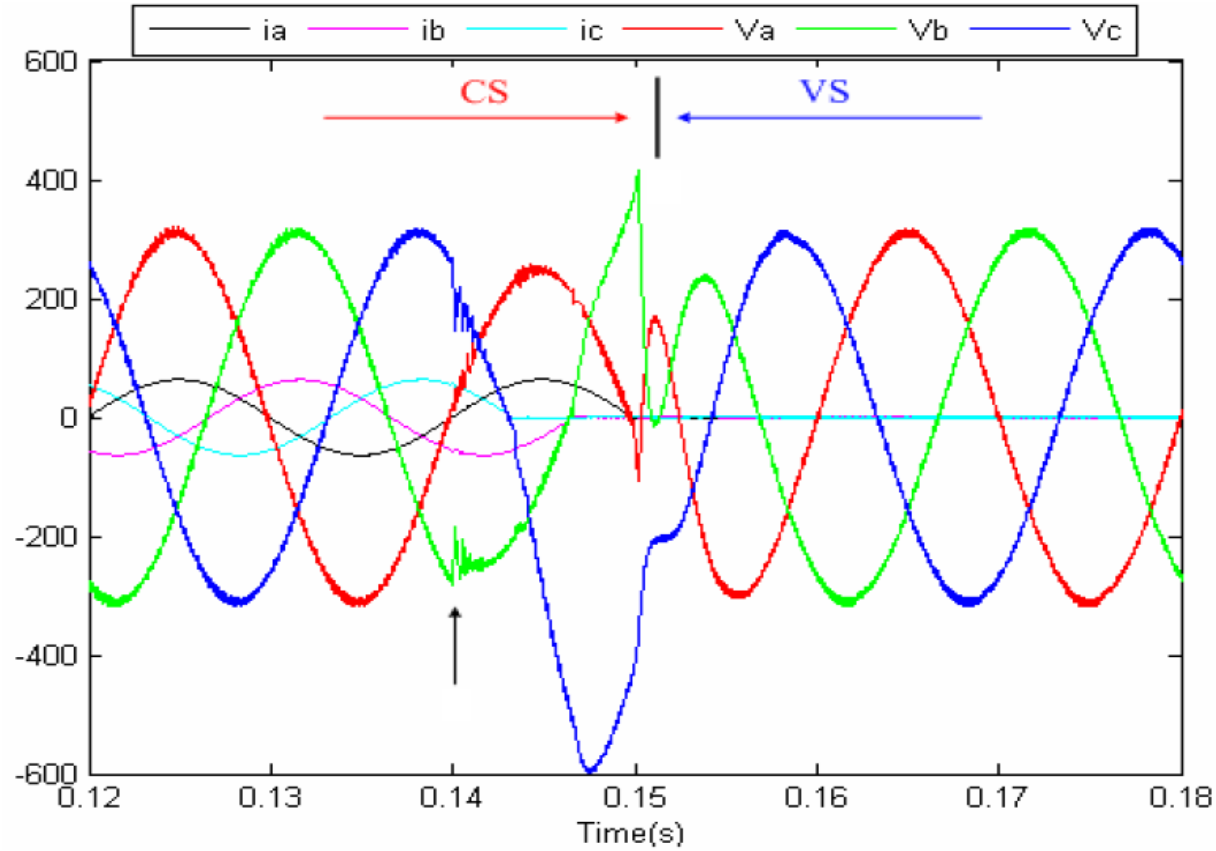

Fig. 5. 1 Simulation waveforms of load voltages and grid currents during the grid disconnection [38]

In order to solve this transition problem, this chapter presents the development and test of a control strategy for DG capable of working in intentional islanding connection mode with a seamless transition from grid-connected to stand-alone operation modes. The control scheme proposed is based on a voltage-controlled method for the stand-alone DG inverter. The stand-alone mode with voltage control is featured with a grid condition detection algorithm to detect the instant at which the DG is cut from the main grid, a load shedding algorithm to disconnect part of the load in order to steer the power system from potential dangers, and a voltage controller with seamless transition from grid-connected to stand-alone operation modes.

5.2. Grid Condition Detection

The instant at which the DG is cut off from the main grid must be detected in order for the system to change between grid-connected to stand-alone modes [53]. This detection is achieved by using a PLL which consists of Clarke's transformation (Eq. 5.1), Park's transformation (Eq. 5.2), a PI regulator, and an integrator [5, 54]. The schematic of the PLL is illustrated in Fig. 5.2.

$$\begin{bmatrix} V_\alpha \\ V_\beta \end{bmatrix} = \begin{bmatrix} 2/3 & 1/3 \\ 0 & 1/\sqrt{3} \end{bmatrix} \begin{bmatrix} V_{ab} \\ V_{bc} \end{bmatrix} \tag{5.1}$$

$$\begin{bmatrix} V_d \\ V_q \end{bmatrix} = \begin{bmatrix} -\cos\theta & \sin\theta \\ \sin\theta & \cos\theta \end{bmatrix} \begin{bmatrix} V_\alpha \\ V_\beta \end{bmatrix} \tag{5.2}$$

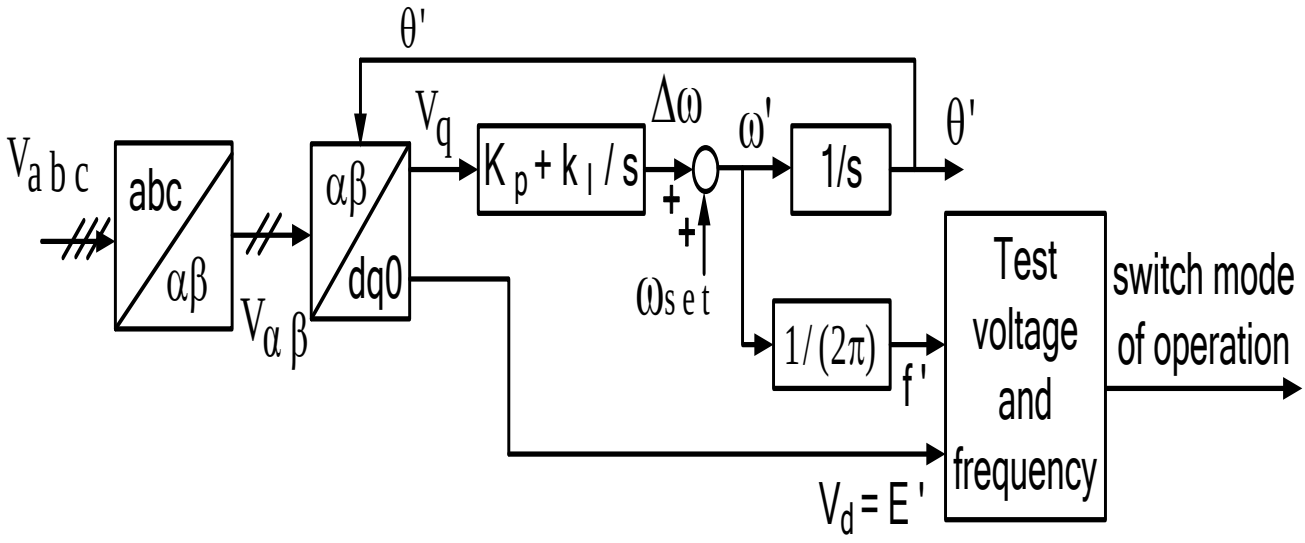

Fig. 5. 2 PLL structure

The lock is realized by setting V_q to zero. A PI regulator can be used to control this variable and the output of this regulator is the grid frequency [55]. As can be noticed in Fig. 5.1, in addition to the frequency, the PLL is capable of tracking the magnitude of its input signals (V_d and V_q), e.g. the grid voltages. These two parameters, frequency or voltage magnitude, are used in the loss of main detection algorithm to detect the grid condition [28]. The algorithm sends a signal that switches the inverter to the suitable interface control.

Fig. 5.3 shows the implementation of this algorithm. The output of a comparator block activates a monostable circuit. If the monostable circuit stays in on-state for 0.16 seconds, corresponding to 10 cycles, this is considered as an abnormal condition [28]. This abnormal condition sends a signal that switches the inverter to the suitable interface control.

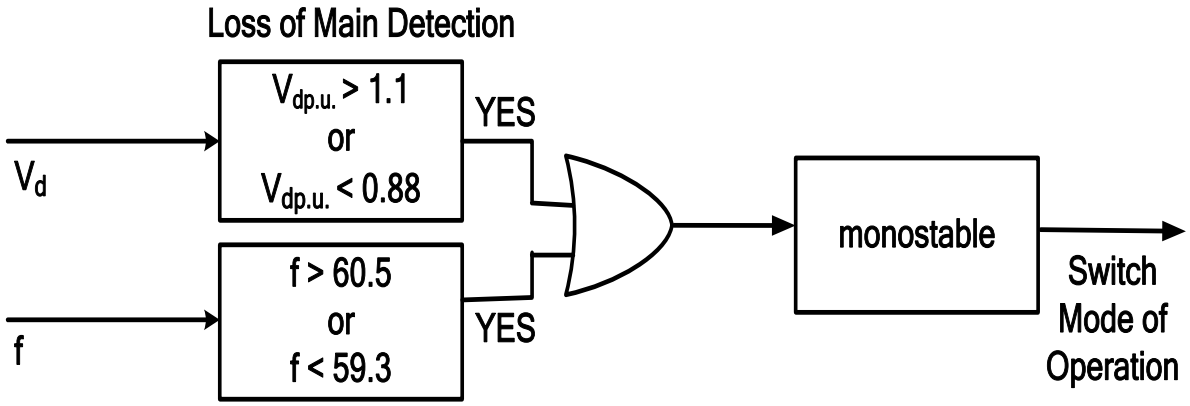

Fig. 5. 3 Loss of Main Detection

This switching between grid-connection and stand-alone operation modes is done by using an over/under frequency method (OFP/UFP) or an over/under voltage method (OVP/UVP) that cause the DG inverter to switch if the frequency or amplitude of the voltage stays outside of prescribed limits. When the grid is disconnected, this causes that the voltage amplitude or frequency changes, as shown in Fig. 5.4. When these changes in voltage or frequency exceed certain thresholds, grid disconnection is considered and the operation mode is consequently switched. The algorithm is shown in Fig. 5.5.

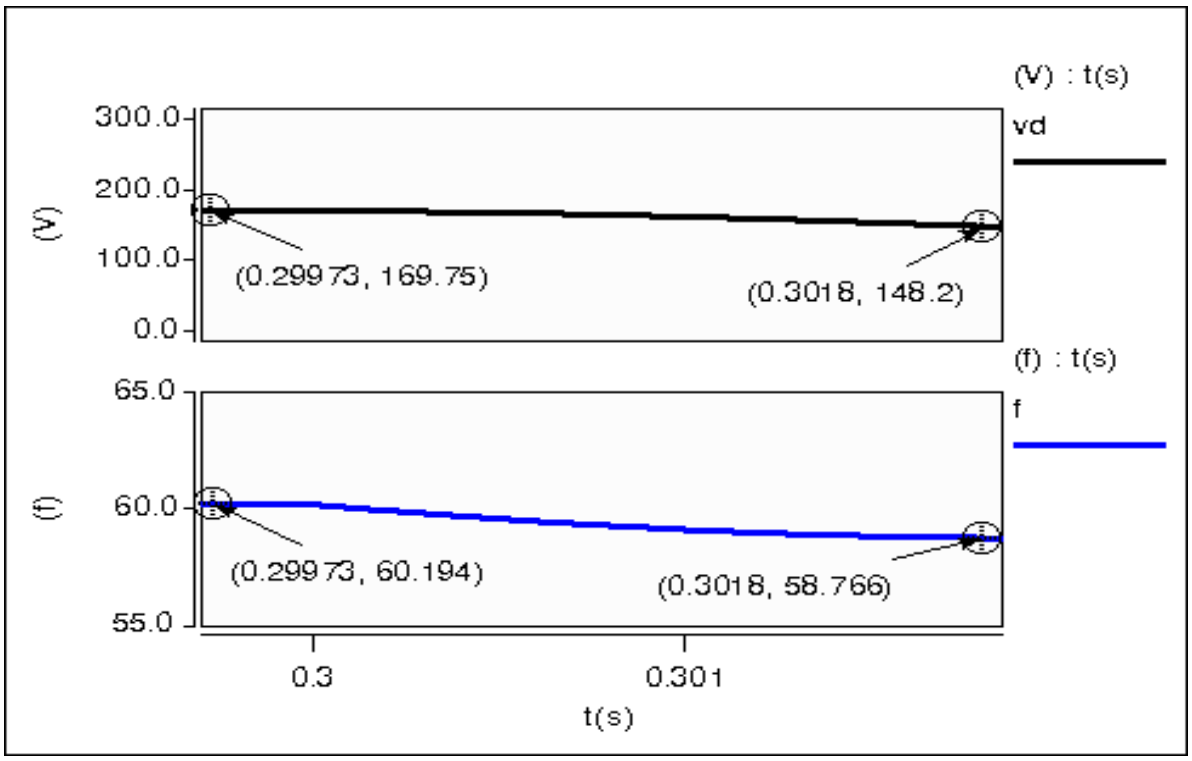

Fig. 5. 4 Voltage or frequency change at grid disconnection

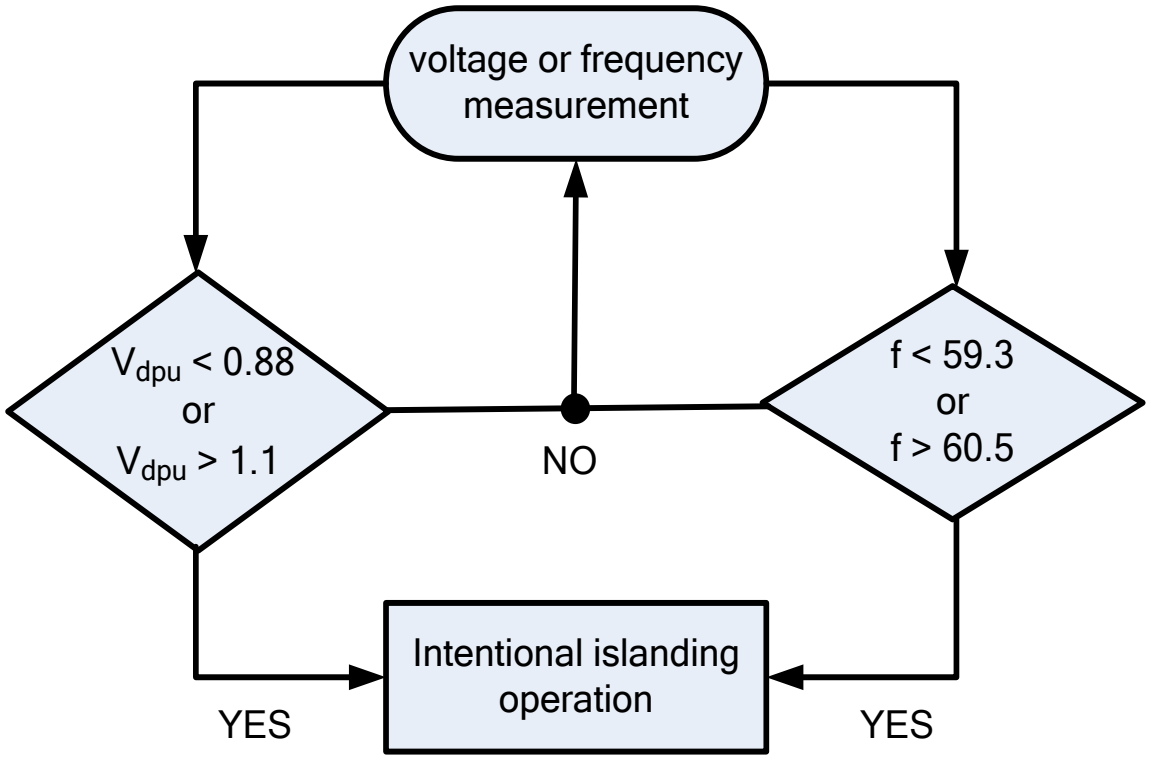

Fig. 5. 5 Islanding Detection Algorithm

While serving as good indications for islanding detection, the quick voltage or frequency variations lead to a serious concern: the DG would operate out of the allowable voltage or frequency range quickly after islanding occurs [56]. To avoid this, intelligent load shedding algorithms need to be implemented in a DG system to make sure that the demand is within available generation by disconnecting some least important loads [57].

5.3. Intelligent Load Shedding

Load shedding is defined as the process in which a part of the system load is disconnected according to a certain priority in order to steer the power system from potential dangers [58-59]. During the grid connected operation, the DG is operated to provide the optimum power to the grid according to many factors such as the availability of energy, energy cost, and so on [39]. The main grid is supplying or absorbing the power difference between the DG and local load demand. When the main power grid is out (power outage), the DG that continues to inject pre-determined optimum power can cause voltage and frequency transients depending on the degree of power difference. The power difference makes the voltage and frequency drift away from the nominal values [37]. When the voltage and frequency drifts have reached certain levels, it is deemed that an islanding is occurring. This methodology is enough for islanding detection. However, it is not enough for intentional islanding operation because often the local DG is either less or greater than local load demand, and intelligent load shedding is needed. Therefore, it is essential to have an analytical solution of the voltage and frequency transients locally for the DG to have information and make decisions, and for intelligent load shedding to secure energy delivery to sensitive loads.

To develop the load shedding algorithm, a constant impedance load is used. Fig. 5.6 shows the theoretical voltage transients for a constant impedance load under various active power differences (from -50% to +50%) after main power outage, while Fig. 5.7 shows the theoretical frequency transients under various reactive power differences. As seen from Figs. 5.6 and 5.7, with no load shedding it would be insufficient for keeping the voltage or frequency within the limits required.

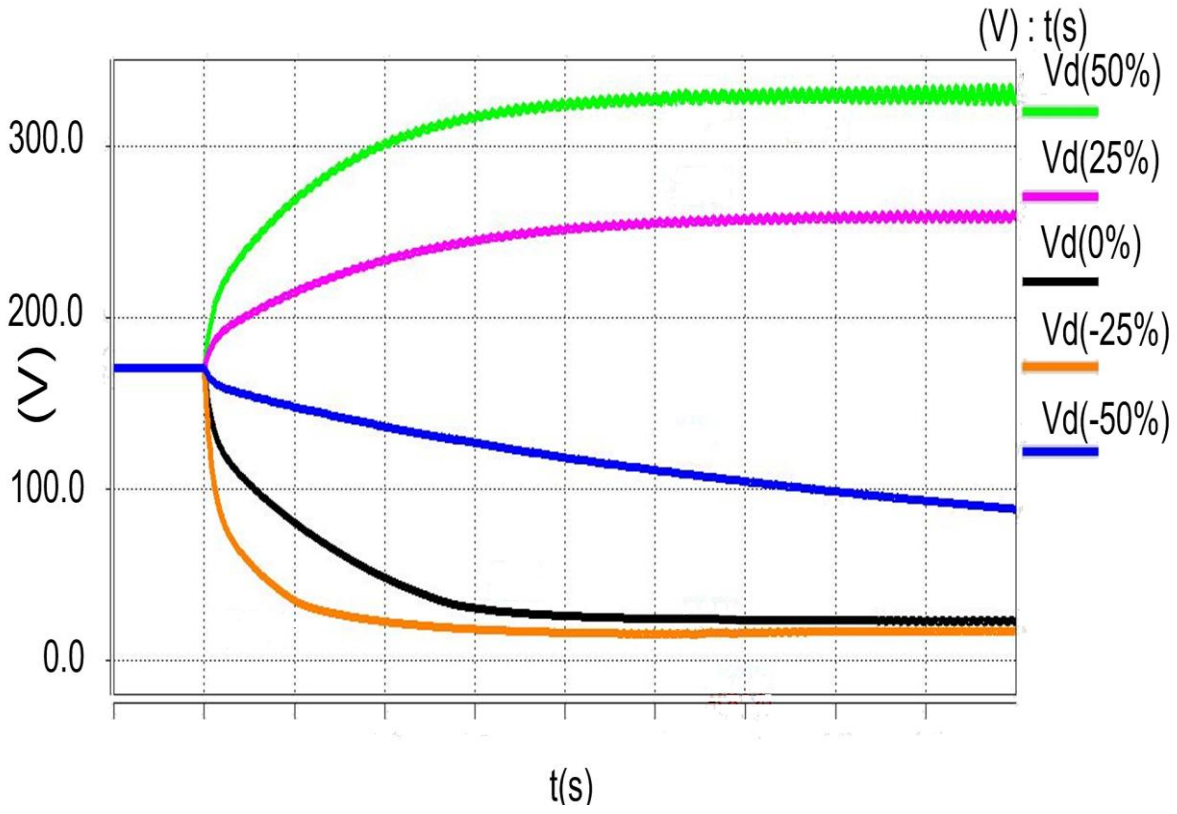

Fig. 5. 6 Voltage Transients under various Active Power Differences

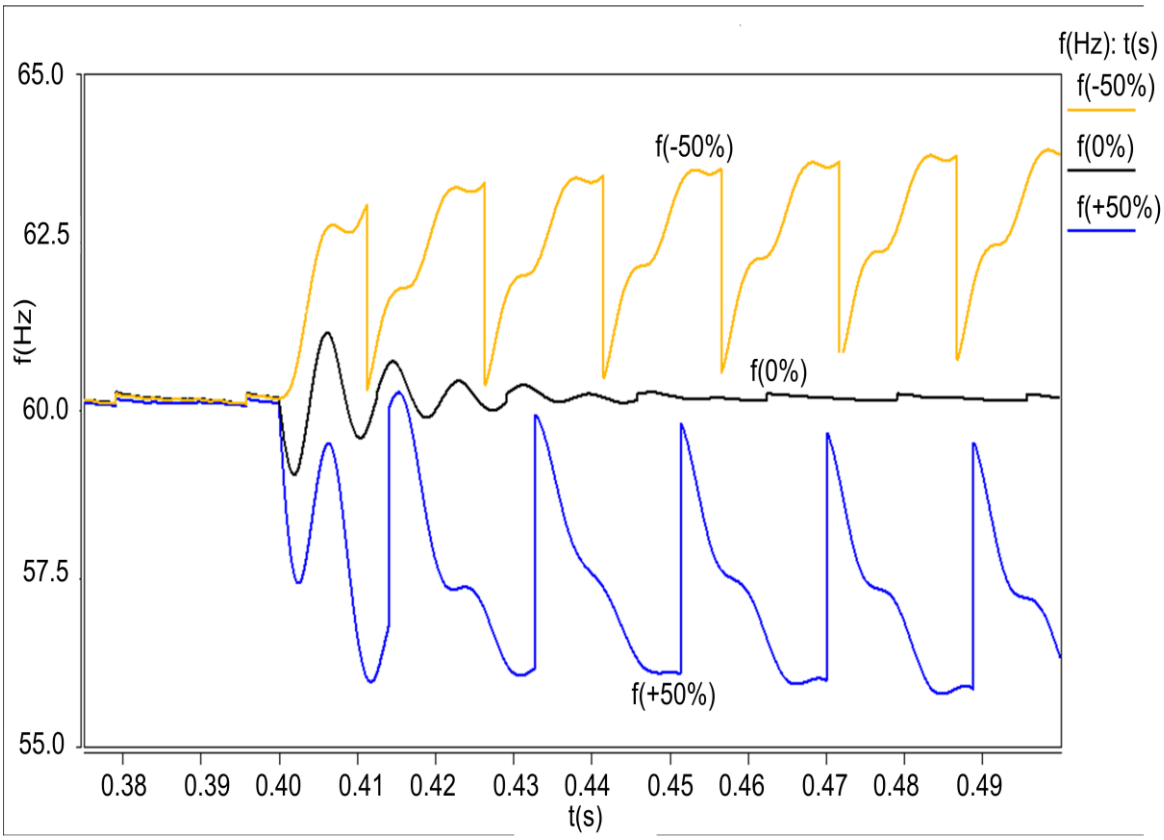

Fig. 5. 7 Frequency Transients under various Reactive Power

The challenge is how to switch the DG inverter system to voltage control mode and bring the voltage back to the normal range (0.88 – 1.1 Vpu) for intentional islanding operation. The analytical solution of the simple case scenario shown in Fig. 5.6 provides a possible solution to this challenge. Fig. 5.6 shows that the voltage change rate is related to the power differences between the DG and load demand. The approach proposed is to detect the voltage change rate and profile after the power outage and determine how much load shedding is needed before going to the intentional islanding operation and switching to the voltage control mode. In order to accomplish this, the system shown in Fig. 5.8 has been analyzed.

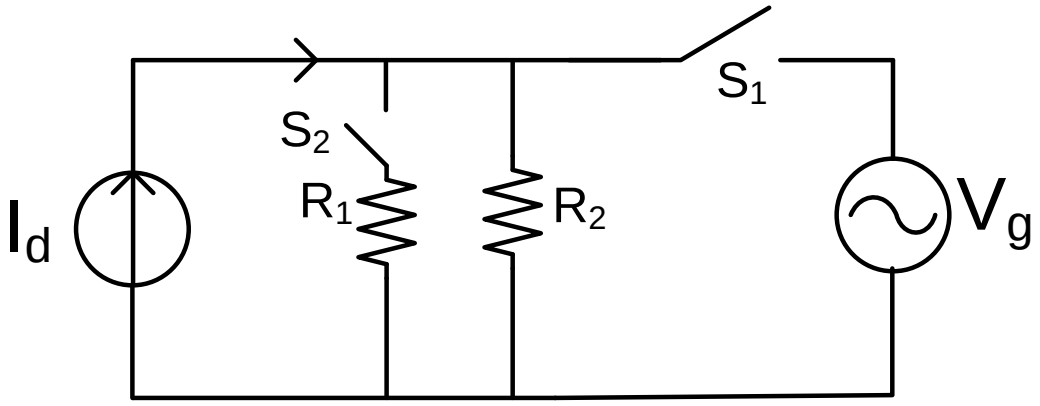

Fig. 5. 8 System to implement load shedding

To determine the amount of load to be disconnected the following algorithm, based on Fig. 5.9, is proposed:

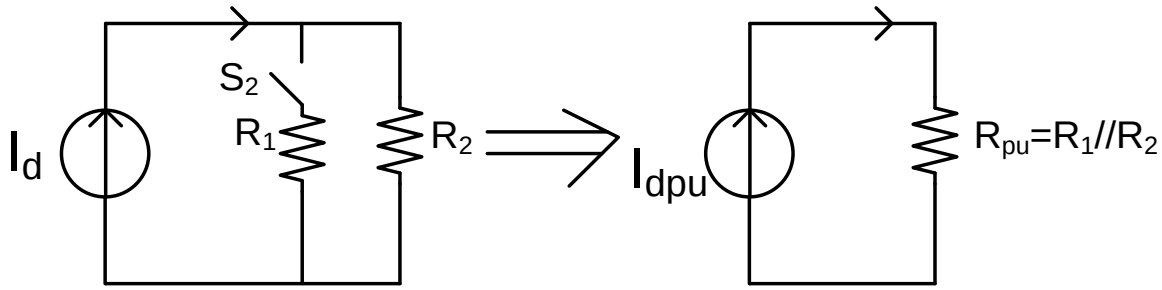

Fig. 5. 9 System in per unit to implement load shedding

- Obtain the voltage amplitude expression for load shedding:

Using the circuit shown in Fig. 5.9, the expressions for the load voltages V_{apu}, V_{bpu}, and V_{cpu} can be found:

$$V_{apu} = I_{dpu} R_{pu} \sin(\omega t + \theta) \tag{5.3}$$

$$V_{bpu} = I_{dpu} R_{pu} \sin\left(\omega t + \theta - \frac{2\pi}{3}\right) \tag{5.4}$$

$$V_{cpu} = I_{dpu} R_{pu} \sin\left(\omega t + \theta + \frac{2\pi}{3}\right) \tag{5.5}$$

Using V_{apu}, V_{bpu}, and V_{cpu} an expression for the voltage amplitude can be found,

$$V_{pk} = \sqrt{\frac{2}{3}}\sqrt{V_{ab}^2 + V_{bc}^2 + V_{ca}^2} \tag{5.6}$$

$$V_{pk} = \sqrt{\frac{2}{3}}\sqrt{3} I_{dpu} R_{pu} \sqrt{\cos^2\left(\omega t + \theta + \frac{\pi}{3}\right) + \cos^2\left(\omega t + \theta\right) + \sin^2\left(\omega t + \theta + \frac{\pi}{6}\right)} \tag{5.7}$$

$$V_{pk} = \sqrt{2} I_{dpu} R_{pu} \sqrt{\cos^2\left(\omega t + \theta + \frac{\pi}{3}\right) + \cos^2\left(\omega t + \theta\right) + \sin^2\left(\omega t + \theta + \frac{\pi}{6}\right)} \tag{5.8}$$

- Derive the slope of the voltage amplitude

$$s = \frac{d\left(V_{pk}(t)\right)}{dt} = \frac{-\sqrt{2} I_{dpu} R_{pu} \omega K}{\sqrt{\cos^2\left(\omega t + \theta + \frac{\pi}{3}\right) + \cos^2\left(\omega t + \theta\right) + \sin^2\left(\omega t + \theta + \frac{\pi}{6}\right)}} \tag{5.9}$$

- Derive I_{dpu}

$$I_{dpu} = \frac{-s\sqrt{2}\sqrt{\cos^2\left(\omega t + \theta + \frac{\pi}{3}\right) + \cos^2\left(\omega t + \theta\right) + \sin^2\left(\omega t + \theta + \frac{\pi}{6}\right)}}{2\omega R_{pu} K} \tag{5.10}$$

Using

$$R_{pu} = R_{1pu} // R_{2pu} \tag{5.11}$$

and solving for R_1, where R_1 represents the load to be shed,

$$R_{1pu} = \frac{-\sqrt{2}\omega I_{dpu} K}{s\sqrt{\cos^2\left(\omega t+\theta+\frac{\pi}{3}\right)+\cos^2\left(\omega t+\theta\right)+\sin^2\left(\omega t+\theta+\frac{\pi}{6}\right)+\sqrt{2}\omega I_{dpu} K}} \tag{5.12}$$

where

$$K = \sin\left(\omega t+\theta+\frac{\pi}{3}\right)\cos\left(\omega t+\theta+\frac{\pi}{3}\right)-\sin\left(\omega t+\theta+\frac{\pi}{6}\right)\cos\left(\omega t+\theta+\frac{\pi}{6}\right)+\sin\left(\omega t+\theta\right)\cos\left(\omega t+\theta\right) \tag{5.13}$$

5.4. Transition from Grid-connected to Stand-alone: Proposed Controller

The proposed voltage closed loop control for stand-alone operation with seamless transition is shown in Fig. 5.10. The control works as voltage regulation through current compensation. The controller uses voltage compensators to generate current references for the current regulation.

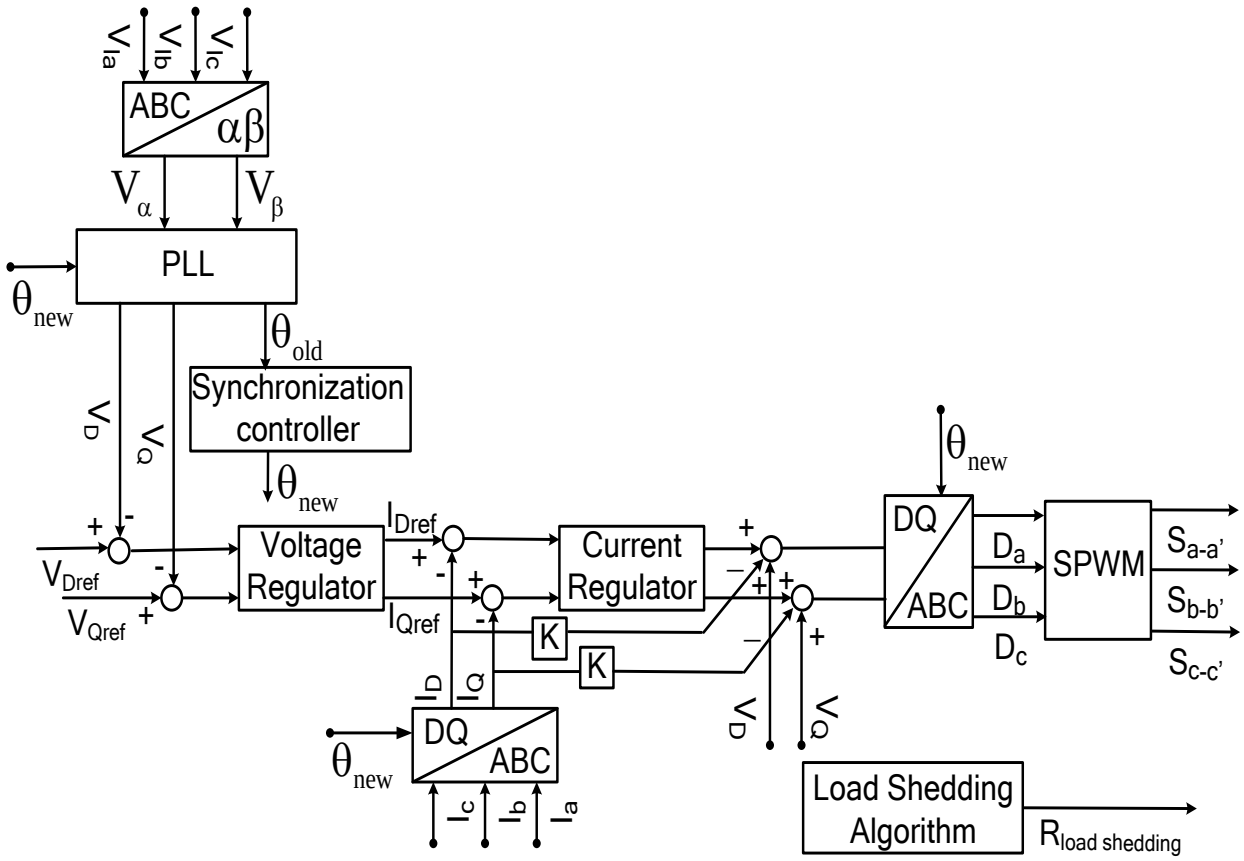

Fig. 5. 10 Voltage controlled inverter

As shown, the load voltage, V_D and V_Q, are forced to track their references (V_{Dref} and V_{Qref}) by using a voltage regulator (PI compensator). The outputs of this compensator, I_{Dref} and I_{Qref}, are compared with the load current (I_D and I_Q), and the error is fed to a current regulator (PI compensator). The output of the current regulator acts as the voltage reference signal that is fed to the sinusoidal pulse-width modulator (SPWM) to generate the high frequency gating signals for driving the three-phase voltage source inverter. The current loop is included to stabilize the system and to improve the system dynamic response by rapidly compensating for near-future variations in the load voltages [11]. In order to get a good dynamic response V_{DQ} is

fed forward. This is done because the terminal voltage of the inverter is treated as a disturbance and the feed-forward is used to compensate for it [60].

A compensation coefficient, K, is added to the current control loop as a feedforward control unit. This feedforward control achieves accurate tracking of the sinusoidal reference. The compensation coefficient processes the magnitude of the input voltage of the PWM modulator and counterattacks the severe transitions influenced by the grid disconnection. Then, this input voltage is fed to the PWM modulator to produce the drive signals for the inverter switches. Therefore, the modulated wave does not include the transient components that resulted from the grid disconnection.

5.5. Transfer Functions

Fig. 5.11 shows the block diagram of the DG interface control for intentional islanding operation.

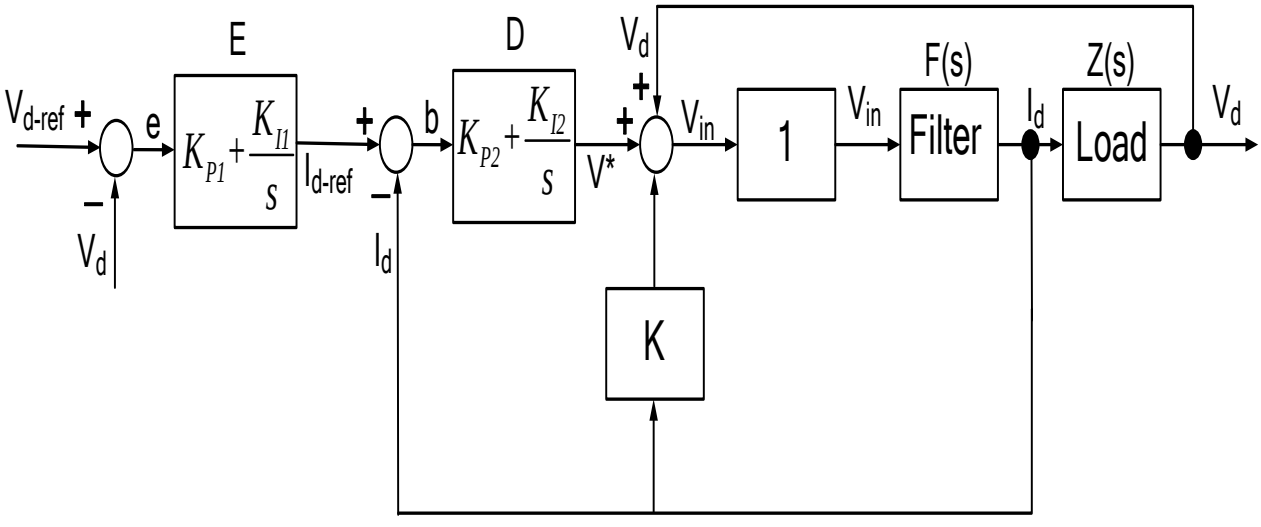

Fig. 5. 11 Block diagram of the voltage controlled inverter

The PI controllers produce a signal that is proportional to the time integral of the controller. The transfer functions of the PI controllers are given by:

$$E = K_{P1} + \frac{K_{I1}}{s} \tag{5.14}$$

$$D = K_{P2} + \frac{K_{I2}}{s} \tag{5.15}$$

where K_P are the proportional gains and K_I the integral gains.

The inverter stage does not have any significant transient time associated with it and hence it is modeled as an ideal gain. This ideal gain can be given by $G_I(s) = 1$.

The transfer function of the LCL filter is given by:

$$F(s) = \frac{I_d(s)}{V_{in}(s)} = \frac{1}{s^3 C_f L_1 L_2 + s^2 C_f L_1 Z + s\left(L_1 + L_2\right) + Z} \tag{5.16}$$

The transfer function of a parallel RLC load, *Z(s)*, is given by:

$$Z(s) = \frac{sL_L R_L}{s^2 R_L C_L L_L + sL_L + R_L} \tag{5.17}$$

Using Fig. 5.11 and equations (5.14) to (5.17), the transfer function of the current controlled system is derived as:

$$H(s) = \frac{V_d(s)}{V_{d\text{-}ref}(s)} = \frac{FZDE}{\left(1 + KF - FZ + FD + FZDE\right)} \tag{5.18}$$

By using $K = 0.9425$, $R_L = 4.33\Omega$, $L_L = 4.584mH$, $C_L = 1.535mF$, $L_1 = 1mH$, $L_2 = 0.5mH$, $C_f = 31\mu F$, $K_{P1} = 0.8$, $K_{I1} = 25$, $K_{P2} = \frac{1}{0.8}$, $K_{I2} = \frac{1}{25}$, then,

$$E = 0.8 + \frac{25}{s} \tag{5.19}$$

$$D = 1.25 + \frac{1}{25s} \tag{5.20}$$

$$H(s) = \frac{4.203x10^{13}\left(s^2 + 31.282s + 1\right)}{s^6 + 150.454s^5 + 9.8219x10^7 s^4 + 1.5601x10^{11}s^3 + 7.7068x10^{13}s^2 + 2.1418x10^{16}s + 4.0878x10^{14}} \tag{5.21}$$

5.6. Simulation Results

The performance of the proposed control strategy was evaluated by computer simulation using SABER. Fig. 5.12 shows the simulated system.

The R load was adjusted to consume 10 kW. The DG system was designed to supply 10 kW and zero reactive power. The system was operated initially in grid-connected operation. The grid was disconnected at 0.3 seconds. After the island was detected the control mode was changed from current controlled to voltage controlled operation. Fig. 5.13 shows the currents at the PCC before and after grid disconnection without the seamless transition controller implemented, while Fig. 5.14 shows the currents at the PCC before and after grid disconnection with the seamless transition controller implemented.

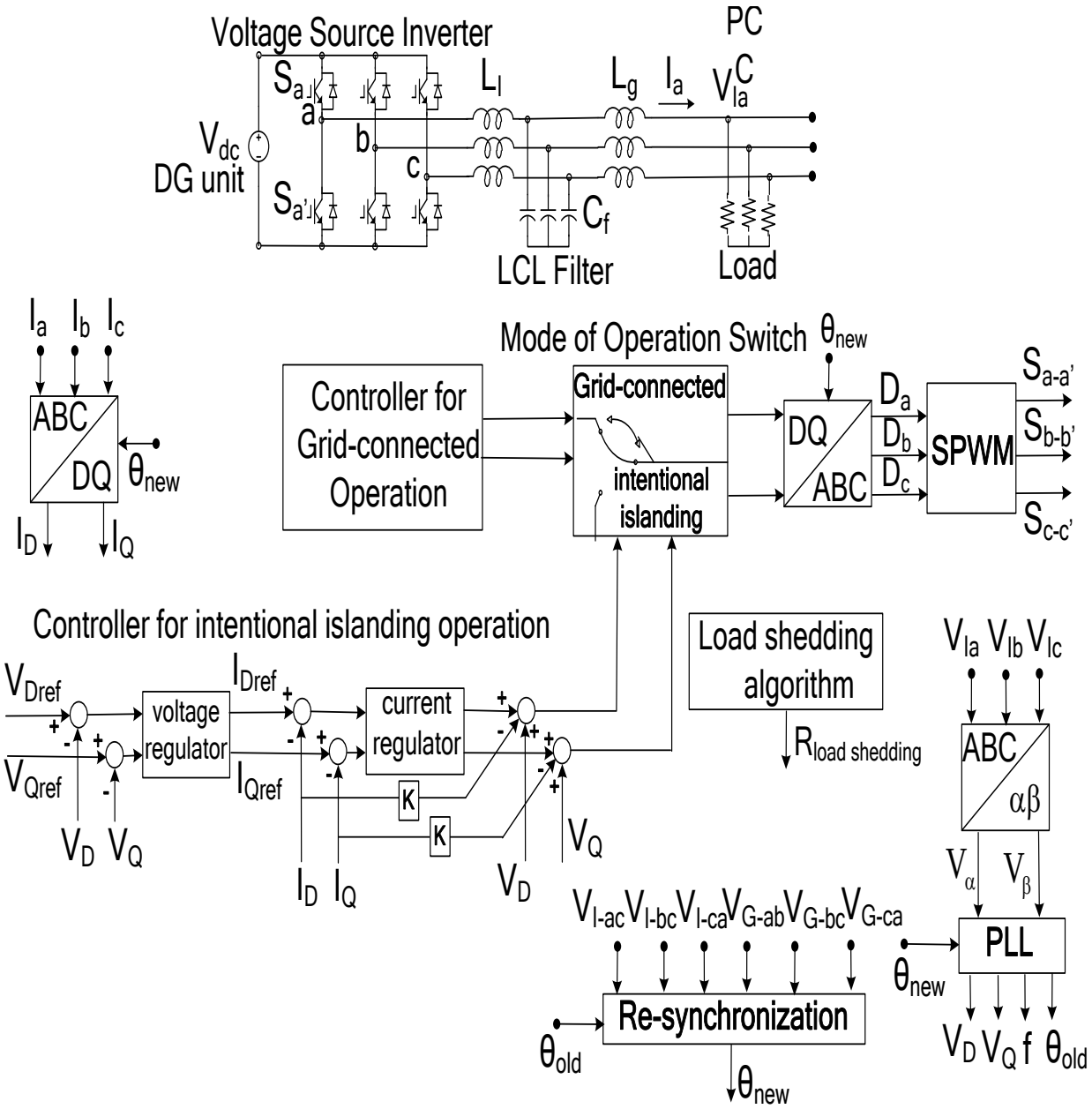

Fig. 5. 12 Simulated systems

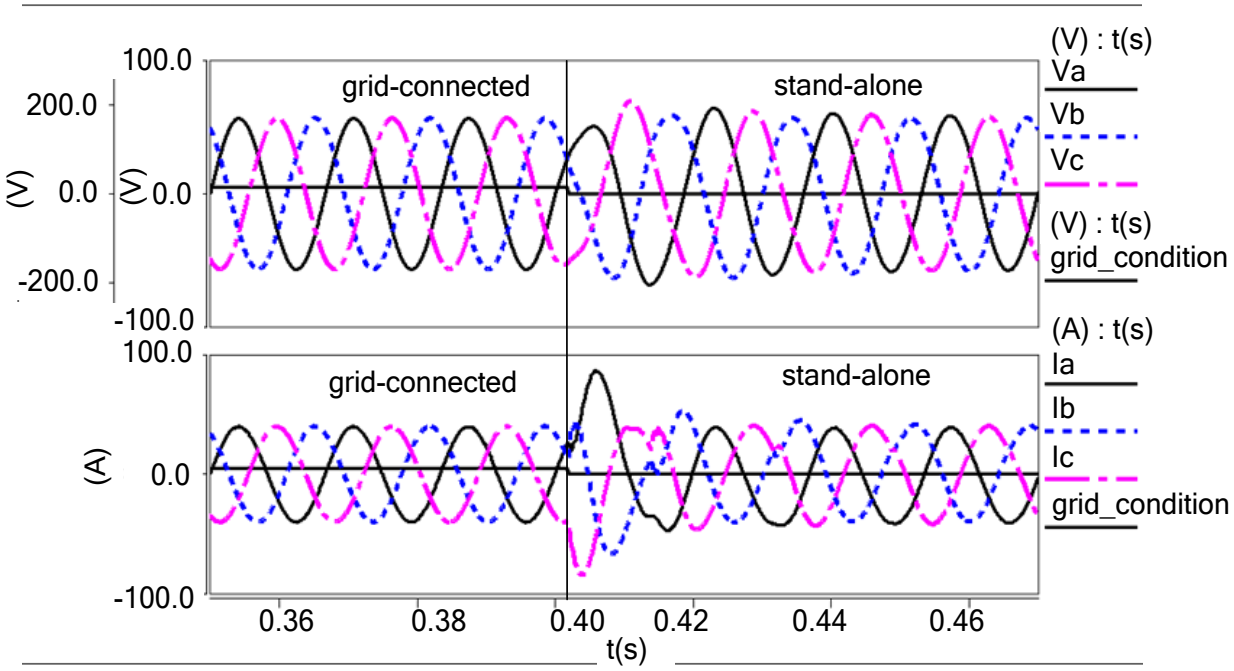

Fig. 5. 13 From grid-connected to stand-alone operation with severe transients

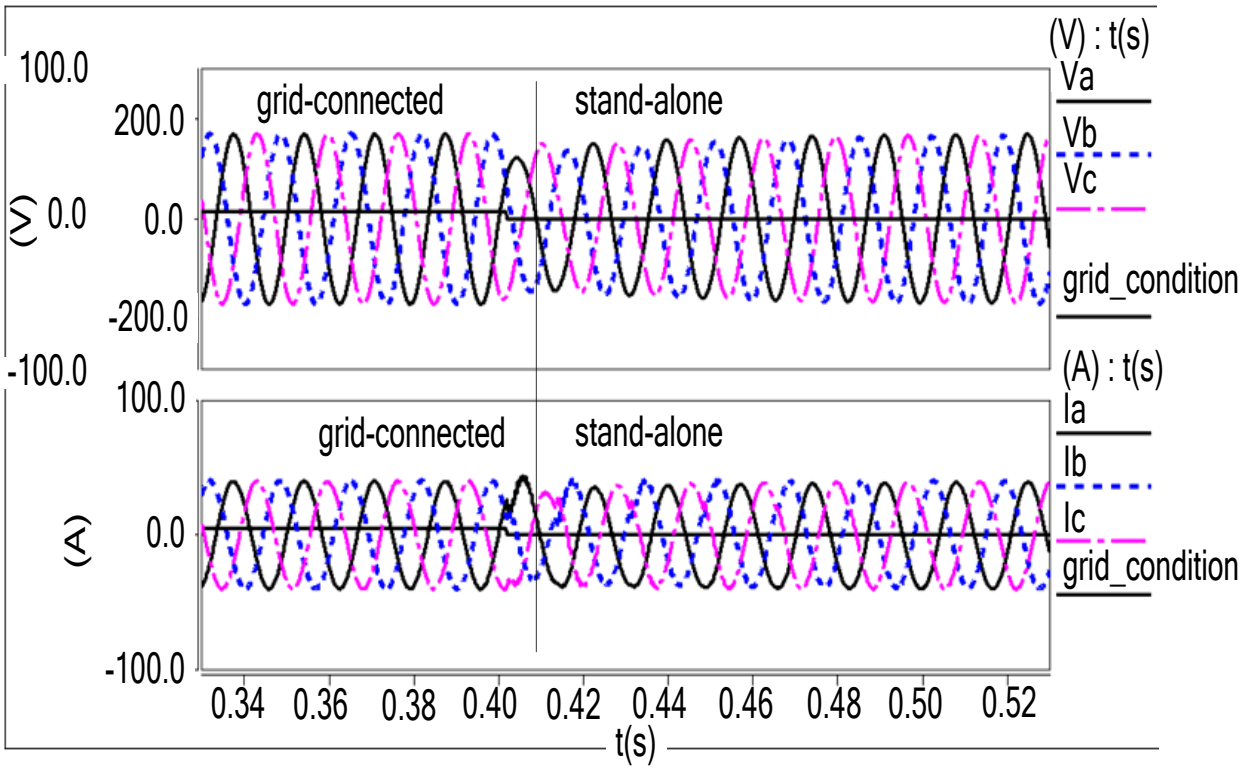

Fig. 5. 14 From grid-connected to stand-alone operation without severe transients

Fig. 5.15 shows a line-to-line voltage and a phase current at the PCC before and after grid disconnection with the seamless transition controller implemented. As can be noticed, the proposed controller successfully suppresses the severe transients caused by the disconnection of the grid.

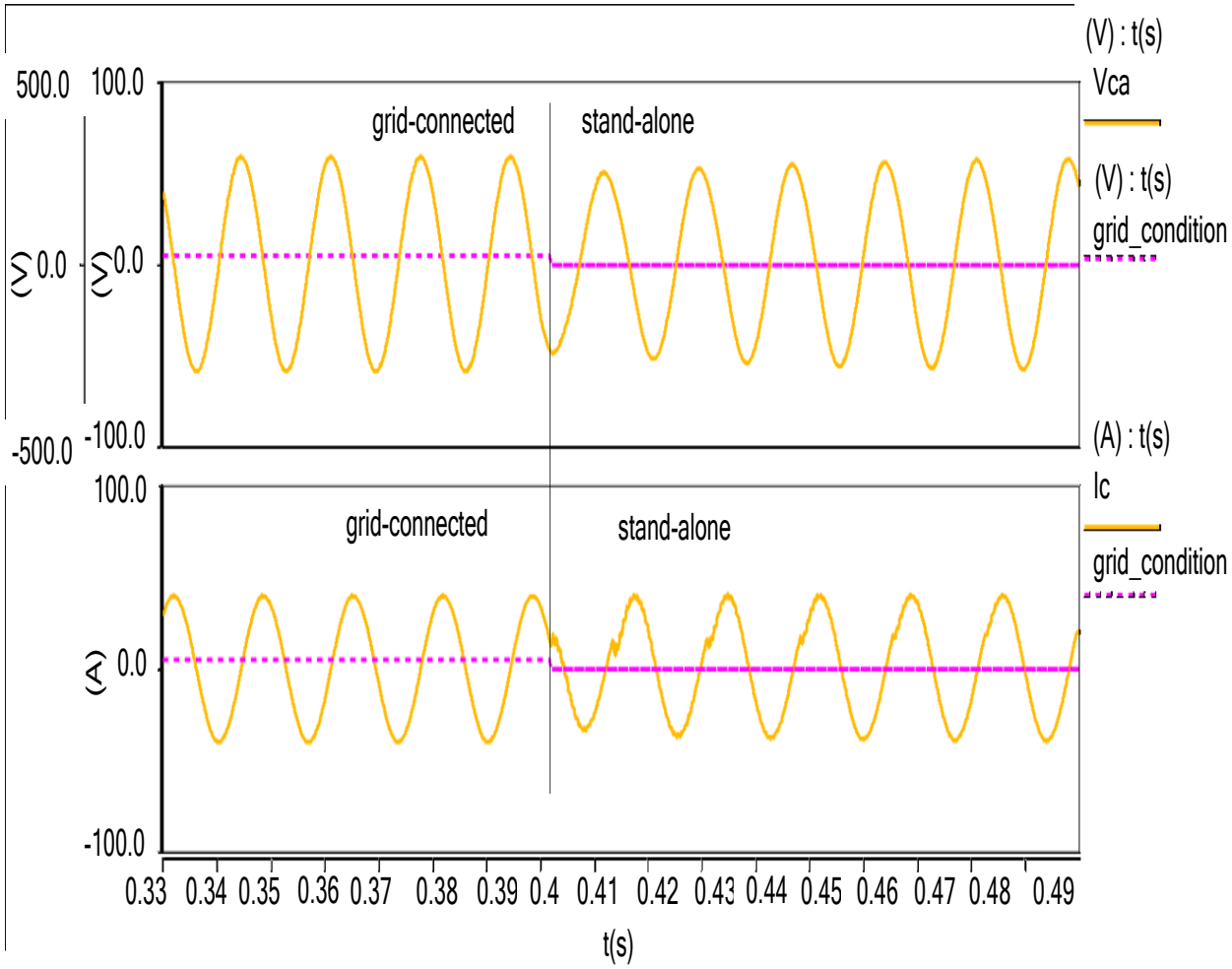

Fig. 5. 15 From grid-connected to stand-alone operation without severe transients

To keep the magnitude of the voltage in its normal operational range when there is a power mismatch, the load shedding algorithm proposed was implemented. Fig. 5.16 shows the theoretical voltage transients under a power difference without the load shedding algorithm implemented. For this case, when the voltage is out of the normal operating point, the load

shedding algorithm cut off the power difference from the load and the voltage was brought back to the normal range. Fig 5.17 shows that the suitable load disconnection results in voltage recovery, compared to the case of "no load shedding".

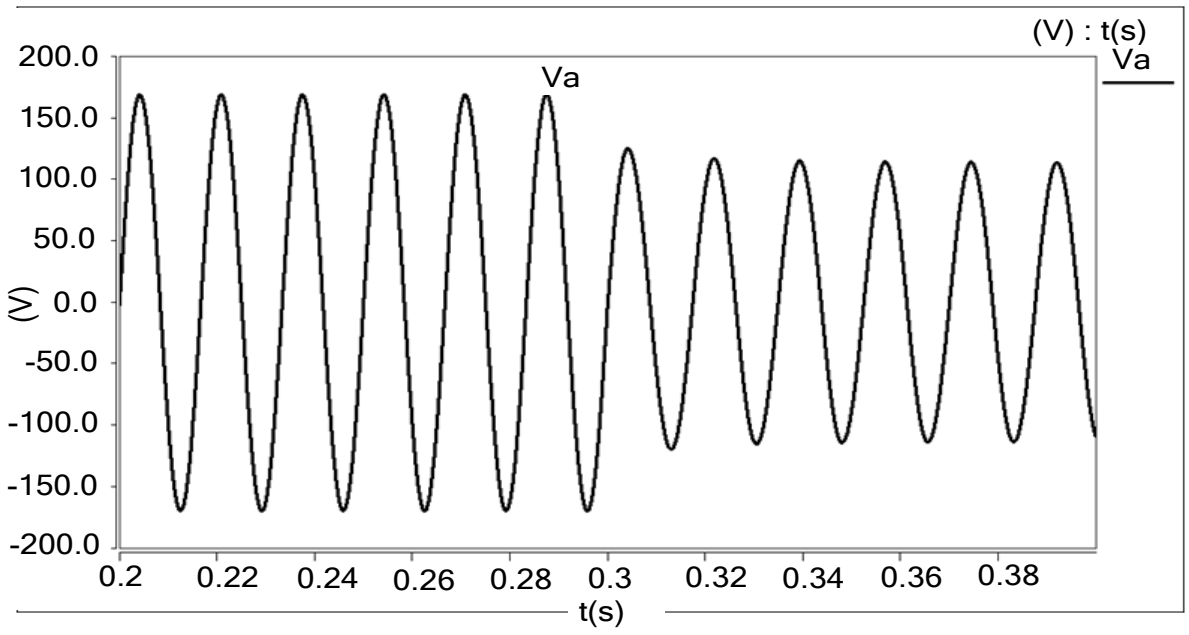

Fig. 5. 16 Phase voltage V_a without load shedding algorithm

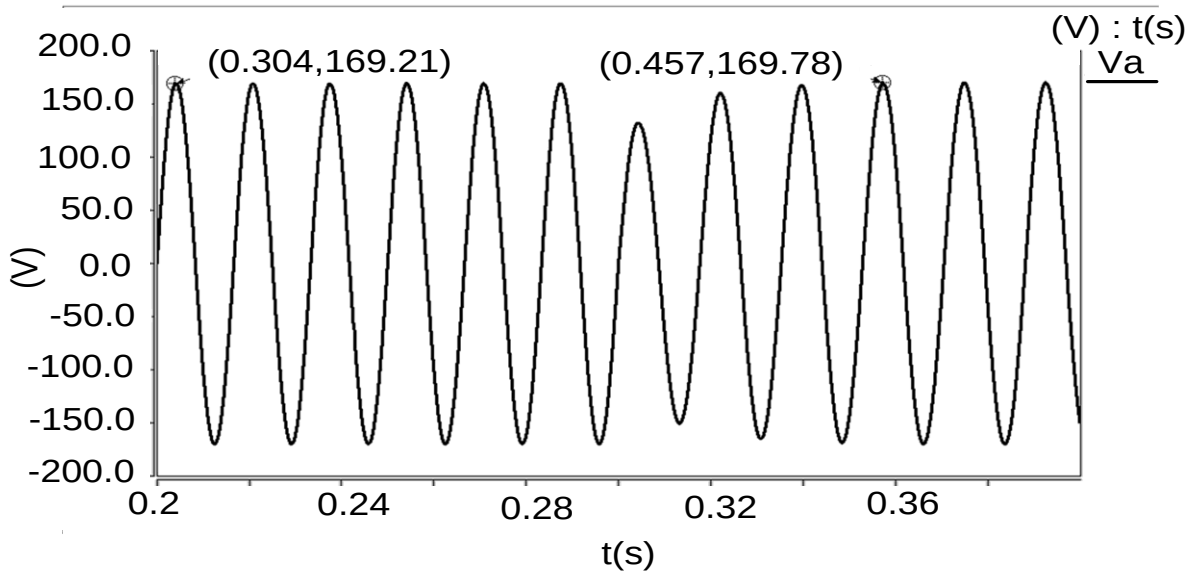

Fig. 5. 17 Phase voltage V_a with load shedding algorithm

5.7. Experimental Results

The DG is started up in grid-connected operation mode, and then the separation device is opened. When the DG is disconnected from the grid it operates in stand-alone mode. Fig. 5.18 shows a voltage and phase currents when the disconnection device is opened and the seamless controller from grid-connected to stand alone is not implemented.

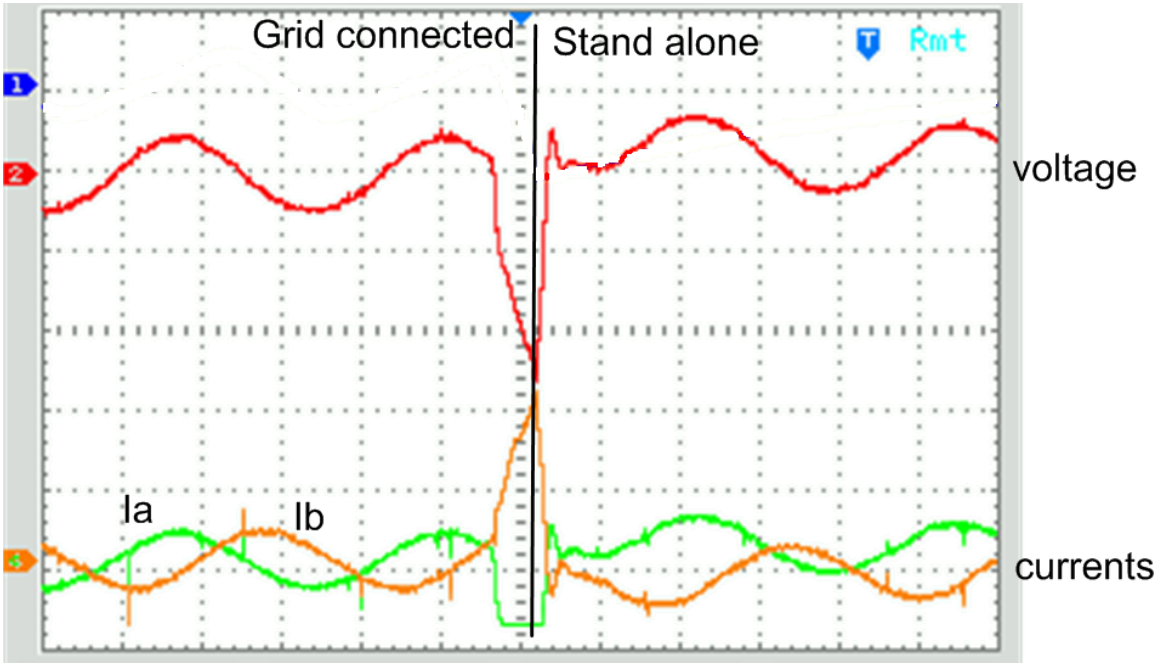

Fig. 5. 18 Transition from grid-connected to stand-alone operation with severe transients

Fig. 5.19 shows the grid voltage, the DG line to line voltage, and the phase current before and after grid disconnection with the seamless transition controller implemented. As can be noticed, the proposed controller successfully suppresses the severe transients caused by the disconnection of the grid.

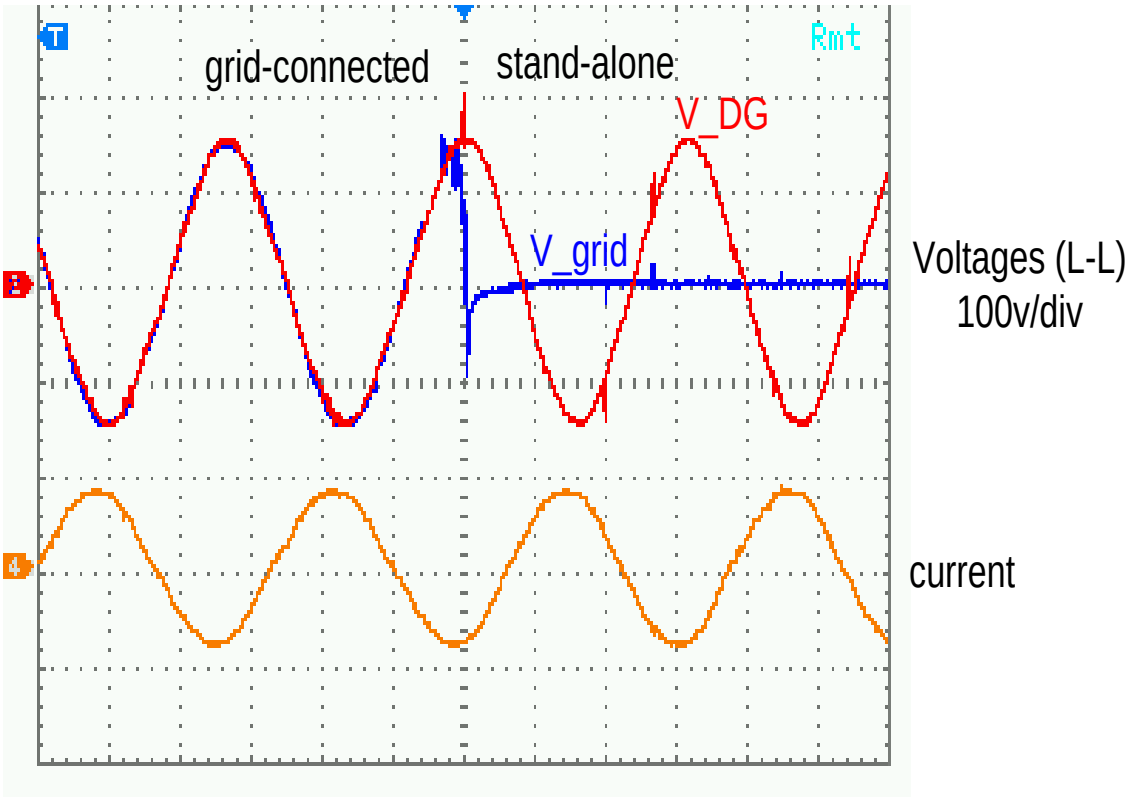

Fig. 5. 19 Transition from grid-connected to intentional islanding operation without severe transients

Fig. 5.20 shows the line to line voltage for the grid and the DG when the system is operating in the islanding mode. Also shown are the load currents for the same type of operation. Fig. 5.21 shows the line to line voltages of the DG and the phase currents when the system is operating in the islanding mode. As can be seen, the proposed control scheme is capable of maintaining the voltages within the designed levels.

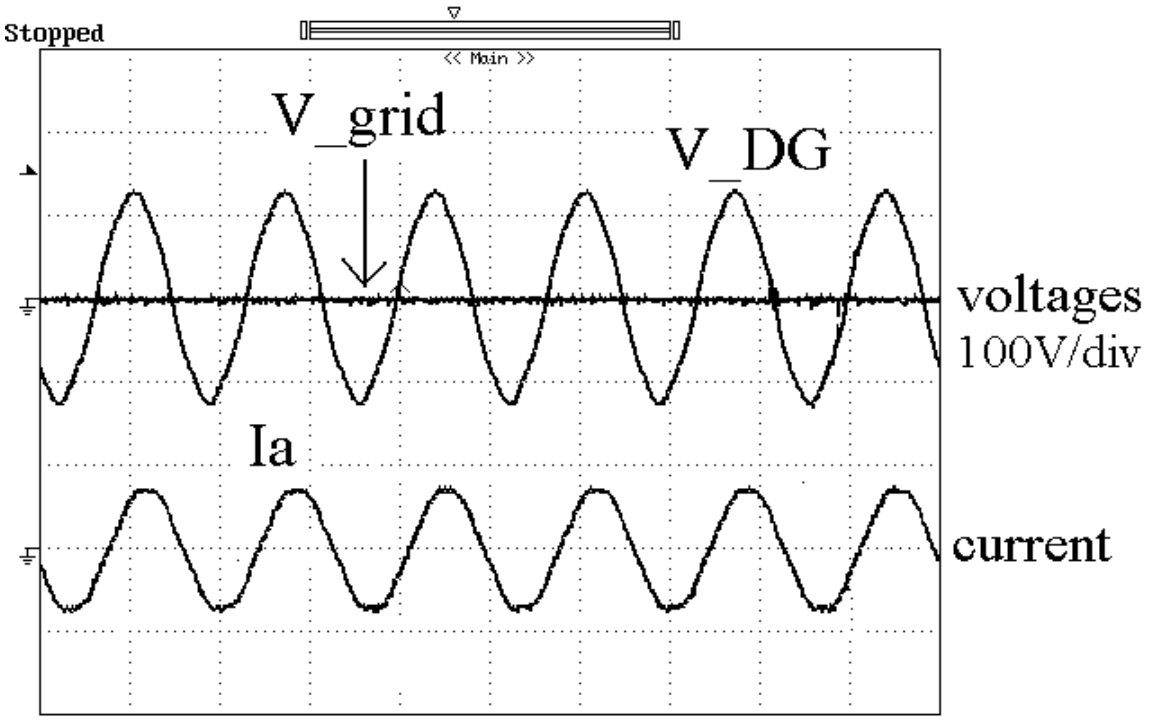

Fig. 5. 20 Line to line voltages and phase currents during intentional islanding operation

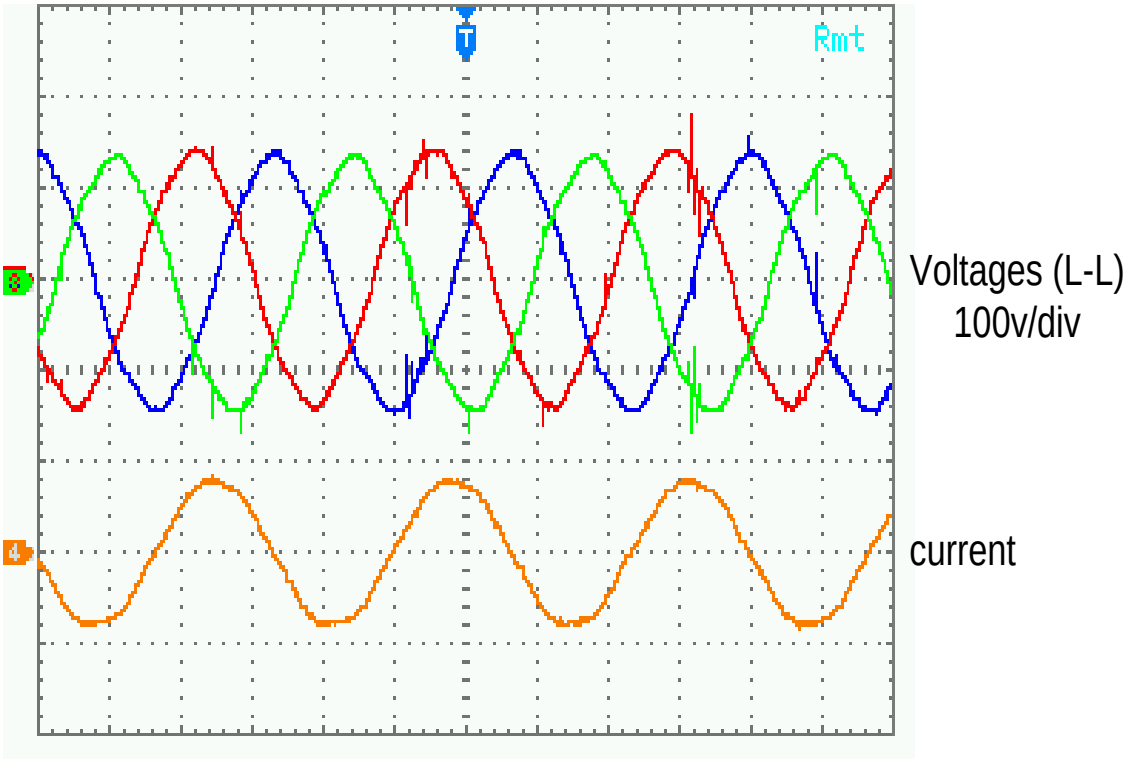

Fig. 5. 21 DG line to line voltages and phase currents during intentional islanding operation

To test the load shedding algorithm, a test case where the islanded network is supplying 330W and importing 330W of active power from the grid was analyzed. Starting from this point, in steady-state, the DG is disconnected and the network will become islanded. As shown in Fig. 5.22 it can be noticed that the suitable load disconnection results in voltage recovery. A total load of around 640 W is curtailed to 320 W through load shedding, which is within the DG capabilities. It can also be noticed from Fig. 5.21 that the load shedding assists the voltage to reach acceptable values above the threshold selected.

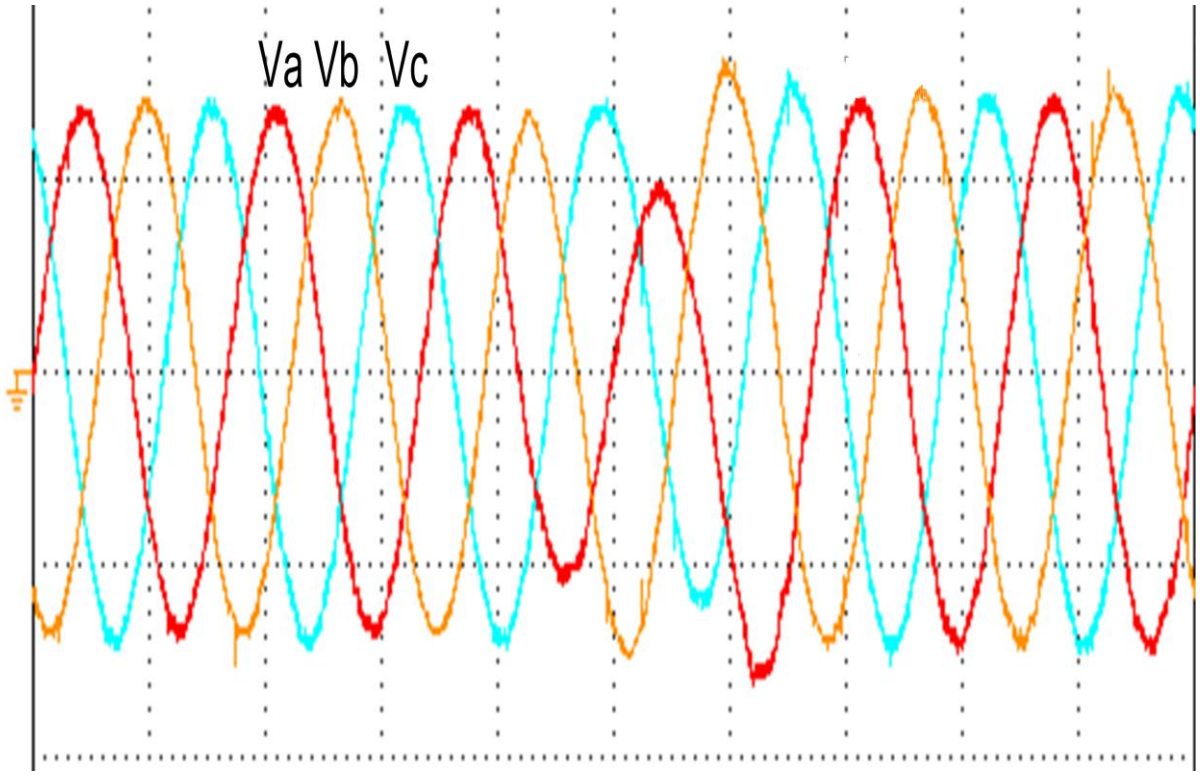

Fig. 5. 22 Implementation of the load shedding algorithm

CHAPTER 6. CONCLUSIONS AND FUTURE WORKS

6.1 Conclusions

This research presented the development and test of a control strategy for DG capable of working in both intentional-islanding (stand-alone) and grid-connected modes. The stand-alone control featured an output voltage controller capable of handling excess or deficit of generated power and synchronization for grid reconnection with a seamless transition from stand-alone to grid-connected operation modes. The grid-connected mode with current control was also enabled for the case of power grid connection. This grid-connected control featured an output current controller capable of loss of main detection, synchronization with the grid, and seamless transition from grid-connected to stand-alone operation modes.

An automatic mode switch method based on a PLL controller was described in order to detect the power grid disconnection or recovery and switch the operation mode accordingly.

The proposed control strategy has the following characteristics:

- Interface with AC System
- Power quality
- Synchronization with the Grid
- Loss of Main Detection or Islanding
- Transitions from grid-connected to stand-alone
- Load shedding
- Reclosing

- Transitions from stand-alone to grid-connected

The simulation results showed that the detection algorithm can distinguish between islanding events and changes in the loads and apply the load shedding algorithms when needed. The experimental results showed that the proposed control schemes are capable of maintaining the voltages within the standard permissible levels during grid-connected and islanding operation modes. In addition, it was shown that the re-closure algorithm causes the DG to resynchronize itself with the grid. Also, the simulation and experimental results show that seamless transfer has been achieved.

6.2 Future Works

There are some issues that could be explored in the future related to this work:

- Throughout this thesis, the DG unit was modeled by an ideal DC source and therefore, the dynamic of the input source was neglected. As a future work, the effect of these dynamic on the islanding detection and control of islanded systems can be studied.
- A situation particular to the three-phase signals is the concept of unbalance. The three-phase signals are unbalanced if they either have unequal magnitudes or phase-displacements unequal to 120 degrees. The performance of the three phase PLL algorithm presented is not good when the utility voltage presents voltage unbalances. If these unbalances are not taking into account, the information of the utility voltage, obtained from PLL structures, can present undesired errors. Based on the theory of symmetrical components, an unbalanced set of signals can be decomposed into positive-, negative- and zero-sequence components. The positive-sequence component is a

balanced set of signals. To eliminate the distorted utility voltage effects, a positive sequence computation block can be used with good performance. This situation can be considered as a future work.

- One of the selling points for DG is that the local generation follows a scalable system model, where due to the typical small size of the units, one can install as many units as needed to satisfy the requests of the loads, without having too much of extra capacity sitting idle. This concept requires that DGs can be installed in parallel without any restrictions.
- Storage need to be incorporated to satisfy the instantaneous power balance as a new load comes on-line without penalizing the quality of other network quantities, such as bus voltage magnitude. Load changes resulting in fast transients that exceed the ramping capability of generation require storage availability from which to draw the required transient energy. This inertia-less system presented is not well suited to handle step changes in the requested output power.

APPENDICES

Appendix 1. Transfer Functions of the current controlled inverter

Fig. A1.1 shows the block diagram of the DG interface control for grid-connected operation.

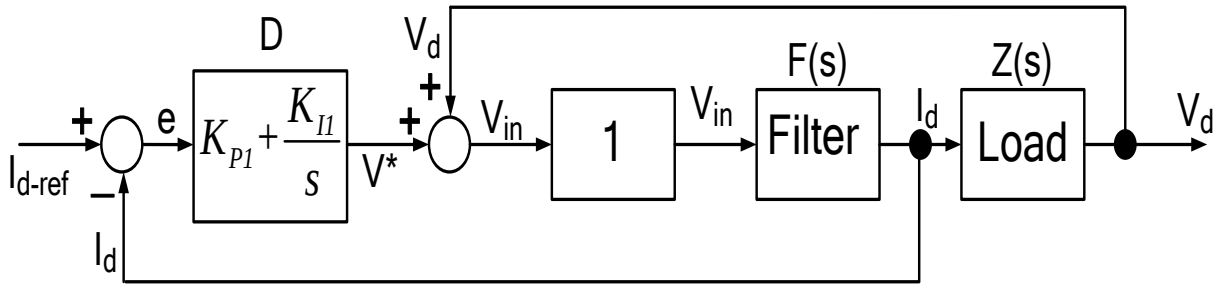

Fig. A1. 1 Block diagram of the current controlled inverter

The PI controller produces a signal that is proportional to the time integral of the controller. The transfer function of the PI controller is given by:

$$D = K_{P1} + \frac{K_{I1}}{s} \tag{A1.1}$$

where k_p is the proportional gain and k_I the integral gain.

The inverter stage does not have any significant transient time associated with it and hence it is modeled as an ideal gain. This ideal gain can be given by $G_I(s) = 1$.

The schematic circuit of the filter stage is shown in Fig. A1.2. It consists of an LCL filter and a parallel RLC load.

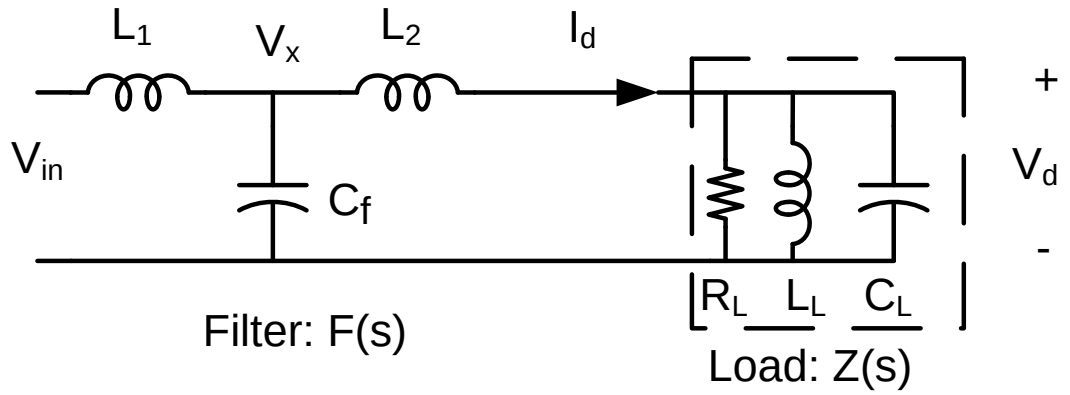

Fig. A1. 2 LCL Filter and parallel RLC load

The transfer function of the filter is given by:

$$F(s) = \frac{I_d(s)}{V_{in}(s)} \tag{A1.2}$$

By Kirchhoff Current Law, the following expression is obtained:

$$\frac{V_x - V_{in}}{sL_1} + sC_f V_x + I_d(s) = 0 \tag{A1.3}$$

Equation (A1.3) can be re-expressed as:

$$\frac{V_x}{sL_1} - \frac{V_{in}}{sL_1} + sC_f V_x + I_d(s) = 0 \tag{A1.4}$$

Using Ohm's Law, the current I_d is given by:

$$I_d(s) = \frac{V_x - 0}{sL_2 + Z(s)} \tag{A1.5}$$

From equation (A1.5), the voltage V_x is given by:

$$V_x = I_d(sL_2 + Z) \tag{A1.6}$$

Substituting equation (A1.6) into equation (A1.4)

$$\frac{I_d(sL_2 + Z)}{sL_1} - \frac{V_{in}}{sL_1} + sC_f\left(I_d(sL_2 + Z)\right) + I_d(s) = 0 \tag{A1.7}$$

Equation (A1.7) can be re-expressed as:

$$\frac{sI_dL_2}{sL_1} + \frac{I_dZ}{sL_1} - \frac{V_{in}}{sL_1} + I_d + s^2C_fI_dL_2 + sC_fI_dZ = 0 \tag{A1.8}$$

$$I_d\left[s^2C_fL_2 + sC_fZ + \frac{Z}{sL_1} + \frac{L_2}{L_1} + 1\right] = \frac{V_{in}}{sL_1} \tag{A1.9}$$

$$\frac{V_{in}}{I_d} = sL_1\left[s^2 C_f L_2 + sC_f Z + \frac{Z}{sL_1} + \frac{L_2}{L_1} + 1 \right] \tag{A1.10}$$

$$\frac{V_{in}}{I_d} = s^3 C_f L_1 L_2 + s^2 C_f L_1 Z + s\left(L_1 + L_2\right) + Z \tag{A1.11}$$

Then, the transfer function of the filter, *F(s)*, is given by:

$$F(s) = \frac{I_d(s)}{V_{in}(s)} = \frac{1}{s^3 C_f L_1 L_2 + s^2 C_f L_1 Z + s\left(L_1 + L_2\right) + Z} \tag{A1.12}$$

The transfer function of the load, *Z(s)*, is given by:

$$Z(s) = \frac{V_d(s)}{I_d(s)} \tag{A1.13}$$

By Kirchhoff Current Law:

$$I_d = I_{R_L} + I_{L_L} + I_{C_L} \tag{A1.14}$$

$$I_d = \frac{V_d}{R_L} + \frac{V_d}{sL_L} + sC_L V_d \tag{A1.15}$$

Equation (A1.15) can be re-expressed as:

$$I_d = V_d \left[\frac{1}{R_L} + \frac{1}{sL_L} + sC_L \right] \tag{A1.16}$$

$$\frac{I_d}{V_d} = \left[\frac{1}{R_L} + \frac{1}{sL_L} + sC_L \right] \tag{A1.17}$$

Then, the transfer function of the load, *Z(s)*, is given by:

$$Z(s) = \frac{V_d(s)}{I_d(s)} = \frac{1}{\frac{1}{R_L} + \frac{1}{sL_L} + sC_L} \tag{A1.18}$$

This can be re-expressed as:

$$Z(s) = \frac{sL_L R_L}{s^2 R_L C_L L_L + sL_L + R_L} \tag{A1.19}$$

Using Fig. A1.2 and equations (A1.12) and (A1.19), the transfer function of the current controlled system is derived as:

$$H(s) = \frac{V_d(s)}{I_{d-ref}(s)} \tag{A1.20}$$

$$I_{d-ref} - I_d = e \tag{A1.21}$$

$$eD = V^* \tag{A1.22}$$

$$V^* + V_d = V_{in} \tag{A1.23}$$

$$V_{in} F = I_d \tag{A1.24}$$

$$I_d Z = V_d \tag{A1.25}$$

From equation (A1.25),

$$I_d = \frac{V_d}{Z} \tag{A1.26}$$

Substituting equation (A1.25) into equation (A1.24)

$$V_{in} F = \frac{V_d}{Z} \tag{A1.27}$$

Equation (A1.27) can be re-expressed as:

$$V_{in} = \frac{V_d}{FZ} \tag{A1.28}$$

Substituting equation (A1.27) into equation (A1.23)

$$V^{*} + V_d = \frac{V_d}{FZ} \tag{A1.29}$$

Substituting equation (A1.22) into equation (A1.29)

$$eD + V_d = \frac{V_d}{FZ} \tag{A1.30}$$

From equation (A1.30)

$$e = \left(\frac{V_d}{FZ} - V_d \right) \frac{1}{D} \tag{A1.31}$$

From equation (A1.31)

$$I_{d-ref} - \frac{V_d}{Z} = \left(\frac{1}{FZ} - 1 \right) \frac{V_d}{D} \tag{A1.32}$$

Equation (A1.32) can be re-expressed as:

$$I_{d-ref} = \frac{V_d}{FZD} - \frac{V_d}{D} + \frac{V_d}{Z} \tag{A1.33}$$

$$I_{d-ref} = \left[\frac{1}{FZD} - \frac{1}{D} + \frac{1}{Z}\right] V_d \tag{A1.34}$$

$$\frac{I_{d-ref}}{V_d} = \frac{1}{FZD} - \frac{1}{D} + \frac{1}{Z} \tag{A1.35}$$

$$\frac{I_{d-ref}}{V_d} = \frac{1 - ZF + FD}{FZD} \tag{A1.36}$$

Then, the transfer function of the voltage controller, H(s), is given by:

$$H(s) = \frac{V_d(s)}{I_{d-ref}(s)} = \frac{FZD}{(1 - FZ + FD)} \tag{A1.37}$$

Where

$$Z(s) = \frac{sL_L R_L}{s^2 R_L C_L L_L + sL_L + R_L}$$

$$F(s) = \frac{1}{s^3 C_f L_1 L_2 + s^2 C_f L_1 Z + s(L_1 + L_2) + Z}$$

$$C = K_{P1} + \frac{K_{I1}}{s}$$

$$R_L = 4.33\Omega$$

$$L_L = 4.584mH$$

$$C_L = 1.535mF$$

$$L_1 = 1mH$$

$$L_2 = 0.5mH$$

$$C_f = 31\mu F$$

$$K_{P1} = 0.8$$

$$K_{I1} = 25$$

$$Z(s) = \frac{651.466s}{s^2 + 150.454s + 142117}$$

$$F(s) = \frac{6.4516x10^{10}\left(s^2 + 150.454s + 142117\right)}{s^5 + 150.454s^4 + 9.8219x10^7 s^3 + 1.456x10^{10}s^2 + 5.5783x10^{13}s + 0.4187}$$

$$D = 0.8 + \frac{25}{s}$$

$$H(s) = \frac{3.365x10^{13}s^2 + 1.051s}{s^6 + 150.108s^5 + 9.83x10^7 s^4 + 6.62x10^{10} s^3 + 2.31x10^{13}s^2 + 7.58x10^{15}s + 2.28x10^{17}}$$

Appendix 2. Derivation of the Load Shedding Equations

The approach proposed is to detect the voltage change rate and profile after the power outage and determine how much load shedding is needed before going to the intentional islanding operation and switching to the voltage control mode. In order to accomplish this, the system shown in Fig. A2.1 has been analyzed.

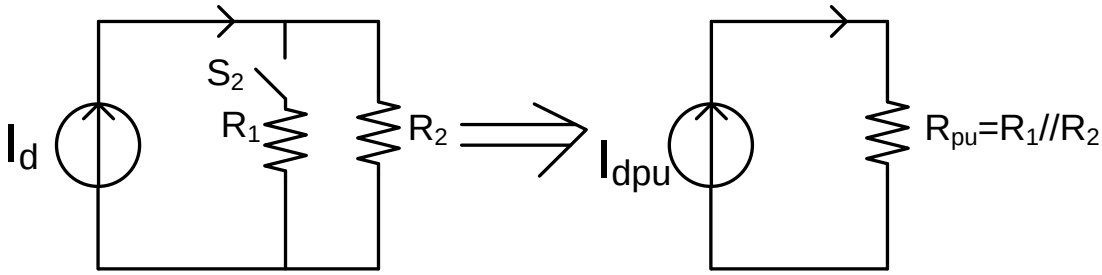

Fig. A2. 1 System to implement load shedding

○ Obtain the voltage amplitude expression before load shedding. The expressions for the load voltages V_{apu}, V_{bpu}, and V_{cpu} can be found:

$$\frac{V_a}{R} = I_d \sin(\omega t + \theta) \tag{A2.1}$$

$$\frac{V_b}{R} = I_d \sin\left(\omega t + \theta - \frac{2\pi}{3}\right) \tag{A2.2}$$

$$\frac{V_c}{R} = I_d \sin\left(\omega t + \theta + \frac{2\pi}{3}\right) \tag{A2.3}$$

In per unit:

$$\frac{V_{apu}}{R_{pu}} = I_{dpu} \sin(\omega t + \theta) \tag{A2.4}$$

$$\frac{V_{bpu}}{R_{pu}} = I_{dpu}\sin\left(\omega t+\theta-\frac{2\pi}{3}\right) \quad \text{(A2.5)}$$

$$\frac{V_{cpu}}{R_{pu}} = I_{dpu}\sin\left(\omega t+\theta+\frac{2\pi}{3}\right) \quad \text{(A2.6)}$$

Solving for the voltages:

$$V_{apu} = I_{dpu}R_{pu}\sin(\omega t+\theta) \quad \text{(A2.7)}$$

$$V_{bpu} = I_{dpu}R_{pu}\sin\left(\omega t+\theta-\frac{2\pi}{3}\right) \quad \text{(A2.8)}$$

$$V_{cpu} = I_{dpu}R_{pu}\sin\left(\omega t+\theta+\frac{2\pi}{3}\right) \quad \text{(A2.9)}$$

- Using V_{apu}, V_{bpu}, and V_{cpu} an expression for the voltage amplitude can be found,

$$V_{pk} = \sqrt{\frac{2}{3}}\sqrt{V_{ab}^2+V_{bc}^2+V_{ca}^2} \quad \text{(A2.10)}$$

$$V_{abpu} = V_{apu}-V_{bpu} = I_{dpu}R_{pu}\sin(\omega t+\theta)-I_{dpu}R_{pu}\sin\left(\omega t+\theta-\frac{2\pi}{3}\right) \quad \text{(A2.11)}$$

$$V_{abpu} = I_{dpu}R_{pu}\left[\sin(\omega t+\theta)-\sin\left(\omega t+\theta-\frac{2\pi}{3}\right)\right] \quad \text{(A2.12)}$$

$$V_{abpu} = I_{dpu}R_{pu}\left[\sqrt{3}\sin\left(\omega t+\theta+\frac{\pi}{6}\right)\right] \quad \text{(A2.13)}$$

$$V_{abpu} = \sqrt{3}I_{dpu}R_{pu}\sin\left(\omega t+\theta+\frac{\pi}{6}\right) \quad \text{(A2.14)}$$

$$V_{bcpu} = V_{bpu}-V_{cpu} = I_{dpu}R_{pu}\sin\left(\omega t+\theta-\frac{2\pi}{3}\right)-I_{dpu}R_{pu}\sin\left(\omega t+\theta+\frac{2\pi}{3}\right) \quad \text{(A2.15)}$$

$$V_{bcpu} = I_{dpu}R_{pu}\left[\sin\left(\omega t+\theta-\frac{2\pi}{3}\right)-\sin\left(\omega t+\theta+\frac{2\pi}{3}\right)\right] \quad \text{(A2.16)}$$

$$V_{bcpu} = I_{dpu} R_{pu} \left[-\sqrt{3} \cos\left(\omega t + \theta\right) \right] \tag{A2.17}$$

$$V_{bcpu} = -\sqrt{3} I_{dpu} R_{pu} \cos\left(\omega t + \theta\right) \tag{A2.18}$$

$$V_{capu} = V_{cpu} - V_{apu} = I_{dpu} R_{pu} \sin\left(\omega t + \theta + \frac{2\pi}{3} \right) - I_{dpu} R_{pu} \sin(\omega t + \theta) \tag{A2.19}$$

$$V_{capu} = I_{dpu} R_{pu} \left[\sin\left(\omega t + \theta + \frac{2\pi}{3} \right) - \sin(\omega t + \theta) \right] \tag{A2.20}$$

$$V_{capu} = I_{dpu} R_{pu} \left[\sqrt{3} \cos\left(\omega t + \theta + \frac{\pi}{3} \right) \right] \tag{A2.21}$$

$$V_{capu} = \sqrt{3} I_{dpu} R_{pu} \cos\left(\omega t + \theta + \frac{\pi}{3} \right) \tag{A2.22}$$

$$V_{abpu}^2 = 3 I_{dpu}^2 R_{pu}^2 \sin^2\left(\omega t + \theta + \frac{\pi}{6} \right) \tag{A2.23}$$

$$V_{bcpu}^2 = 3 I_{dpu}^2 R_{pu}^2 \cos^2\left(\omega t + \theta\right) \tag{A2.24}$$

$$V_{capu}^2 = 3 I_{dpu}^2 R_{pu}^2 \cos^2\left(\omega t + \theta + \frac{\pi}{3} \right) \tag{A2.25}$$

$$\begin{aligned} & V_{abpu}^2 + V_{bcpu}^2 + V_{capu}^2 \\ & = 3 I_{dpu}^2 R_{pu}^2 \left[\cos^2\left(\omega t + \theta + \frac{\pi}{3} \right) + \cos^2\left(\omega t + \theta\right) + \sin^2\left(\omega t + \theta + \frac{\pi}{6} \right) \right] \end{aligned} \tag{A2.26}$$

$$\begin{aligned} & \sqrt{V_{abpu}^2 + V_{bcpu}^2 + V_{capu}^2} \\ & = \sqrt{3} I_{dpu} R_{pu} \sqrt{\cos^2\left(\omega t + \theta + \frac{\pi}{3} \right) + \cos^2\left(\omega t + \theta\right) + \sin^2\left(\omega t + \theta + \frac{\pi}{6} \right)} \end{aligned} \tag{A2.27}$$

$$V_{pk} = \sqrt{\frac{2}{3}} \sqrt{V_{ab}^2 + V_{bc}^2 + V_{ca}^2} \tag{A2.28}$$

$$V_{pk} = \sqrt{\frac{2}{3}}\sqrt{3} I_{dpu} R_{pu} \sqrt{\cos^2\left(\omega t + \theta + \frac{\pi}{3}\right) + \cos^2\left(\omega t + \theta\right) + \sin^2\left(\omega t + \theta + \frac{\pi}{6}\right)} \tag{A2.29}$$

$$V_{pk} = \sqrt{2} I_{dpu} R_{pu} \sqrt{\cos^2\left(\omega t + \theta + \frac{\pi}{3}\right) + \cos^2\left(\omega t + \theta\right) + \sin^2\left(\omega t + \theta + \frac{\pi}{6}\right)} \tag{A2.30}$$

- Derive the slope of the voltage amplitude

$$s = \frac{d\left(V_{pk}(t)\right)}{dt} \tag{A2.31}$$

$$s = \frac{-\sqrt{2} I_{dpu} R_{pu} \omega K}{\sqrt{\cos^2\left(\omega t + \theta + \frac{\pi}{3}\right) + \cos^2\left(\omega t + \theta\right) + \sin^2\left(\omega t + \theta + \frac{\pi}{6}\right)}} \tag{A2.32}$$

where

$$K = \sin\left(\omega t + \theta + \frac{\pi}{3}\right)\cos\left(\omega t + \theta + \frac{\pi}{3}\right) - \sin\left(\omega t + \theta + \frac{\pi}{6}\right)\cos\left(\omega t + \theta + \frac{\pi}{6}\right) + \sin\left(\omega t + \theta\right)\cos\left(\omega t + \theta\right) \tag{A2.33}$$

Solving for I_{dpu}

$$I_{dpu} = \frac{-s\sqrt{2}\sqrt{\cos^2\left(\omega t + \theta + \frac{\pi}{3}\right) + \cos^2\left(\omega t + \theta\right) + \sin^2\left(\omega t + \theta + \frac{\pi}{6}\right)}}{2\omega R_{pu} K} \tag{A2.34}$$

Using $R_{pu} = R_1 // R_2$ and solving for R_1, where R_1 represents the load to be shed,

$$R_{1pu} = \frac{-\sqrt{2}\omega I_{dpu} K}{s\sqrt{\cos^2\left(\omega t + \theta + \frac{\pi}{3}\right) + \cos^2\left(\omega t + \theta\right) + \sin^2\left(\omega t + \theta + \frac{\pi}{6}\right) + \sqrt{2}\omega I_{dpu} K}} \tag{A2.35}$$

Appendix 3. Transfer Functions of the voltage controlled inverter

Fig. A3.1 shows the block diagram of the DG interface control for intentional islanding operation.

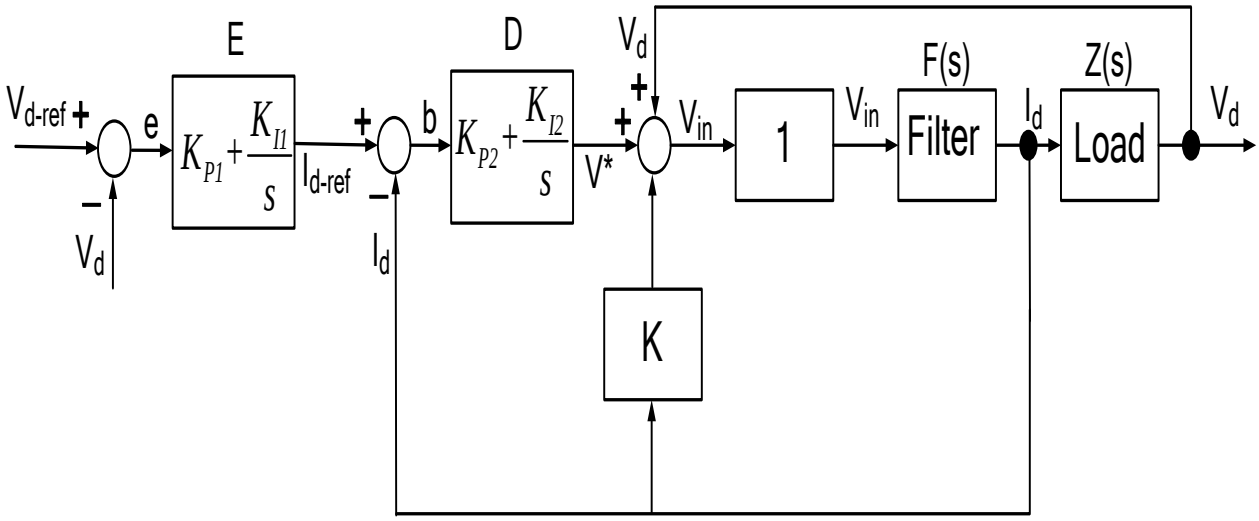

Fig. A3. 1 Block diagram of the voltage controlled inverter

The PI controllers produce a signal that is proportional to the time integral of the controller. The transfer functions of the PI controllers are given by:

$$E = K_{P1} + \frac{K_{I1}}{s} \tag{A3.1}$$

$$D = K_{P2} + \frac{K_{I2}}{s} \tag{A3.2}$$

The inverter stage does not have any significant transient time associated with it and hence it is modeled as an ideal gain. This ideal gain can be given by $G_I(s) = 1$.

The schematic circuit of the filter stage is shown in Fig. A3.2. It consists of an LCL filter and a parallel RLC load.

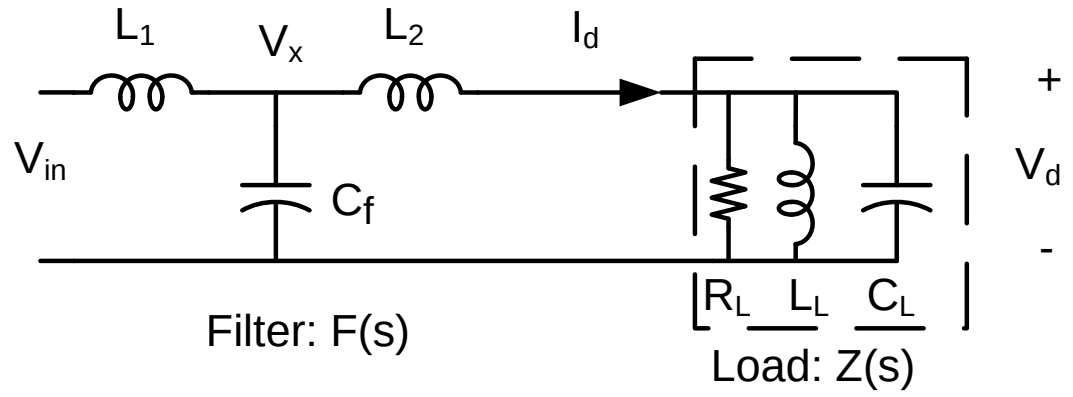

Fig. A3. 2 LCL Filter and parallel RLC load

The transfer function of the filter is given by:

$$F(s)=\frac{I_d(s)}{V_{in}(s)}=\frac{1}{s^3C_fL_1L_2+s^2C_fL_1Z+s\left(L_1+L_2\right)+Z} \tag{A3.3}$$

The transfer function of the load, *Z(s)*, is given by:

$$Z(s)=\frac{sL_LR_L}{s^2R_LC_LL_L+sL_L+R_L} \tag{A3.4}$$

Using Fig. A3.9 and equations (A3.3) to (A3.4), the transfer function of the current controlled system is derived as:

$$H(s)=\frac{V_d(s)}{V_{d-ref}(s)} \tag{A3.5}$$

$$V_{d-ref}-V_d=e \tag{A3.6}$$

$$eE=I_{d-ref} \tag{A3.7}$$

$$eE - I_d = b \tag{A3.8}$$

$$bD + V_d - KI_d = V_{in} \tag{A3.9}$$

$$V_{in}F = I_d \tag{A3.10}$$

$$I_d Z = V_d \tag{A3.11}$$

From (A3.11),

$$I_d = \frac{V_d}{Z} \tag{A3.12}$$

(A3.12) in (A3.10)

$$V_{in}F = \frac{V_d}{Z} \tag{A3.13}$$

From (A3.13)

$$V_{in} = \frac{V_d}{FZ} \tag{A3.14}$$

(A3.14) in (A3.9)

$$bD + V_d - K\frac{V_d}{Z} = \frac{V_d}{FZ} \tag{A3.15}$$

From (A3.15)

$$b = V_d\left(\frac{1}{FZ} - 1 + \frac{K}{Z}\right)\frac{1}{D} \tag{A3.16}$$

(A3.16) and (A3.12) in (A3.8)

$$eE - \frac{V_d}{Z} = \left(\frac{1}{FZ} - 1 + \frac{K}{Z}\right)\frac{V_d}{D} \tag{A3.17}$$

From (A3.17)

$$e = \left(\frac{1}{FZD} + \frac{K}{ZD} - \frac{1}{D} + \frac{1}{Z}\right)\frac{V_d}{E} \tag{A3.18}$$

(A3.18) in (A3.6)

$$V_{d-ref} = e + V_d \tag{A3.19}$$

$$V_{d-ref} = \left(\frac{1}{EFZD} + \frac{K}{EZD} - \frac{1}{ED} + \frac{1}{ZE} + 1 \right) V_d \tag{A3.20}$$

From (A3.0)

$$H(s) = \frac{V_d(s)}{V_{d-ref}(s)} = \frac{FZDE}{\left(1 + KF - FZ + FD + FZDE\right)} \tag{A3.21}$$

Using $K = 0.9425$, $R_L = 4.33\Omega$, $L_L = 4.584mH$, $C_L = 1.535mF$, $L_1 = 1mH$, $L_2 = 0.5mH$,

$C_f = 31\mu F$, $K_{P1} = 0.8$, $K_{I1} = 25$, $K_{P2} = \frac{1}{0.8}$, $K_{I2} = \frac{1}{25}$, then,

$$Z(s) = \frac{651.466s}{s^2 + 150.454s + 142117} \tag{A3.22}$$

$$F(s) = \frac{6.4516x10^{10}\left(s^2 + 150.454s + 142117\right)}{s^5 + 150.454s^4 + 9.8219x10^7 s^3 + 1.456x10^{10} s^2 + 5.5783x10^{13} s + 0.4187} \tag{A3.23}$$

$$E = 0.8 + \frac{25}{s} \tag{A3.24}$$

$$D = 1.25 + \frac{1}{25s} \tag{A3.25}$$

$$H(s) = \frac{V_d(s)}{V_{d-ref}(s)} = \frac{FZDE}{\left(1 + KF - FZ + FD + FZDE\right)} \tag{A3.26}$$

$$H(s) = \frac{4.203x10^{13}\left(s^2 + 31.282s + 1\right)}{s^6 + 150.454s^5 + 9.8219x10^7 s^4 + 1.5601x10^{11} s^3 + 7.7068x10^{13} s^2 + 2.1418x10^{16} s + 4.0878x10^{14}} \tag{A3.27}$$

Appendix 4. Block Diagram of the 2407A DSP Controller

Fig. A4.1 shows the block diagram of the basic configuration for the LF2407A DSp controller. The major interfaces of the board include the target RAM, SRAM memory, analog interface, analog signals interface, PWM output signal interfaces, among others functions.

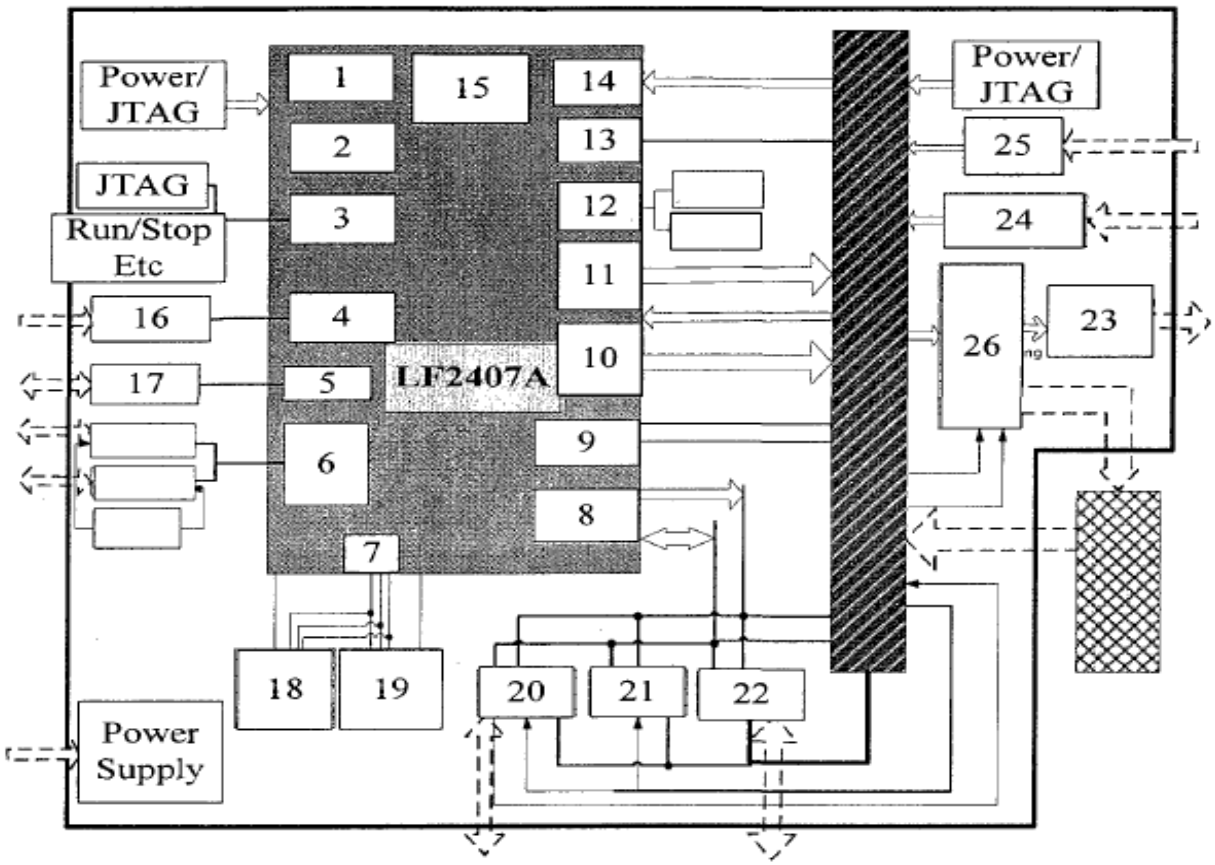

Fig. A4. 1 Block diagram of the 2407A DSP controller

REFERENCES

REFERENCES

[1] A. Ajaja, "Reinventing electric distribution," *Potentials, IEEE,* vol. 29, pp. 29-31, 2010.

[2] E. M. Stewart, *et al.*, "Analysis of a Distributed Grid-Connected Fuel Cell During Fault Conditions," *Power Systems, IEEE Transactions on,* vol. 25, pp. 497-505, 2010.

[3] J. C. Vasquez, *et al.*, "Adaptive Droop Control Applied to Voltage-Source Inverters Operating in Grid-Connected and Islanded Modes," *Industrial Electronics, IEEE Transactions on,* vol. 56, pp. 4088-4096, 2009.

[4] C.-S. Wu, *et al.*, "Design of intelligent utility-interactive inverter with AI detection," in *Electric Utility Deregulation and Restructuring and Power Technologies, 2008. DRPT 2008. Third International Conference on*, 2008, pp. 2012-2017.

[5] G. Franceschini, *et al.*, "Synchronous Reference Frame Grid Current Control for Single-Phase Photovoltaic Converters," in *Industry Applications Society Annual Meeting, 2008. IAS '08. IEEE,* 2008, pp. 1-7.

[6] J. Selvaraj and N. A. Rahim, "Multilevel Inverter For Grid-Connected PV System Employing Digital PI Controller," *Industrial Electronics, IEEE Transactions on,* vol. 56, pp. 149-158, 2009.

[7] M. ROPP, *et al.*, "Sandia Smart Anti-Islanding Project; Summer 2001: Task II Investigation of the Impact of Single-Phase Induction Machines in Islanded Loads: Summary of Results," SAND2002-1320; TRN: US200222%%275, 2002.

[8] T. C. Green and M. Prodanovic, "Control of inverter-based micro-grids," *Electric Power Systems Research,* vol. 77, pp. 1204-1213, 2007.

[9] M. E. Haque, *et al.*, "A Novel Control Strategy for a Variable-Speed Wind Turbine With a Permanent-Magnet Synchronous Generator," *Industry Applications, IEEE Transactions on,* vol. 46, pp. 331-339, 2010.

[10] J. C. Vasquez, *et al.*, "Hierarchical Control of Intelligent Microgrids," *Industrial Electronics Magazine, IEEE,* vol. 4, pp. 23-29, 2010.

[11] L. Yunwei, "Development of power conditioners and controllers for Microgrids," DOCTOR OF PHILOSOPHY, School of Electrical and Electronic Engineering, Nanyang Technological University, 2005.

[12] R. A. Prata, "Impact of distributed generation connection with distribution grids - two case-studies," in *Power Engineering Society General Meeting, 2006. IEEE*, 2006, p. 8 pp.

[13] N. Pogaku, "Analysis, Control and Testing of Inverter-Based Distributed Generation in Standalone and Grid-Connected Applications," Ph.D., University of London, 2006.

[14] Y. Zhou, *et al.*, "Grid-connected and islanded operation of a hybrid power system," in *Power Engineering Society Conference and Exposition in Africa, 2007. PowerAfrica '07. IEEE*, 2007, pp. 1-6.

[15] V. T. Consortium on Energy Restructuring. (2008, *Distributed Generation Education Modules*. Available: http://www.history.vt.edu/Hirsh/CER/CER-Base.htm

[16] S. P. Chowdhury, *et al.*, "UK scenario of islanded operation of active distribution networks — A survey," in *Power and Energy Society General Meeting - Conversion and Delivery of Electrical Energy in the 21st Century, 2008 IEEE*, 2008, pp. 1-6.

[17] A. A. Bayod-Rújula, "Future development of the electricity systems with distributed generation," *Energy*, vol. 34, pp. 377-383, 2009.

[18] A. A. Salam, *et al.*, "A 50kW PEM fuel cell inverter-based distributed generation system for grid connected and islanding operation," in *TENCON 2009 - 2009 IEEE Region 10 Conference*, 2009, pp. 1-5.

[19] M. Ciobotaru, *et al.*, "Accurate and less-disturbing active anti-islanding method based on PLL for grid-connected PV Inverters," in *Power Electronics Specialists Conference, 2008. PESC 2008. IEEE*, 2008, pp. 4569-4576.

[20] R. A. Walling and N. W. Miller, "Distributed generation islanding-implications on power system dynamic performance," in *Power Engineering Society Summer Meeting, 2002 IEEE*, 2002, pp. 92-96 vol.1.

[21] P. Piagi, "Microgrid Control," PhD, Department of Electrical and Computer Engineering, University of Wisconsin - Madison, Madison, 2005.

[22] R. Majumder, *et al.*, "Power System Stability and Load Sharing in Distributed Generation," in *Power System Technology and IEEE Power India Conference, 2008. POWERCON 2008. Joint International Conference on*, 2008, pp. 1-6.

[23] S. Carley, "Distributed generation: An empirical analysis of primary motivators," *Energy Policy*, vol. 37, pp. 1648-1659, 2009.

[24] T. S. Basso, "System Impacts from Interconnection of Distributed Resources: Current Status and Identification of Needs for Further Development," NREL/TP-550-44727; TRN: US200908%%14, 2009.

[25] A. Cardenas, *et al.*, "An Active Anti-Islanding Algorithm for Inverter Based Multi-Source DER Systems," in *Power and Energy Engineering Conference, 2009. APPEEC 2009. Asia-Pacific*, 2009, pp. 1-6.

[26] W. Fei and Z. Chengcheng, "Protection and Control for Grid Connected Photovoltaic Power Generation System Based on Instantaneous Power Theory," in *Circuits, Communications and Systems, 2009. PACCS '09. Pacific-Asia Conference on*, 2009, pp. 356-359.

[27] W. Fei and M. Zengqiang, "Passive Islanding Detection Method for Grid Connected PV System," in *Industrial and Information Systems, 2009. IIS '09. International Conference on*, 2009, pp. 409-412.

[28] "IEEE Standard for Interconnecting Distributed Resources With Electric Power Systems," *IEEE Std 1547-2003*, pp. 0_1-16, 2003.

[29] L. Varnado and M. Sheehan, "Connecting to the Grid: A Guide to Distributed Generation Interconnection Issues. ," *Interstate Renewable Energy Council Connecting to the Grid Project*, 2009.

[30] R. Tirumala, *et al.*, "Seamless transfer of grid-connected PWM inverters between utility-interactive and stand-alone modes," in *Applied Power Electronics Conference and Exposition, 2002. APEC 2002. Seventeenth Annual IEEE*, 2002, pp. 1081-1086 vol.2.

[31] L. Yunwei, *et al.*, "Design, analysis, and real-time testing of a controller for multibus microgrid system," *Power Electronics, IEEE Transactions on*, vol. 19, pp. 1195-1204, 2004.

[32] T. Thacker, *et al.*, "Islanding Control of a Distributed Generation Unit's Power Conversion System to the Electric Utility Grid," in *Power Electronics Specialists Conference, 2005. PESC '05. IEEE 36th*, 2005, pp. 210-216.

[33] T. Thacker, *et al.*, "Implementation of control and detection algorithms for utility interfaced power conversion systems," in *Applied Power Electronics Conference and Exposition, 2006. APEC '06. Twenty-First Annual IEEE*, 2006, p. 6 pp.

[34] H. Zeineldin, *et al.*, "Intentional islanding of distributed generation," in *Power Engineering Society General Meeting, 2005. IEEE*, 2005, pp. 1496-1502 Vol. 2.

[35] G. Fang and M. R. Iravani, "A Control Strategy for a Distributed Generation Unit in Grid-Connected and Autonomous Modes of Operation," *Power Delivery, IEEE Transactions on*, vol. 23, pp. 850-859, 2008.

[36] G. Iwanski and W. Koczara, "Autonomous power system for island or grid-connected wind turbines in distributed generation," *European Transactions on Electrical Power*, vol. 18, pp. 658-673, 2008.

[37] R. Majumder, *et al.*, "Control of parallel converters for load sharing with seamless transfer between grid connected and islanded modes," in *Power and Energy Society General Meeting - Conversion and Delivery of Electrical Energy in the 21st Century, 2008 IEEE*, 2008, pp. 1-7.

[38] H. Shengli, *et al.*, "Control algorithm research on seamless transfer for distributed resource with a LCL filter," in *Electric Utility Deregulation and Restructuring and Power Technologies, 2008. DRPT 2008. Third International Conference on*, 2008, pp. 2810-2814.

[39] D. N. Gaonkar, *et al.*, "Seamless Transfer of Microturbine Generation System Operation Between Grid-connected and Islanding Modes," *Electric Power Components and Systems*, vol. 37, pp. 174 - 188, 2009.

[40] C. Chien-Liang, *et al.*, "Design of Parallel Inverters for Smooth Mode Transfer Microgrid Applications," *Power Electronics, IEEE Transactions on*, vol. 25, pp. 6-15, 2010.

[41] L. Qin, *et al.*, "Multi-loop control algorithms for seamless transition of grid-connected inverter," in *Applied Power Electronics Conference and Exposition (APEC), 2010 Twenty-Fifth Annual IEEE*, 2010, pp. 844-848.

[42] Y. Zhilei, *et al.*, "Seamless Transfer of Single-Phase Grid-Interactive Inverters Between Grid-Connected and Stand-Alone Modes," *Power Electronics, IEEE Transactions on*, vol. 25, pp. 1597-1603, 2010.

[43] K. H. Ahmed, *et al.*, "Passive Filter Design for Three-Phase Inverter Interfacing in Distributed Generation," in *Compatibility in Power Electronics, 2007. CPE '07*, 2007, pp. 1-9.

[44] J. Dannehl, *et al.*, "Limitations of Voltage-Oriented PI Current Control of Grid-Connected PWM Rectifiers With "LCL" Filters," *Industrial Electronics, IEEE Transactions on*, vol. 56, pp. 380-388, 2009.

[45] O. Vodyakho and C. C. Mi, "Three-Level Inverter-Based Shunt Active Power Filter in Three-Phase Three-Wire and Four-Wire Systems," *Power Electronics, IEEE Transactions on*, vol. 24, pp. 1350-1363, 2009.

[46] B. Singam and L. Y. Hui, "Assessing SMS and PJD Schemes of Anti-Islanding with Varying Quality Factor," in *Power and Energy Conference, 2006. PECon '06. IEEE International*, 2006, pp. 196-201.

[47] G. Hernandez-Gonzalez and R. Iravani, "Current injection for active islanding detection of electronically-interfaced distributed resources," *Power Delivery, IEEE Transactions on*, vol. 21, pp. 1698-1705, 2006.

[48] H. Karimi, *et al.*, "Negative-Sequence Current Injection for Fast Islanding Detection of a Distributed Resource Unit," *Power Electronics, IEEE Transactions on,* vol. 23, pp. 298-307, 2008.

[49] "IEEE Recommended Practice for Utility Interface of Photovoltaic (PV) Systems," *IEEE Std 929-2000,* p. i, 2000.

[50] S. Alepuz, *et al.*, "Control Strategies Based on Symmetrical Components for Grid-Connected Converters Under Voltage Dips," *Industrial Electronics, IEEE Transactions on,* vol. 56, pp. 2162-2173, 2009.

[51] M. Castilla, *et al.*, "Linear Current Control Scheme With Series Resonant Harmonic Compensator for Single-Phase Grid-Connected Photovoltaic Inverters," *Industrial Electronics, IEEE Transactions on,* vol. 55, pp. 2724-2733, 2008.

[52] M. Brucoli, *et al.*, "Modelling and Analysis of Fault Behaviour of Inverter Microgrids to Aid Future Fault Detection," in *System of Systems Engineering, 2007. SoSE '07. IEEE International Conference on,* 2007, pp. 1-6.

[53] A. Pigazo, *et al.*, "Wavelet-Based Islanding Detection in Grid-Connected PV Systems," *Industrial Electronics, IEEE Transactions on,* vol. 56, pp. 4445-4455, 2009.

[54] T. Thacker, *et al.*, "Islanding Detection Using a Coordinate Transformation Based Phase-Locked Loop," in *Power Electronics Specialists Conference, 2007. PESC 2007. IEEE,* 2007, pp. 1151-1156.

[55] R. M. Santos Filho, *et al.*, "Comparison of Three Single-Phase PLL Algorithms for UPS Applications," *Industrial Electronics, IEEE Transactions on,* vol. 55, pp. 2923-2932, 2008.

[56] L. Qin, *et al.*, "Islanding control of DG in microgrids," in *Power Electronics and Motion Control Conference, 2009. IPEMC '09. IEEE 6th International*, 2009, pp. 450-455.

[57] S. Hirodontis and H. Li, "An adaptive load shedding method for intentional islanding," in *Clean Electrical Power, 2009 International Conference on*, 2009, pp. 300-303.

[58] H. Gaztanaga, *et al.*, "Real-Time Analysis of the Control Structure and Management Functions of a Hybrid Microgrid System," in *IEEE Industrial Electronics, IECON 2006 - 32nd Annual Conference on,* 2006, pp. 5137-5142.

[59] G. Iwanski and W. Koczara, "DFIG-Based Power Generation System With UPS Function for Variable-Speed Applications," *Industrial Electronics, IEEE Transactions on,* vol. 55, pp. 3047-3054, 2008.

[60] J. M. Espi Huerta, *et al.*, "A Synchronous Reference Frame Robust Predictive Current Control for Three-Phase Grid-Connected Inverters," *Industrial Electronics, IEEE Transactions on,* vol. 57, pp. 954-962, 2010.